REAL TIME MONITORING OF VOLUMETRIC WATER CONTENT IN RECLAIMED MINE WASTE USING CONE PENETRATION – TIME DOMAIN REFLECTOMETRY

A Thesis

Submitted to the College of Graduate and Postdoctoral Studies

In Partial Fulfillment of the Requirements

for the

Degree of Master of Science

in the

Department of Civil, Geological and Environmental Engineering

University of Saskatchewan

Saskatoon

By

SPENCER MCLEAN CHUHANIUK

©Copyright Spencer McLean Chuhaniuk, July, 2018. All rights reserved

PERMISSION TO USE

In presenting this thesis/dissertation in partial fulfillment of the requirements for a Postgraduate degree from the University of Saskatchewan, I agree that the Libraries of this University may make it freely available for inspection. I further agree that permission for copying of this thesis/dissertation in any manner, in whole or in part, for scholarly purposes may be granted by the professor or professors who supervised my thesis/dissertation work or, in their absence, by the Head of the Department or the Dean of the College in which my thesis work was done. It is understood that any copying or publication or use of this thesis/dissertation or parts thereof for financial gain shall not be allowed without my written permission. It is also understood that due recognition shall be given to me and to the University of Saskatchewan in any scholarly use which may be made of any material in my thesis/dissertation.

Requests for permission to copy or to make any other use of material in this thesis in whole or in part should be addressed to:

Head of Department of Civil, Geological and Environmental Engineering

University of Saskatchewan

Engineering Building

57 Campus Drive

Saskatoon, Saskatchewan

Canada, S7N 5A9

OR

Dean

College of Graduate and Postdoctoral Studies

University of Saskatchewan

116 Thorvaldson Building, 110 Science Place

Saskatoon, Saskatchewan S7N 5C9

Canada

ABSTRACT

Reclamation soil covers over mine waste are designed to store water as a means of controlling water balance in order to support re-vegetation and minimize the net percolation of water into mine waste. Measurement of stored volumes of water in reclamation material is a critical element in monitoring the performance of the soil cover.

The purpose of this project is to undertake laboratory and field trials of a sensor to measure volumetric water content profiles through reclaimed mine waste using a new time domain reflectometry (TDR) component added to conventional geotechnical cone penetration testing (CPT). Time domain reflectometry measures the volumetric water content of a soil by characterizing the dielectric constant of the soil – a property that is strongly dependant on volumetric water content. The sensor design is constrained by the ability to be adapted to standard CPT equipment as well as being operational in soils with elevated electrically conductivity (EC). The engineering problem addressed in this project is the measurement of detailed profiles of stored water volume over large areas of reclaimed mine waste (i.e. soil covers placed over tailings or overburden) in real time. If successful, this will be a new method to obtain real time, spatial distributions of stored water volume to depths of up to 10 m within reclaimed mine closure landscapes. Other methods exist to obtain stored water volume profiles however these methods are rather complicated.

The laboratory component of this project was intended to measure the accuracy and operational range of the device using prepared samples under a controlled setting. Two field based calibration studies were used to assess the robustness of the device under extreme forces and to evaluate its performance under actual field conditions. It is expected that the developed CPT-TDR probe can be utilized by industry to evaluate the performance of reclamation covers in a wide variety of closure designs.

ACKNOWLEDGEMENTS

I would like to thank my supervisor, Dr. Lee Barbour for the opportunity, guidance and support throughout my graduate studies. During tougher times, he guided me through with his experience, wisdom and humility. I am also appreciative of my committee members, Dr. Dave Elwood and Dr. Eric Salt as their advice led me to explore different ideas in engineering.

I am very grateful for the funding provided through my graduate studies from NSERC Syncrude-IRC, O'Kane Consultants Inc. and the Gabriel Dumont Institute. In addition to funding, my research would not be possible without the field program from Syncrude Canada Ltd.

I would like to thank Adam Hammerlindl and Helen Yin for their help throughout my laboratory program. Also, Mike Amos, my predecessor who explained to me exactly what I was getting into and for advice along the way. Thanks to Eric Neil for sharing equipment and to Dyan Pratt for coordinating our field trips.

My fellow graduate students deserve thanks, James Tipman, Matthew Buchinski, Shahab Alam and Spencer Chad. Our conservations kept my spirits up and long days in the field are always better with good company.

I have to thank my family and friends too. Although they may have been confused as to what I actually do as a student they showed their support no matter what.

I would also like to thank the Lord as I have been blessed my entire life with the opportunity to go to school and move forward with my education. Through ups and downs in life, having faith kept me on track and brought me to where I am today.

TABLE OF CONTENTS

LIST OF TABLES

LIST OF FIGURES

1 INTRODUCTION

Soil covers over mine waste are used in part of mine reclamation to decrease the net percolation of water into the mine waste material. The cover material also acts to support vegetation and control the overall water balance. Measuring volumes of water from rain and snow all play a role in monitoring the performance of the cover. The most critical element in monitoring the performance of the cover is measuring the stored volumes of water within the cover material.

The purpose of this project is to develop a device to measure the stored volume of water in a soil depth profile. This device is comprised of a sensor that measures the volumetric water content of soil using time domain reflectometry (TDR) added to conventional geotechnical cone penetration testing (CPT). Time domain reflectometry is an indirect measurement of volumetric water content as the dielectric constant is actually being measured which is strongly dependent on the volumetric water content.

Conventional practice has been to install TDR systems over shallow depths (< 2m) to monitor volumetric water content with time at a few selected locations. The engineering problem addressed in this project is the measurement of detailed profiles of stored water volume over large areas of reclaimed mine waste (i.e. soil covers placed over tailings or overburden). If successful, this will be the only known method to obtain real time, vertical and spatial distributions of stored water volume within reclaimed mine closure landscapes to depths of up to 10 meters. The goal of this work is to adapt a preliminary laboratory based design of a CPT-TDR for application to reclaimed sand and fluid fine tailings from the oil sands industry.

This project builds upon the previous MSc research of Amos (2014). His research attempted to calibrate a prototype CPT-TDR using laboratory trials. He was able to develop an appropriate configuration of TDR probes for use with CPT-TDR and was also able to mitigate the loss of signal in highly electrically conductive soils by insulating the TDR probes. However, the experimental program was limited to laboratory scale testing without evaluating the performance of the system under field conditions.

The current research advances this work in two broad areas. The first area is the modification of the probe construction to make it sufficiently robust for testing under field conditions using conventional TDR instrumentation and CPT equipment. The second area was to explore the use of the modified CPT-TDR under both field and laboratory conditions for a range soil types including sand tailings as well as fluid fine tailings (FFT).

The objectives that addressed these problems are as follows:

1) Design a CPT-TDR probe that has sufficient durability and strength to be utilized in the field using conventional TDR readers and CPT push rigs.
2) Define the accuracy and range of operation of the CPT-TDR in two types of oil sands mine waste: sand tailings (with and without high EC pore-water) and Fluid Fine Tailings (FFT).

The design of the CPT-TDR will have insulation and steel between the TDR waveguides taking place of what would otherwise be soil. It is hypothesized that this will likely cause a reduction in sensitivity when compared to conventional TDR. If this hypothesis holds true than a custom calibration of the CPT-TDR will be required.

A section on literature provides the background of TDR and CPT. The Materials and Methods section describe the design of the equipment and the test methods. All the results from testing are presented and discussed in the Results and Analysis section followed by the Conclusions and Recommendations section.

2 LITERATURE REVIEW

2.1 Introduction

Selected papers that introduce key issues associated with the use of TDR to determine the volumetric water content of soil are reviewed in this chapter. This information provided the literature context for the research and guided the design of the CPT-TDR and analysis of test results.

2.2 TDR Theory

TDR was originally developed to locate breaks as part of electrical cable testing (Fellner-Feldegg 1969). In these applications, the velocity at which an electrical pulse propagated down the cable was defined based on the dielectric properties of the insulation. However, it was soon realized that the TDR method could also be used to measure the dielectric properties of the material surrounding the cable based on the observed velocity of wave propagation. This provided the opportunity to measure the dielectric properties of soil in which a section of cable (i.e. metal rod) was installed. This is accomplished by having a pulse generator create an electromagnetic wave that travels along a coaxial cable. As the wave reaches parallel probes connected to the coaxial cable, part of that wave is reflected back at the end of the probes (Fellner-Feldegg 1969, Jones et al. 2002). The reflection coefficient, ρ (rho) is the ratio of the reflected wave amplitude to the initial wave amplitude (MOHR Test and Measurement LLC 2017). The travel time for the reflected wave is displayed on an oscilloscope as a reflection coefficient and an apparent length as shown in Figure 2.1. The length of probes remains constant, but the apparent length changes with changes in the dielectric constant of the soil water medium.

The dielectric constant can be calculated from the waveform using the following equation by Jones et al. (2002):

$$\varepsilon_b = \left(\frac{x_2 - x_1}{V_p L}\right)^2 \tag{2-1}$$

where ($x_2 - x_1$) is the apparent length (m), V_p is the propagation velocity of the wave relative to the speed of light (m/s) and L is the length (m) of the probes (Jones et al. 2002). Ultimately the higher soil water content results in a higher dielectric constant. As the water content increases the propagation velocity of the wave decreases (Jones, Wraith and Or 2002). It should be noted that

the apparent length and distance are used synonymously in this research, both referring to the apparent length ($X_2 - X_1$) of the TDR waveguides.

The dielectric constant from Equation 2-1 may then be used to estimate the volumteric water content of a soil water medium. Topp et al. (1980) developed an empirical equation, known as Topp's equation, to determine the volumetric water content in soils from the dielectric constant:

$$\theta_v = -5.3\ x\ 10^{-2} + 2.92\ x\ 10^{-2}\varepsilon_b - 5.5\ x\ 10^{-4}\varepsilon_b^2 + 4.3\ x\ 10^{-6}\varepsilon_b^3 \qquad (2\text{-}2)$$

where θ_v is the volumetric water content and ε_b is the dielectric constant. Equation 2-2 was developed using 5 different soils and mediums. Topp et al. (1980) concluded that the dielectric constant was strongly dependent on water content and weakly dependent on soil type.

Sorta et al. (2013) found that for soils with very high volumetric water contents (e.g. above 0.45 m^3/m^3) Topp's equation underestimated the actual water content. Sorta et al. (2013) developed their own equation:

$$\theta_v = -3.08\ x\ 10^{-5}\varepsilon_b^3 - 7.40\ x\ 10^{-3}\varepsilon_b^2 + 2.05\varepsilon_b - 3.04 \qquad (2\text{-}3)$$

Jones et al. (2002) found good results using a mixing model approach. In this case the dielectric constants from the three soil constituents (air, water and solids) are used to arrive at a bulk dielectric constant (Jones, Wraith and Or 2002). In order to determine the volumetric water content of the soil using the bulk dielectric constant the porosity of the soil must be known or estimated (Jones, Wraith and Or 2002).

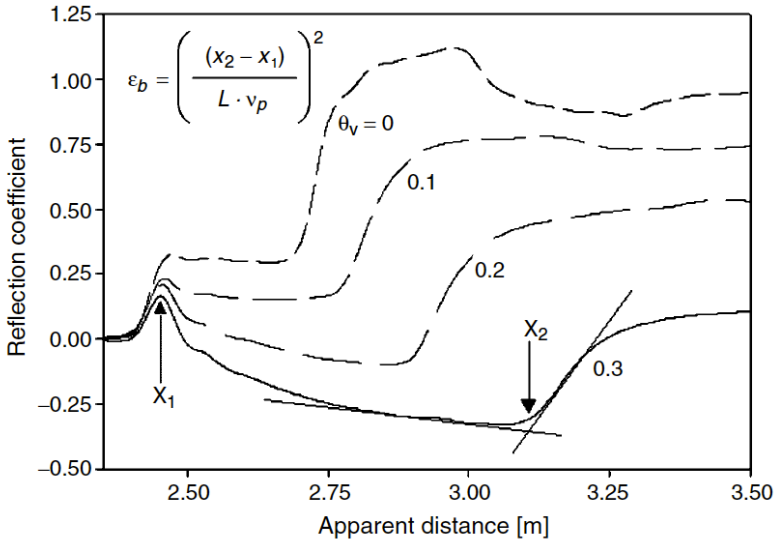

Figure 2.1: Sample TDR waveforms of various volumetric water contents. Labels X_1 and X_2 mark the points of the waveform for the apparent length (Jones et al. 2002).

2.3 Complications with TDR

The water content reading obtained with TDR is based on a measured dielectric constant, which is independent of soil type and salinity (Topp et al. 1980). However; in the case of highly electrical conductive soils (e.g. saline mine tailings or clays) the energy within the electromagnetic wave is lost into the conductive medium and consequently very little of the energy is reflected back. This results in difficulties in interpreting the time (apparent length) at which the voltage pulse is reflected, as illustrated in Figure 2.2 (Mojid et al. 1998, Dalton and Van Genuchten 1986 and Fujiyasu, et al. 2004).

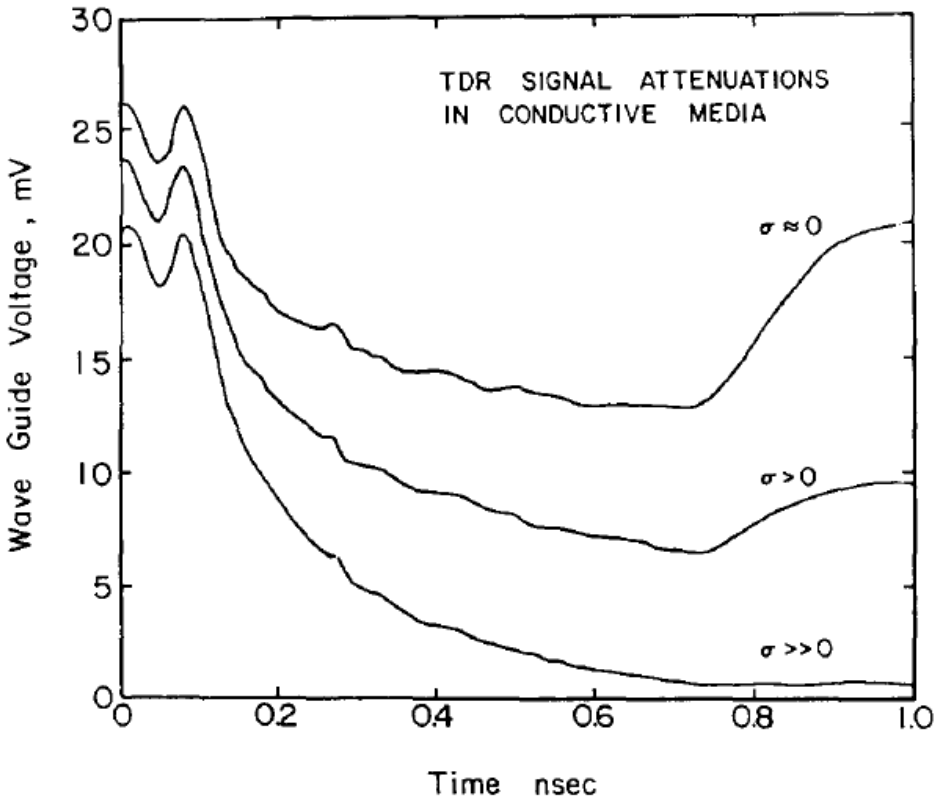

Figure 2.2: TDR waveforms in low, medium and high electrical conductivity mediums. As the electrical conductivity increases the upward slope of the waveform marking the pulse reflection becomes less pronounced. The upward slope is non-existent in high electrically conductive mediums (Dalton and Van Genuchten 1986).

The use of long coaxial cables also presents a challenge with TDR. As the cable length is increased the rise time of the voltage step also increases. This causes an underestimation in the

dielectric constant in soils (Heimovaar 1993, Fellner-Feldegg 1969). Using 50 Ω cable, Heimovaara (1993) found reproducible results with 24 m cable lengths.

The goal of the current research is to obtain water content profiles to depths of approximately 10 m or greater. Even though the cable lengths fall under the maximum length proposed by Heimovaara (1993), challenges with the coaxial cable remain due to its fragility and the concomitant damage caused by bending or crushing of the cable during employment in the field. The use of coaxial cable may be eliminated altogether with the use of an 'in-probe, down-hole' processor. This however is not in the scope of this project.

2.4 TDR Probe Length and Configuration

Selection of an appropriate probe length is an important decision for installation of the TDR. The metal probes that are in contact with the soil measure the length-weighted water content along the probes (Ferre, et al. 1998). Short probes will handle electrically conductive soils better than long probes due to the reduced potential for energy loss into the soil (Dalton and Van Genuchten 1986). The minimum recommended probe length is 100 mm, since any probe less than 100 mm in length is likely to produce erroneous readings (Ferre and Topp, 2002).

Dalton and van Genuchten (1986) provide the following equation to help estimate an optimal length of probe:

$$L_{max} = \frac{\ln V_t/V_r\sqrt{\epsilon(\theta)}}{120\pi\sigma(\theta,\sigma_w)} \quad (2\text{-}4)$$

where $\varepsilon(\theta)$ is the volumetric water content, $\sigma(\theta, \sigma_w)$ is the conductivity as a function of water content and salinity in dS/m, V_t/V_r the ratio of transmitted and reflected voltages.

The selection of the spacing between paired (i.e. two-rod probes) will define the volume of soil being measured. The sample volume/area is reduced when using three-rod TDR probes (Ferre, et al. 1998). The sample volume is estimated to be 20 times the probe length as defined by an eliptical shape around the probes (Topp, et al. 1980). Amos (2014) found good results using conventional two rod probes embedded in a plastic cylinder for use in CPT-TDR prototype. The rod lengths in this case were 111 mm.

2.5 TDR Probe Sheathing

The loss in a TDR return voltage in electrically conductive soils may be mitigated with the use of an insulating rod coating (Fujiyasu, et al. 2004, Nichol, et al. 2002). With an insulating coating the sensitivity of the TDR readings becomes reduced because the dielectric constant of the insulating material is much lower than the surrounding soil. Soil mineral grains have a dielectric constant ranging from 3 to 5 where the dielectric constant of the plastic material used in Amos' research ranges from 3 to 4 (DuPont Engineering Polymers n.d.). The optimum dielectric constant of the insulating material is around 35, nearly half of the dielectric constant for water (80) (Fujiyasu, et al. 2004).

In this project the TDR probes will be partially embedded in a plastic cylinder with a relatively low dielectric constant. The plastic cylinder will be place axially on a steel shaft. Due to the high dielectric constant of steel, calibrations should not be required because of the steel shaft. Calibration may be required due to the partially embedded probes (Lin, et al. 2006).

2.6 CPT Theory

Cone penetration testing (CPT) is a site characterization tool used extensively in geotechnical engineering. The main components of the tool are the cone tip and the friction sleeve. Both have load sensors and thus the resistance from the friction sleeve and load from the cone tip are known. In addition, a pore water pressure transducer is often used to measure pore-pressures developed during pushing as well as to observe rates of pore-pressure dissipation when pushing ceases. A large body of empirical relationships have been developed which enable to relate tip and shaft resistance during pushing to soil type and condition (Robertson and Cabal 2012).

Typical CPT equipment is shown in Figure 2.3 and 2.4. A large rig is used to push the cone into the soil at a rate of 20 mm/s (Robertson and Cabal 2012). As the cone is advanced into the ground additional rods are threaded onto the previous rod below to keep advancing the test.

The advantages and disadvantages of CPT are as follows:

Advantages of CPT:

- Fast and continuous profiling
- Repeatable and reliable data (not operator-dependent)
- Economical and productive
- Strong theoretical basis for interpretation

Disadvantages of CPT:

- Relatively high capital investment
- Requires skilled operators
- No soil sample, during a CPT
- Penetration can be restricted in gravel/cemented layers (Robertson and Cabal 2012)

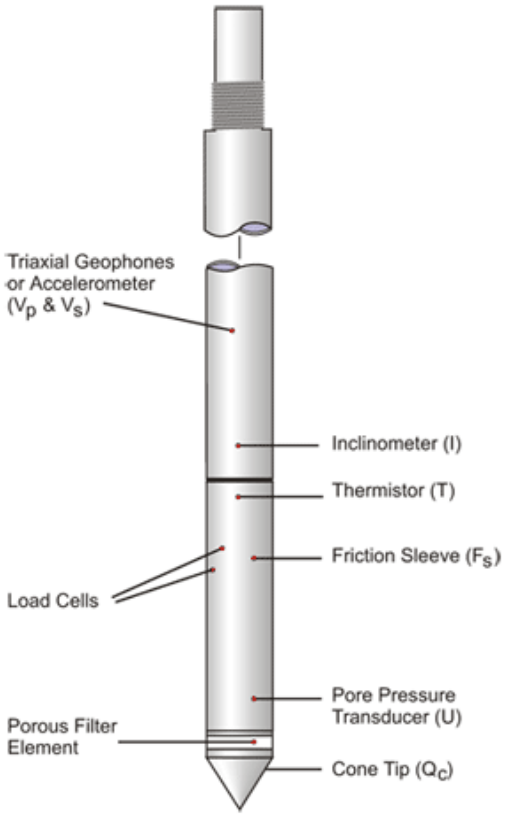

Figure 2.3: Diagram of a typical CPT tool (Robertson and Cabal 2012).

Figure 2.4: Rig used for CPT. Other types of rigs may be used in CPT varying from fully enclosed units integrated into on-highway trucks to amphibious units (Robertson and Cabal 2012).

Additional tools may be integrated into CPT shafts for other parameters of interest. In addition to pore-pressure monitoring, electrical resistivity is often monitored during pushing. Site access has become less of problem for CPT with the development of smaller rigs, soft terrain rigs and amphibious rigs (Robertson and Cabal 2012).

2.7 Previous CPT-TDR and Soil Water Content Work

There has been a number of previous attempts to configure TDR probes with some form of penetration testing reported in the literature. Lin et al. (2006) embedded copper strips into an insulating Delrin sheath connected to a cone penetration shaft and tip (Fig. 2.5). Lin et al. (2006) found that advancing the probe resulted in errors in the dielectric constant measurements. The configuration of the probes does not have a large effect on the sensitivity of the measurements (Lin et al. 2006).

A similar 2 rod configuration was also utilized by Lefebvre (1997). The 2 probe design has high precision for apparent length measurements. However this design was targeted for use in very soft soils with shallow penetration depths. The reported results were promising and a custom calibration was recommended.

One factor that is not well defined in the work to date is whether advancing the probe results in compaction or displacement of the soil adjacent to the probe which might alter the observed water contents (Vaz and Hopmans 2001).

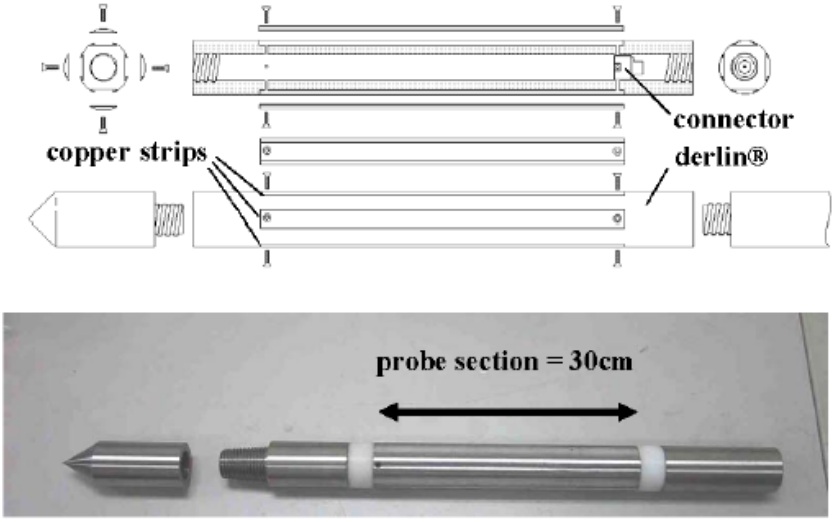

Figure 2.5: Design and actual prototype of TDR probe by Lin et al. (2006).

A different type of CPT moisture sensor in which rings were used as waveguides was evaluated by Shinn II et al. (1998). These researchers mounted stainless steel rings onto a CPT shaft directly behind the CPT load cell. A down-hole processor was used to convert the dielectric reading to a voltage. The voltage was sent to another computer where a calibration curve was used to convert the voltage to a volumetric water content reading. The use of down-hole electronics has the advantage of eliminating the need for a coaxial cable. In addition, it also provides the opportunity to vary operational frequencies to mitigate electircal conductivity issues.

Overall the challenge of mounting TDR probes onto a shaft to be penetrated into soil has been overcome but not proven to withstand extreme field conditions. Although Shinn II et al. has reached depths of approxiamtelt 55 feet their probe design was unique using steel conductive rings. Their method was also different where resonant frequency modulation was used to determine the dielectric constant.

One method already existing to obtain water content profiles in soils uses a neutron moisture meter and access tube. Volumetric water content of the soil is measured using a neutron moisture meter. Profiling of volumetric water content is achieved by lowering the neutron moisture meter down through the access tube and obtaining readings at specified depths (Evett 2003).

This method acheives the same results as the CPT-TDR with some comparable disadvantages. Mainly a tube must be installed prior to obtaining volumteric water content profiles. Also since the neutron moisture meter is a source of radiation, the operation and storage of the device becomes difficult (Evett 2003).

3 MATERIALS AND METHODS

3.1 Introduction

The overall methodology being followed in this research is to design, construct and test a set of CPT-TDR shafts which can be evaluated in programs of controlled laboratory testing followed by full scale testing within the field. The primary focus of the laboratory testing component will be to evaluate the performance of the probe in a range of soil types (fluid fine tailings or sand tailings) under a range of pore water salinities (freshwater to process affected water). The field testing program will be based on comparing the measured CPT-TDR profiles of water content with those obtained from direct sampling (core samples) over a transect of reclaimed sand tailings at an oil sands mine. Two field programs were completed in 2015 and 2016 at the same site. The 2015 field testing proved that the equipment design needed to be strengthened and the new design was tested in 2016.

3.2 Design of CPT-TDR Probe

The CPT-TDR design is comprised of the structural design of the CPT shaft connections that will hold the insulated TDR waveguides, and the waveguides and coaxial cable connections themselves.

3.2.1 Structural and Shaft Design

The CPT push rig creates large forces on the shaft of the CPT device. The TDR section of the CPT shaft must be able to withstand the large shear, axial and bending forces created with the penetration test. The presence of rocks or variability in strength or stiffness in the ground can also lead to additional bending or abrasion forces.

Preliminary field testing with an early prototype CPT-TDR design highlighted that there were some structural deficiencies in the design under the high stresses associated with advancement of the cone tip. This led to modification of the connections of the TDR unit to the CPT shaft. In Figure 3.1 the initial prototype design is shown at the top with the current design at the bottom. The design changes are noted in the Figure 3.1.

The current shaft design has constraints as follows:

- The shaft must be compatible with standard CPT equipment (push rods and friction reducers)
- The shaft must be robust in order to handle the extreme forces that are involved with CPT. This includes the physical design and the material selection.

Using these constraints as a guide the CPT-TDR shaft shown in Figures 3.1 and 3.2 was developed.

Figure 3.1: First prototype (top) and second prototype (bottom). Changes include the fully embedded waveguides on the second prototype, as well as a stronger cone tip connection.

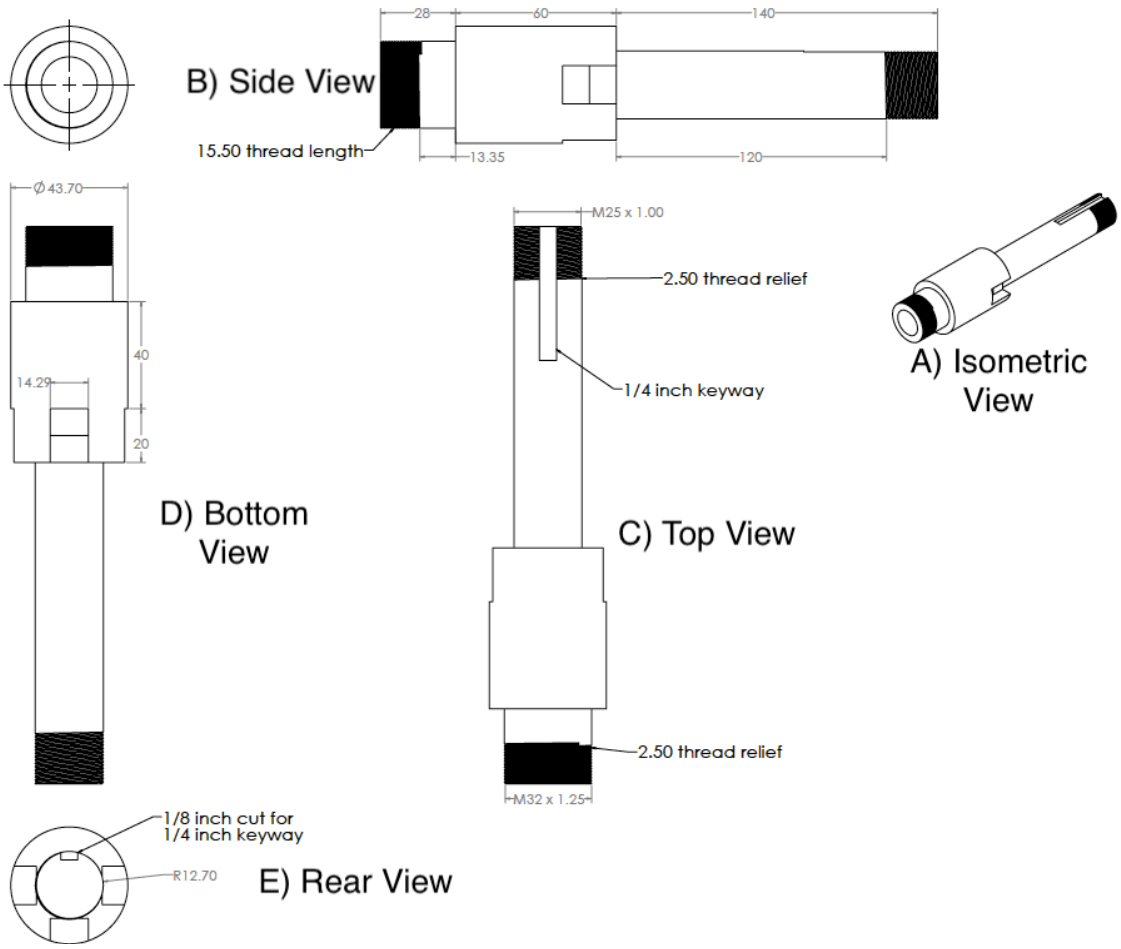

Figure 3.2: Schematic drawings of the CPT-TDR module. All dimensions are in millimeters unless otherwise noted.

The insulated TDR unit is constructed as a polymer cylinder held in place on the CPT shaft as shown in Figure 3.2. The cylinder fits onto the 25 mm by 120 mm portion as in B) side view and C) in Figure 3.2. The polymer cylinder is unable to rotate freely since the keyway prevents this. The shaft is designed to be compatible with conventional CPT push rods and is placed between the cone tip and the friction reducer. Figure 3.3 is an image of the final CPT-TDR tip design showing the tip, TDR probes, friction reducer and coaxially cable installed.

The major change is in the design from the initial prototype was the connection between the CPT-TDR shaft and the tip. The initial design had a relatively small half-inch threaded rod to connect the shaft to the tip. The current design utilizes a larger 25 mm threaded connection between the shaft and the tip.

Figure 3.3: Complete field ready CPT-TDR unit.

3.2.2 Design of Waveguides and Coaxial Cable Connections

The two key design constraints are those associated with the coaxial cable and its connections and those associated with the structural integrity of the rods and tip. However, it is worth noting that the intention is that the TDR section can be easily replaced if worn or damaged.

The number of coaxial cable connections should be kept to a minimum and the connections should be tight fitting in maximize signal transmission and minimize signal noise (M. Amos 2014). The TDR waveguides must be mounted on the shaft in parallel. The probes will have to be connected to a coaxial cable running through the hollow centre of the entire CPT shaft. To meet these constraints the cable and waveguides were connected using banana plugs.

The structural integrity of the waveguides and shaft must be sufficient to resist friction and abrasion. In particular, the TDR waveguides must be protected from becoming dislodged from

the shaft. This was achieved using the more robust tip design described earlier and by embedding the waveguides into the cylinder as in Figure 3.1.

3.3 Laboratory Assessment of CPT-TDR Tip

The device must be able to produce useable data when testing in all soils. Testing in electrically conductive soils such as clay, FFT and any type of soil saturated with saline water will create challenges to obtaining useable data. The two known options to problems with signal loss due to highly conductive soils is through the use of sheathing (Nichol et al. 2002) or the use of shorter rods (Ferre and Topp, 2002). The probe length selected for this design was 10 cm, the minimum length suggested by Ferre and Topp (2002).

A laboratory testing program was used to assess the performance of the CPT-TDR in two different soil types; sand tailings with a range of pore fluid electrical conductivity, and FFT, which already contains saline pore water. Both the sand tailings and fluid fine tailings (FFT) are produced as waste materials as a result of bitumen extraction from oil sands.

3.3.1 Comparison of Conventional TDR to CPT-TDR

Initial testing performed in five sand and water mixtures was used to compare the dielectric readings from conventional TDR to that of CPT-TDR. The water content of each mixture was increased in increments from that of the previous mixture. Careful measurement of the prepared water content was not critical in this set of tests since the comparision was between the measurement from conventional TDR and the CPT-TDR. Care was taken when inserting the waveguides for conventional TDR to ensure the same depth and spacing as CPT-TDR was maintained.

3.3.2 Sand Testing Part 1

The next component of the laboratory program involved evaluating the performance of the CPT-TDR in prepared samples of sand and water mixtures. Initial testing was done by mixing known masses and volumes of sand and water. This allowed for the density and the final volumetric water content to be calculated from the mass of water and dry sand. The volumetric water content (θ_v) for each mixture had a target of 0.15 m^3/m^3. This was calculated using data from the mixtures and the following equation:

$$\theta_v = \frac{M_w \rho_b}{M_s \rho_w} \tag{3-1}$$

where M_w is the mass of water in kg, M_s is the mass of solids in kg, ρ_b is the bulk density of the soil in kg/m^3 and ρ_w is the density of water in kg/m^3. In the case of saturated conditions (specifically FFT) volumetric water content may also be calculated by the following equation:

$$\theta_v = \frac{\theta_g S_g}{1 + \theta_g S_g} \tag{3-2}$$

where θ_g is the gravimetric water content and S_g is the specific gravity of an individual soil particle.

Sodium Chloride salt was also added to the water used for the mixture in order to vary the salinity of the pore water from 0 g/L to 30 g/L of total dissolved solids (TDS). This testing was conducted using only the CPT-TDR. The purpose of this was to define the operational range of the CPT-TDR in electrically conductive soils. All testing was conducted using the CPT-TDR probe and a Mohr CT100 TDR Cable Tester.

The procedure for this portion of the lab testing is as follows:

1. Prepare sand/water/salt mixtures in pails, recording the volume and mass of the water and sand (keeping the masses and volumes consistent). All pails had roughly equal volumetric water contents.
2. When adding the salt, one mixture is kept as fresh water and the other six mixtures have salt content from 0-30 g/L. The salt content was increased in each pail by 5 g/L. Electrical conductivity readings should be taken using a Decagon Devices 5TE sensor and a ProCheck sensor readout device.
3. The CPT-TDR was inserted into mixture ensuring the waveguides are completely in the mixture as in Figure 3.4.
4. The waveform from the Mohr CT100 unit was collected and stored digitally. This waveform can later be revisted to find the apparent waveguide length, calculate the dielectric constant and then the volumetric water content.
5. Physcial samples were collected for each mixture to measure the volumetric water content from the gravimetric water content and the dry density. A thin walled 47 mm diameter steel pipe was inserted into the soil from a hole previously cut in the side of the pail as shown in Figure 3.5. Once the pipe is extracted the total length of soil inside the pipe was measured allowing for the volume to be calculated. The gravimetric water content (and dry mass) of the sample was then measured using standard procedures.

Figure 3.4: Sand and water mixture with CPT-TDR unit inserted. Waveguides are completely buried in sand, as they are not showing.

Figure 3.5: Sampling method using a steel pipe inserted into the sand and water mixture from a hole cut in the side of the pail.

3.3.3 Sand Testing Part 2

This round of testing was conducted to evaluate the CPT-TDR performance for a series of samples with systematic, incremental, changes in volumetric water content. The results from this testing were used to establish a laboratory based calibration curve for the CPT-TDR.

The procedure for this portion of testing is as follows:

1. A container was filled with sand and the dry mass and volume of the sand was recorded.
2. A known volume of water was added to the sand to increase the volumetric water content by approximately 0.02 m^3/m^3. With each increment manual mixing was performed using a steel scoop.
3. The CPT-TDR was inserted into the mixture, ensuring the waveguides are completely covered by the mixture.
4. The waveforms from the Mohr CT100 unit were recorded. This waveform can later be revisted to find the apparent waveguide length, calculate the dielectric constant and then the volumetric water content.
5. The process starting at Step 2 was repeated, incrementally increasing the volumetric of water content of the mixture by 0.02 m^3/m^3. This process was continued until the sample reached saturation.

3.3.4 Density of Soil

Two critical elements for the determination of volumetric water content are the gravimetric water content and the density of the soil. Measurement of gravimetric water content is straightforward, following standard procedures such as ASTM International D4643 (2008). However; the sampling required for density measurements was always subject to two potential sources of error: disturbance of the sample density as a result of sample collection (e.g. densification or loosening) and potential changes in water content as a result of sample collection and extraction. These issues pose a challenge in accurately measuring the volumetric water content under both laboratory and field conditions.

The density and water contents of laboratory prepared mixtures were check through the collection and testing of cylindrical samples as well as estimating the properties from the bulk dry mass, volume and added water for the mixture. Bulk density is the more trusted approach since there are no obvious errors. Cylindrical physical samples may be subject to error in densification and

material losses. It should be noted that in some cases a density value is assumed for the sake of consistency.

3.3.5 FFT Testing

Laboratory testing on FFT was done in a pail that was modified with filter drains in an attempt to dewater the soil. The pail also was fitted with a modified lid, which enabled a higher air pressure to accelerate the dewatering. The filter drains and the entire unit are displayed in Figures 3.6 and 3.7 respectively.

Figure 3.6: Filter drains installed in the pail to contain the FFT.

Figure 3.7: Entire unit set up. Lid is clamped and weight added to secure the lid under pressure. Containers are placed underneath the pail to collect pore fluid.

Filter drains were made from 1-inch rigid PVC tube with 3mm slots cut into the side. The tube was wrapped in geosynthetic fabric. A PVC cap was fitted on the bottom of the tube with a brass fitting to allow pore water to drain in a container. Four filter drains were used in the unit. Sealing of the drains to the bottom of the pail was handled by passing the brass fitting through the bottom of the pail and setting the bottom of the filter drain in silicon sealant.

The FFT was added, ensuring the level was above the filter drains. The lid was secured additionally by clamping and iron weights. The air pressure was then applied and increased to about 35 kPa and the samples were left to drain for at least four days. The pore fluid that was collected was analyzed for aqueous chemistry and electrical conductivity.

Initial volumetric water content readings were taken from physical samples and from the CPT-TDR. Volumetric water contents were then taken three more times as the FFT drained. Calculating the volumetric water content from gravimetric water content readings was done using Equation 3-2 and assuming a specific gravity for the solids of 2.4 (Dompierre and Barbour 2016).

3.4 Field Evaluation of CPT-TDR Shaft

One of the challenges in undertaking a field based assessment of the performance of the CPT-TDR probe is the ability to collect and test undisturbed samples for gravimetric and dry bulk density from which volumetric water content can be calculated. Measurement of gravimetric water content is relatively straightforward (e.g. ASTM D4643-08); however, sampling of hydraulically placed, and track packed sand tailings can be problematic. For example, sampling with a large (three and a half inch) diameter Shelby tube is ideal for creating the least densification of soil. However sample retention in large diameter Shelby tubes is often problematic upon extraction of the sampling tube from the ground. Small diameter piston sampling is more able to hold low cohesive soils in the tube upon extraction; however, small diameter piston sampling can result in densification of the samples. In addition, sampling near the water table (i.e. within the capillary fringe or below the water table) can result in sample disturbance, changes in water content and loss of water from the sample as it is retrieved from the borehole.

The field-testing was performed at Syncude's Southwest Sand Storage (SWSS) tailings facility. This is a partially reclaimed oil sands tailings site. The first step was a full-scale CPT test using standard CPT equipment to obtain tip resistance, pore pressure and resistivity. This was followed by the CPT-TDR push test to a depth below the water table as previously determined from the

CPT test. Lastly samples were taken and later analyzed for comparison to CPT-TDR results. Two separate field testing programs took place: one in November 2015 and the second in August 2016.

3.4.1 Field Testing 2015

This initial test was performed within Cell 32 at Syncrude's SWSS facility in November of 2015. The site is the downstream slope of the tailings dyke. The purpose of this test was to determine how the initial CPT-TDR design would perform in full scale field-testing conditions. Figure 3.8 is the location where the testing took place at SWSS. The dyke contains a pond that holds process water. Reclamation material is placed on top of tailings sand dyke. The slope itself is a series of benches with access roads to research wells labeled BH-LB-07, BH-LB-08 and BH-LB-09 in the inset of Figure 3.8. Initial field testing took place adjacent to these three locations.

Figure 3.9 shows the typical landscape of the SWSS dyke. Vegetation consists mainly of Aspen and Pine trees with a mixture of native grasses.

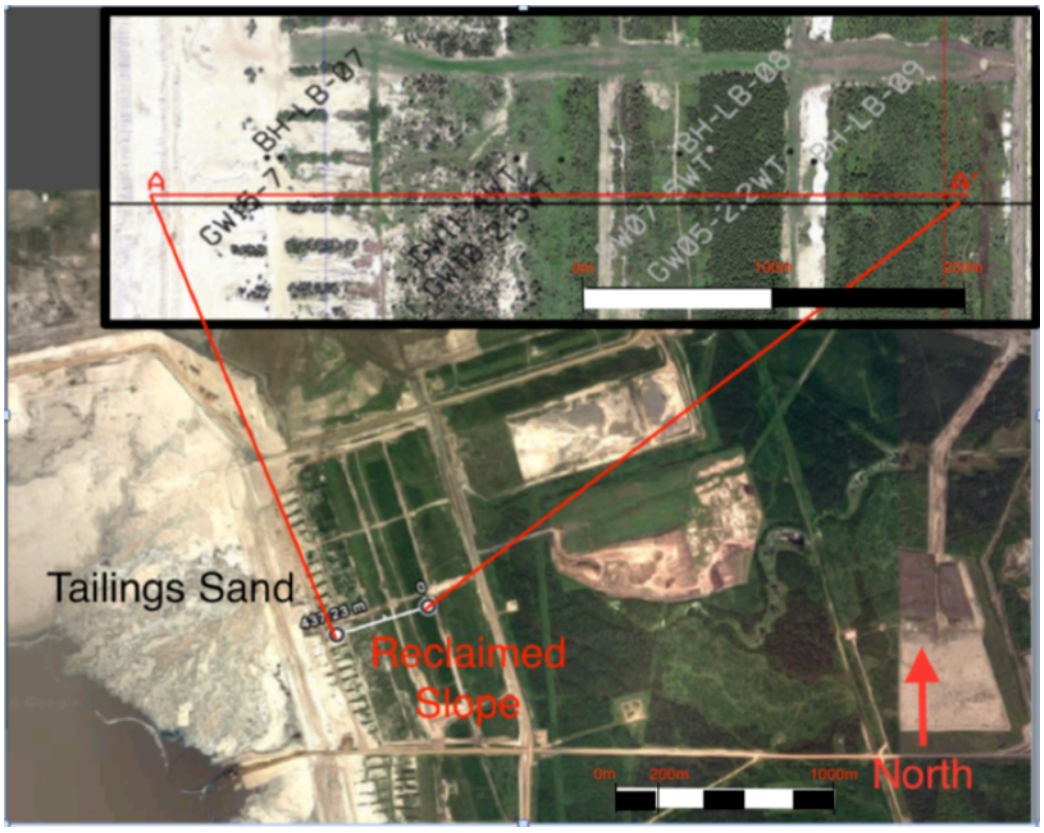

Figure 3.8: Aerial view of location of field testing. Inset is the approximate location where the testing was done.

Figure 3.9: Landscape of SWSS. Photo taken adjacent to a testing site.

The initial field trial was conducted as a series of CPT pushes at the three previously mentioned locations. The first push was a conventional CPT profile to the approximate depth of the water table. This was followed by a second push within a meter of the first hole using the CPT-TDR unit.

The CPT testing included measurements of tip resistance, sleeve resistance, pore pressure and resistivity. The CPT rig then moved ahead slightly to start a new hole. The CPT-TDR was then deployed and advanced in increments of approximately 25 cm. The TDR wave forms were then scanned at least three times at each increment to ensure consistency.

Soil samples were collected from each depth increment using a stationary piston sampler (similar to ASTM D6519-15). Special care was taken to ensure the correct depth readings/intervals are recorded for the samples. The collected sample tubes were sealed to prevent material and evaporative losses. Once the samples were returned to the laboratory, density and gravimetric water content measurements were obtained and used for the results and analysis. Since the samples were collected in cylinders, the length and diameters were easily measured along with the dry and wet masses.

The CPT-TDR testing for the location, BH-LB-07 required two trials. The first attempt failed due to the CPT shaft breaking apart in the ground (broken probe shown in Figure 3.10). The CPT shaft did; however, remain intact during a second attempt using a spare shaft. However; upon extraction of the TDR probes it was observed that there might have been some damage with the connection from the probes to the coaxial cable. The waveforms collected for this location from the TDR were readable.

At BH-LB-08 the CPT-TDR push was undertaken once; however, upon extraction it was noted that the TDR probe had been damaged. The waveforms collected from this trial were analyzed and reasonable water contents were calculated. A single push was also undertaken at BH-LB-09. There was no indication of damage to the probe following extraction; however, it was noted that one of the rods had shifted within the insulated shaft. The waveforms collected from this trial were analyzed and reasonable water contents were calculated.

Figure 3.10: Broken CPT-TDR shaft. This is the initial design.

3.4.2 Field Testing 2016

Field testing using the improved CPT-TDR shaft design commenced in August of 2016. This testing took place within the same dyke Cell (32) as was used in the 2015 testing (Figure 3.8). A total of nine locations were selected for testing and sampling including standard CPT testing to collect measurements of tip resistance, sleeve resistance, pore pressure and resistivity. Core samples were collected at five of the nine locations. The samples were collected using a sonic

sampler and because the samples were considered disturbed, only gravimetric water content measurements were undertaken. The volumetric water content calculations relied on an assumed dry density.

Due to limitations in equipment availability an older Tektronix 1502C TDR unit had to be used in this portion of CPT-TDR testing. This unit was an older model and does not have the capability to save and export waveforms. As a result the waveforms had to be analyzed while CPT-TDR testing was in progress.

CPT-TDR results were successfully collected at each location and the CPT-TDR shaft remained intact over push depths approaching 8m. After testing at all nine locations using the same shaft only scoring on the shaft was apparent with no bending, breakage or waveguides out of position.

3.5 Data Analysis Method

Every waveform collected using the Mohr CT100 unit has the ability to be analyzed on the unit itself or exported for further analsis on a desktop computer. The waveforms in this research were all exported to be analyzed on a desktop computer except for those analyzed in the second field trial. The digital wave forms allow for an easier analysis and the possibility to later revisit the waveform if necessary. The desktop computer program to analyze the waveforms is called CT Viewer 1.2.2.0.

The waveforms obtained from the CPT-TDR are typical to the waveform in Figure 3.11. There is an initial peak followed by a gradual upslope. For determining the apparent length of the waveguide for the calculation of the dielectric constant the initial peak is the first point, or the X_1 position. This first point is always at the same location as long as the cable length, waveguide length and propagation velocity remain constant.

The second point or X_2 position was determined by two ways in this research. The first way is by the method from Jones et al. (2002) called the double tangent method in this project. It is found by taking a line tangent to the low part of the waveform and a line tangent to the upslope of the waveform. The point where the two tangent lines intersect is the X_2 point. This is shown in Figures 2.1 and 3.11. A second method of finding the X_2 point is called the single tangent method in this project. This is found by simply taking a tangent line to the upslope of the waveform. The point where the tangent line initlally contacts the waveform is the X_2 point as shown in Figure 3.11. Throughout this research both methods have been used and the method used is noted in the presentation of the results.

When the Mohr CT Viewer program was used to analyze the waveforms both the single and double tangent methods were easily used to find the apparent length. The CT Viewer has a cursor that moves horizontally along the waveform with a precision of 10^{-4} m. Waveforms may also be zoomed into easily locate the posistion of X_1 and X_2.

Figure 3.11: Typical waveform from the CPT-TDR in unsaturated sand displayed by the Mohr CT Viewer. Locations of X_1 and X_2 shown using both the single and double tangent method. The X-axis has a scale of 0.152 m/major gridline division and the Y-axis scale is 38.734 mRho/major gridline division.

Using Equation 2-1 the dielectric constant may be calculated using the apparent length from X_1 and X_2 and the length of the waveguide. With the dielctric constant calculated the volumetric water content may be calculated using Equation 2-2 or 2-3.

In laboratory testing the actual volumetric water content of the test soil is known from physical samples. Calibration equations may be developed from the actual volumetric water content and the CPT-TDR volumetric water content readings. By plotting one volumetric water content value on the x-axis and the other volumetric water content value on the y-axis an empirical calibration may be found using the equation of the trendline.

4 RESULTS AND ANALYSIS

4.1 Introduction

This chapter presents the results from the laboratory and field-testing of the CPT-TDR. The goal of the laboratory testing was to define the operating limits and calibrate the CPT-TDR. Field-testing results include volumetric water content depth profiles obtained from both CPT-TDR testing in situ as well as from testing of soil samples collected during the field program. The field results are evaluated using both the field measured volumetric water contents as well as water contents corrected using the calibration developed from the laboratory testing.

Laboratory testing of the CPT-TDR followed the methods outlined in Section 3.2. The goal of this work was to:

- Define the operating range of the CPT-TDR with increasing salinity and water content.
- Analyze the response of the CPT-TDR with changing water content.

Since both the Topp and Sorta equations were originally developed using conventional TDR waveguides it was felt that calibration equations would have to be utilized to capture the changes in readings that would arise as a result of the electrical insulation used for the CPT-TDR field probe. It was expected that the presence of the insulation will alter the apparent length of the waveform and calibration will be required to calculate a representative volumetric water content.

Previous CPT-TDR research by Michael Amos (2014) was conducted using equipment similar in design to this author's research. Amos' CPT-TDR probe (Fig. 4.1) had a number of differences from the current study including:

- The use of round waveguides rather than square waveguides
- Electrical connections using simple spring clips
- The use of only the double tangent method in waveguide analysis

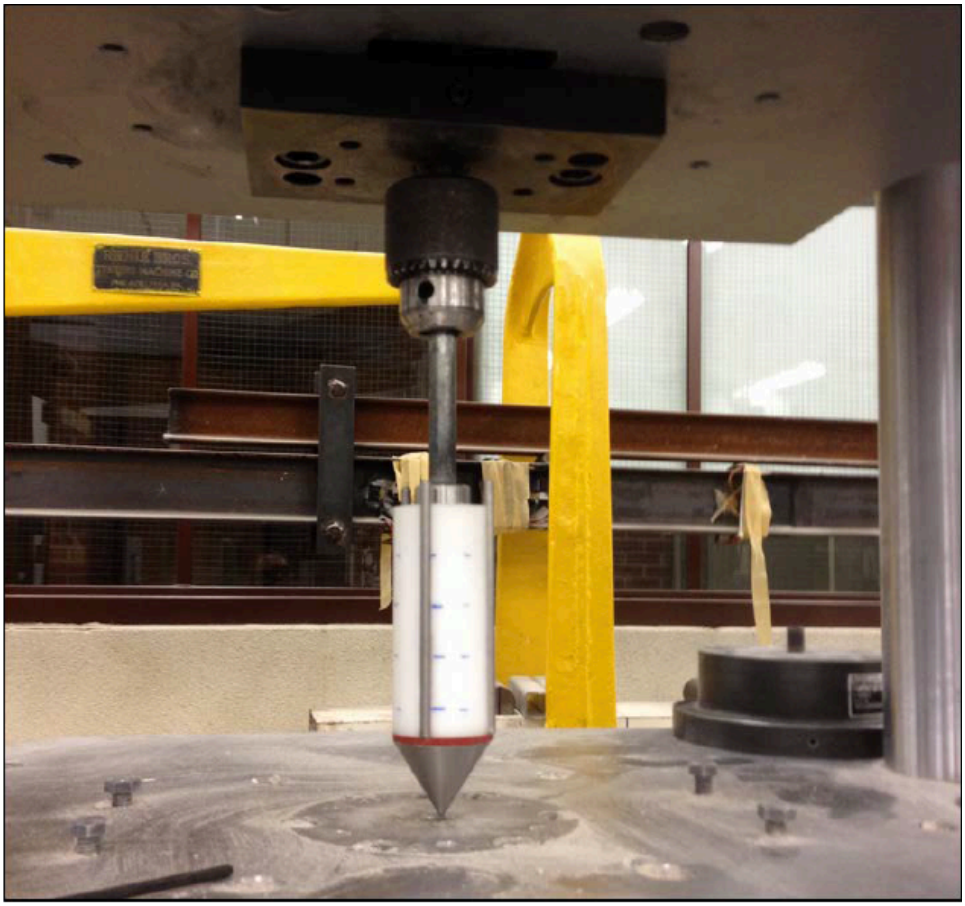

Figure 4.1: Mike Amos' CPT-TDR design (Amos 2014).

Amos (2014) found that although there was a strong linear correlation between measured and actual volumetric water contents, the measurements obtained from his CPT-TDR probe systematically underestimated the volumetric water content (Figures 4.2 and 4.3). In these figures, data points that plot above the 1:1 line indicate an underestimation of volumetric water content by the CPT-TDR.

It is apparent that the CPT-TDR probe developed by Amos (2014) provided a linear relationship to either conventional TDR probes or physical measurements of water content but with a loss of sensitivity. Amos (2014) assumed that this lack of sensitivity in the TDR signal was likely due to altered wave forms produced by the presence of the Delrin® polymer shaft containing the TDR waveguides. This insulating shaft likely altered the electrical field created within the soil by the voltage pulse.

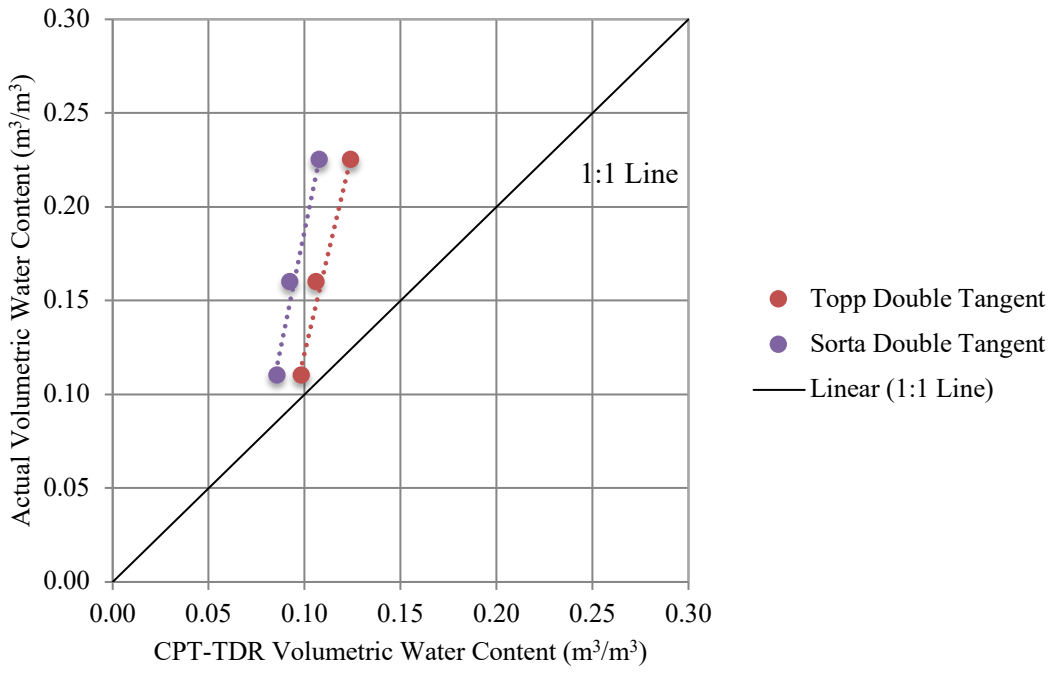

Figure 4.2: Plot of the CPT-TDR volumetric water content calculations and the actual volumetric water content calculations from Amos (2014).

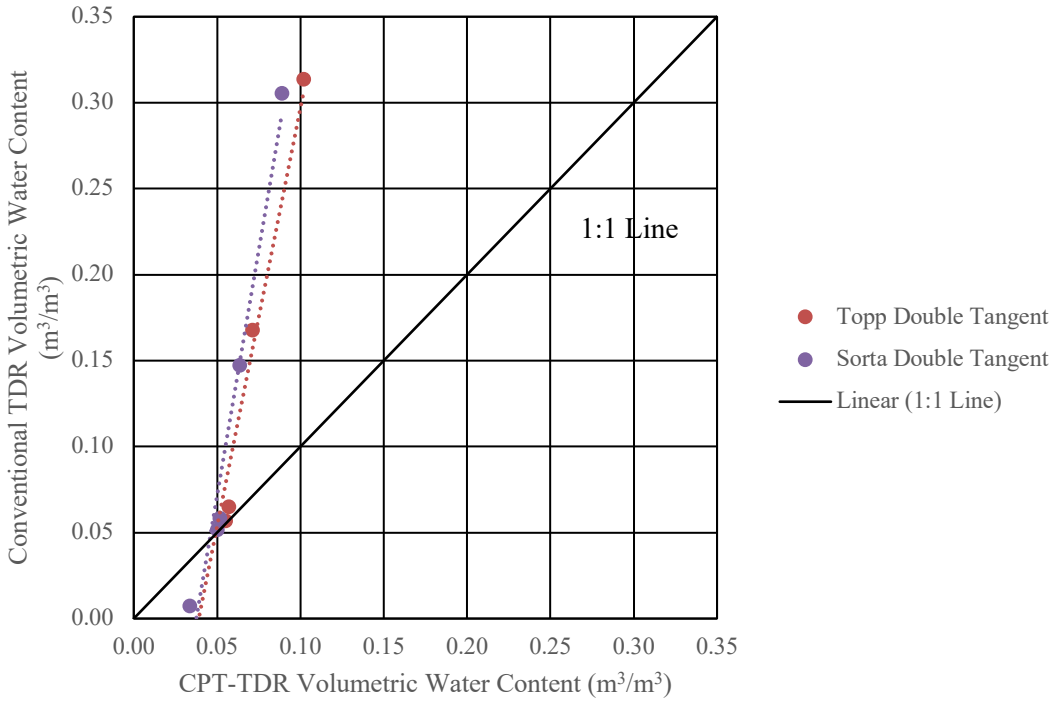

Figure 4.3: Plot of volumetric water content estimation between conventional TDR and CPT-TDR.

4.2 Laboratory Testing

Preliminary testing undertaken as part of this study as well as the results from Amos (2014) indicate the need to calibrate the CPT-TDR. As noted previously, this is assumed to be due to alteration of the electrical field as a result of the polymer shaft containing the TDR waveguides. The presence of the insulation, which takes the place of soil that might be present around the rods in the case of a conventional TDR installation, is assumed to cause a change in the sensitivity of the reading but with the same proportionality between apparent (measured) dielectric properties and the actual soil dielectric properties. If that is the case then calibration of the CPT-TDR in one soil (e.g. sand) could be applicable to a range of materials. This hypothesis will be tested for the FFT test results presented later.

4.2.1 Impact of Water Content and Fluid Electrical Conductivity on Waveform

The CPT-TDR was tested in sand/water mixtures with salinity levels of up to 30 g/L. The CPT-TDR measurements for the mixtures are presented in Table 4.1. Included in Table 4.1 is the electrical conductivity of the mixtures as measured using a Decagon ProCheck sensor read-out. Overall the waveforms are well defined. However, at high water contents and/or elevated pore-fluid salinity the waveforms become less well defined as shown in Figure 4.2. The X_2 point becomes difficult to find using the double tangent method with a less defined upslope; however, in some of these cases the single tangent method may still be used.

Determination of the X_2 point becomes impossible at elevated salinity levels and water contents for both methods. When the waveform was poorly defined the apparent length was calculated using only the single tangent method. If the waveform was very poorly defined then no apparent length could be obtained and the data was left as a dash in Table 4.1. Figure 4.4 is a graph that represents the operating conditions of the CPT-TDR in sand with elevated salinity pore water. The green data points indicated conditions for which the waveforms collected from the CPT-TDR were well defined. The regions of red data points have poorly defined waveforms.

Contours of bulk electrical conductivity for the sand/water mixtures were overlaid on the graph as calculated using Archie's equation:

$$\sigma = \frac{1}{a}\phi^m s^n \sigma_w \tag{4-1}$$

where σ is bulk conductivity (S/m), σ_w is the conductivity of the pore water (S/m). The remaining units are dimensionless: a is tortuosity, ϕ is porosity, m is cementation, s is degree of

saturation, and *n* is the saturation exponent. The values used to calculate σ were chosen to represent similar materials as reported by Reynolds (2011), Cardoso (2016) and Ransom (2017). The chosen tortuosity value is 2 and is kept constant for all calculations. The saturation exponent is kept as 2 and cementation is kept at 1.3 for unconsolidated, un-cemented sand. Pore water electrical conductivity values are based on the salinity levels of the pore water. Porosity is chosen from the average calculated porosity of the tested sand which is 0.33. The degree of saturation is calculated from the water content and porosity.

The EC contours in Figure 4.4 highlight how the combination of pore-fluid salinity (σ_w) and volumetric water content (s) increase the electrical conductivity. This graph might be able to be used to evaluate the feasibility of obtaining reliable wave forms for a given range of salinity (or electrical conductivity) and volumetric water content. For testing in the ranges of water content and salinity in the 'Good Operation' area of green points the CPT-TDR should produce good waveforms. Testing in the ranges of 'Poor Operation' the CPT-TDR would produce poor waveforms. If a CPT-TDR user knows a range of water content and pore water salinity levels to best tested, than the bulk EC could be estimated from the EC contours. From that the user would know if the CPT-TDR would be able to operate (produce readable waveforms) for those specific conditions.

Table 4.1: Volumetric water content and electrical conductivity values for the sand mixtures. Mixture identifications numbers followed by –Sat are saturated and –Dry are air-dried. Dashes represent no reading due to an undefined waveform and/or method to determine the X_2 point.

Mixture Identification	Pore Water Salinity (g/L)	Bulk Electrical Conductivity (dS/m)	θ_v Bulk (m^3/m^3)	θ_v Topp Single Tangent (m^3/m^3)	θ_v Sorta Single Tangent (m^3/m^3)	θ_v Topp Double Tangent (m^3/m^3)	θ_v Sorta Double Tangent (m^3/m^3)
1	0.00	0.17	0.28	0.22	0.20	0.16	0.14
2	5.00	0.26	0.14	0.08	0.07	0.06	0.05
3	10.00	0.22	0.13	0.15	0.13	0.15	0.13
4	15.00	0.25	0.14	0.17	0.15	0.13	0.11
5	20.00	0.38	0.14	0.14	0.12	0.08	0.07

6	25.00	1.07	0.14	0.08	0.07	0.07	0.06
7	30.00	1.09	0.15	0.18	0.16	-	-
1-Sat	0.00	0.01	0.31	0.25	0.23	0.19	0.17
2-Sat	5.00	2.35	0.34	0.26	0.24	0.24	0.22
3-Sat	10.00	4.29	0.38	0.29	0.28	-	-
4-Sat	15.00	4.85	0.33	-	-	-	-
1-Dry	10.00	0.04	0.07	0.05	0.04	0.04	0.04
2-Dry	15.00	0.02	0.04	0.03	0.03	-	-

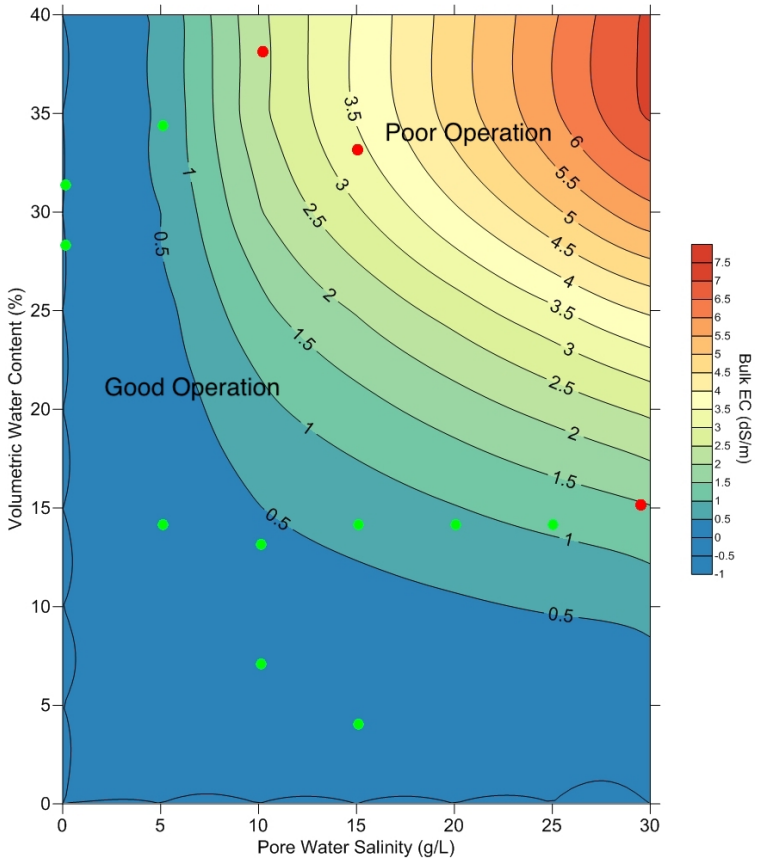

Figure 4.4: Graph defining the operational range of the CPT-TDR over increasing water content and salinity. Regions of green data points represent where waveforms are well defined. Regions of red data points represent where waveforms are poorly defined. Each point corresponds to specific values of volumetric water content (Y-axis), pore water salinity and electrical conductivity (X-axis) and bulk electrical conductivity (background contours).

With the increase in electrical conductivity the return portion of the waveform at the X_2 point becomes flatter and less well defined as shown in Figure 4.5. As long as the X_2 point can be defined then the apparent length may be found and the volumetric water content calculated.

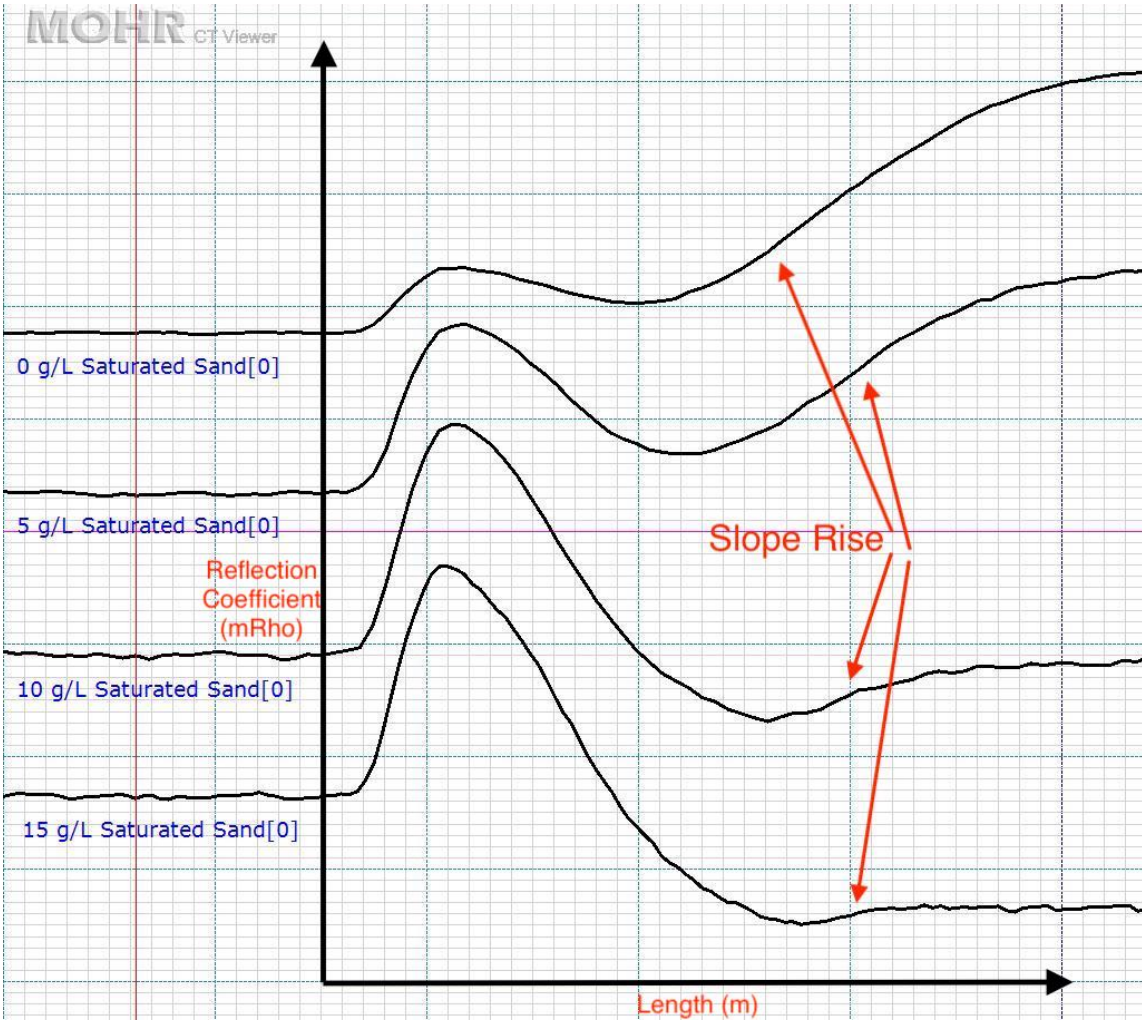

Figure 4.5: Example of selected waveforms used to create Figure 4.4. Waveforms for 0 g/L and 5 g/L saturated sand are considered well defined and readable. Waveforms for 10 g/L and 15 g/L saturated are not considered readable due to attenuation (little or no rise in slope for X_2 determination). The X-axis scale is 0.274 m/major gridline division.

It was only at the highest tested water contents and salinity values that the waveforms become uninterpretable. For example, this occurred at full water saturation and pore-water salinity levels

approaching 10 g/L. At less than saturated conditions it was only extreme levels of salinity of 30 g/L that cause undefined waveforms. The salinity levels for oil sands tailings process water might be as high as 3 g/L (Levesque 2014). Ultimately if a CPT-TDR user is concerned about the operation in elevated electrically conductivity soils than the chart in Figure 4.4 would be useful to determine the usability of the CPT-TDR. From the chart the operational range of the CPT-TDR is in electrically conductive conditions of up to 1.5 dS/m.

4.2.2 Presentation of Laboratory Calibration Data

The test results from laboratory testing of sand as outlined in Section 3.2 are presented in Figure 4.6. This includes data from this authors tests results along with data from Amos (presented only for double tangent analysis as square symbols). The CPT-TDR may be calibrated by fitting trend lines through a plot of the CPT-TDR volumetric water content versus the actual volumetric water content. This calibration should be applicable to other materials since equations 2-2 and 2-3 are independent of soil material (Topp 1980). The data series also covers a broad range of volumetric water content, up to saturation.

Data series are plotted in Figure 4.6 using the Topp and Sorta (Equations 2-2 and 2-3) equations. The dielectric constants used for each equation were those obtained using the single tangent and double tangent methods as described in Section 3.4. The two different equations with two different methods of waveform analysis yields four data series in Figure 4.6. Trend line parameters are found in Table 4.2. The R-squared and root mean square error (RMSE) values quantify how close the data is to a fitted regression line (Mann 2010) (Anderson and Woessner 1992). Root mean square error is the average of the squared difference in measured and actual values (Anderson and Woessner 1992).

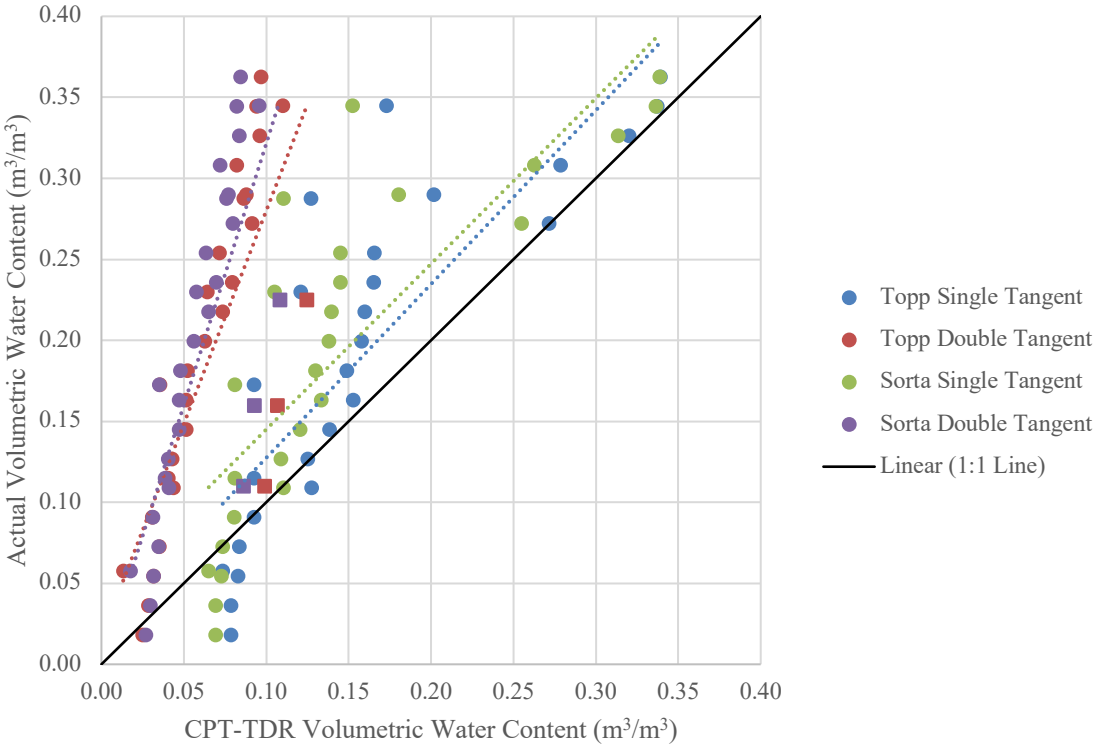

Figure 4.6: Plot of the CPT-TDR volumetric water content calculations and the actual volumetric water content calculations from laboratory testing. The CPT-TDR underestimates the volumetric water content.

Table 4.2: Trend line parameters from Figure 4.6.

Trend Line	Slope	Y-Intercept	R^2	RMSE
Topp Single Tangent	1.07	0.02	0.70	0.07
Topp Double Tangent	2.63	0.02	0.61	0.15
Sorta Single Tangent	1.02	0.04	0.67	0.08
Sorta Double Tangent	3.23	0.00	0.60	0.15

The double tangent method results appear to provide a more precise relationship (i.e. less scatter and with the lowest R-squared values) as compared to the single tangent method. Interestingly; however, the double tangent method also shows less sensitivity to changes in volumetric water content. The single tangent interpretation is more variable but appears to track more closely with the actual volumetric water contents. This may be observed upon visual examination and from the slope/Y-intercept values of each trend line. In each case, it is possible to develop a calibration curve based on the data in Figure 4.6 and Table 4.2. This type of calibration would likely only be applicable over a similar range of water content.

It is important to note that the R-squared values for the double tangent method are actually lower when compared with the single tangent method. It is clear upon visual examination that the data is more linear and closer to the trend lines. However, when the six data points from Amos are included (e.g. square symbols) in Figure 4.6 the R-squared values are lowered for the double tangent method. The RMSE values for the double tangent methods are higher when compared to the single tangent methods. The calibration should bring the CPT-TDR volumetric water content values closer to the actual volumetric water content values and therefore decrease the RMSE values for both the double and single tangent methods.

The greater scatter of the Single Tangent results may be due to difficulty in selecting the X_2 point as well as the reliance on this single point in the calculation. The return portion of the waveform where the X_2 point is found is not well defined on all waveforms. Since the single tangent method only depends on this portion of the waveform this may result in inconsistencies in the selection of the X_2 point. For example, in Figure 4.7 the top waveform labelled 1[0] has a fairly consistent upward slope when compared to the bottom waveform labelled 20[0]. This waveform has an upward slope that is changing throughout the portion of the curve where the X_2 point is selected. Therefore the X_2 point location is inconsistent on these waveforms and thus the volumetric water content values are somewhat unreliable. Somewhat surprisingly, the trend line slope values of near 1.0 (Figure 4.6) highlight that the loss of sensitivity as a result of the polymer insulation does not appear to affect the volumetric water content readings using this method of interpretation. The Single tangent method of analysis plots closer to the actual volumetric water content with a tradeoff of lower precision when compared to the double tangent method of analysis.

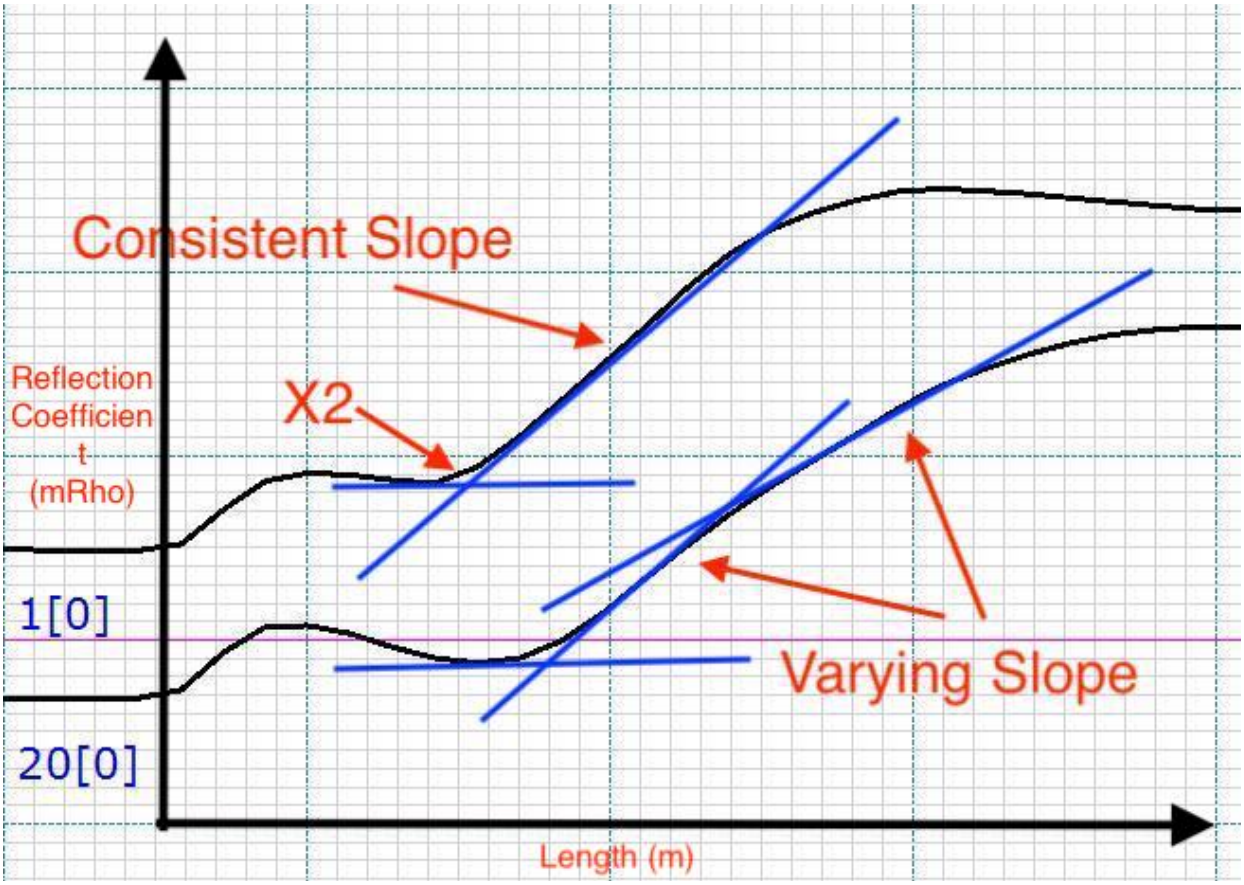

Figure 4.7: Selection of waveforms analyzed to calculate CPT-TDR volumetric water content values in Figure 4.6. Waveform labelled 1[0] corresponds to an actual measured volumetric water content of 0.02 m^3/m^3 and waveform labelled 20[0] corresponds to an actual measured volumetric water content of 0.36 m^3/m^3. The slopes of the two waveforms differ which is cause for inconsistent in single tangent waveform analysis. On waveform labelled 1[0] there is only one tangent line on the upward slope since the slope is constant. One the waveform labelled 20[0] there is multiple tangent lines on the upward slope since the slope is changing. Therefore, there is inconsistent X_2 values. The X-axis scale is 0.319 m/major gridline division.

4.2.3 Presentation of FFT Results

Waveforms collected from the CPT-TDR in FFT are presented in Figure 4.8. These waveforms are not as well defined when compared to those collected from non-elevated salinity sand (due to a smaller return slope as in Figure 4.5). However, the X_2 point could be extracted from all the waveforms. The challenge in this stage of testing was the ability to dewater the FFT as drainage becomes restricted by the buildup of solids. The restricted drainage made it difficult to obtain a wide range in volumetric water contents for testing. Manual mixing of the material between

drainage cycles helped with drainage of the material. It should be noted that even though the material was dewatered, it still remained saturated.

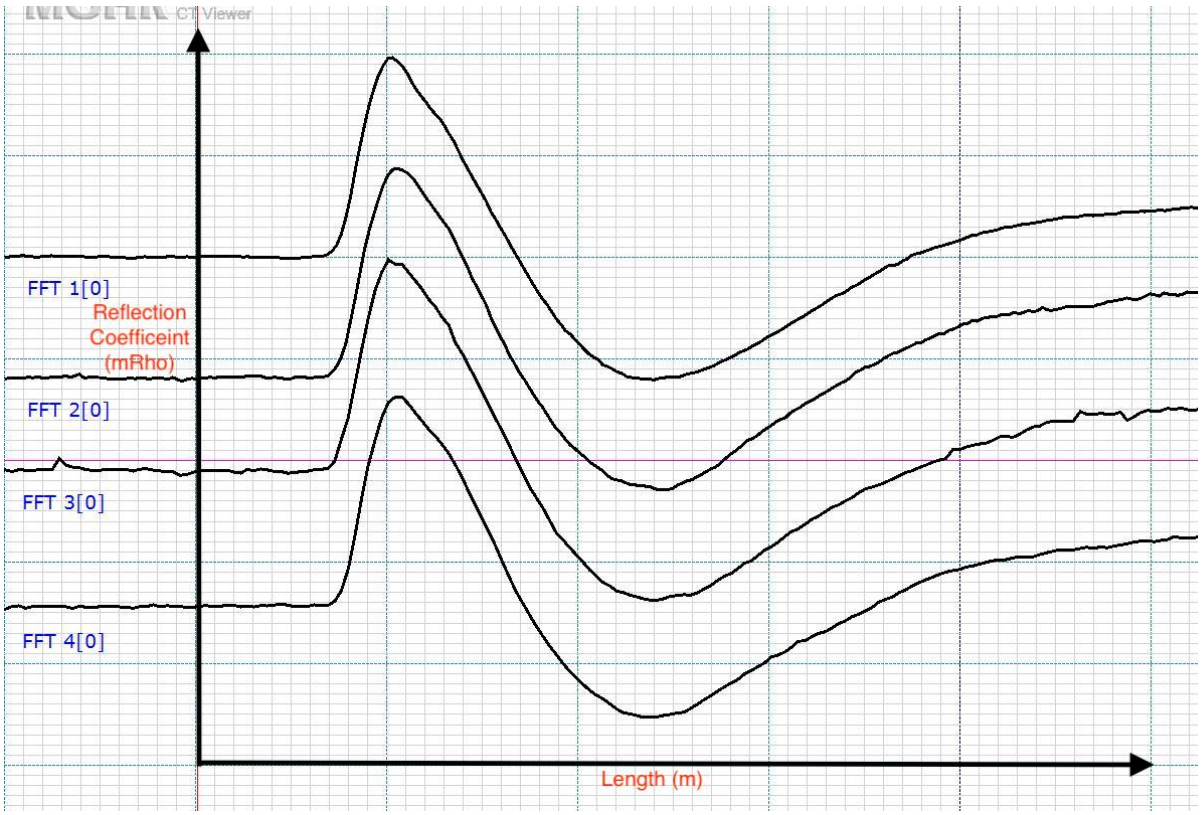

Figure 4.8: Waveforms for FFT collected from the CPT-TDR. The X-axis scale is 0.332 m/major gridline division.

Results from the volumetric water content readings from the samples and CPT-TDR are plotted in Figure 4.9 with the trend line parameters in Table 4.3. A total of four drainage cycles were completed with CPT-TDR readings and sample for each cycle. The CPT-TDR volumetric water content readings are calculated using only the Sorta single and double tangent methods. The Topp equation is not used since it is not applicable beyond volumetric water contents of 0.45 m^3/m^3.

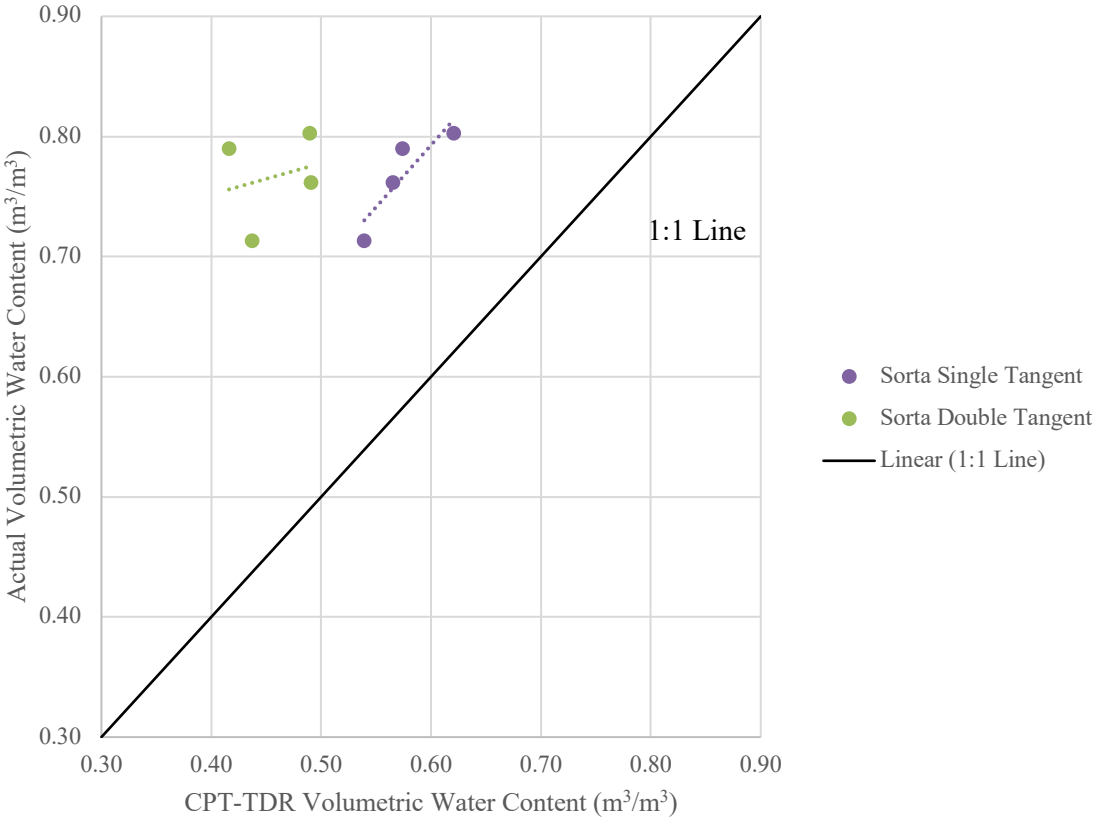

Figure 4.9: Plot of the CPT-TDR volumetric water content calculations and the actual volumetric water content calculations for FFT.

Table 4.3: Trend line parameters from Figure 4.9.

Trend Line	Slope	Y-Intercept	R^2	RMSE
Sorta Single Tangent	1.03	0.18	0.79	0.19
Sorta Double Tangent	0.26	0.65	0.06	0.31

The CPT-TDR readings for volumetric water content underestimate the actual volumetric water content calculated from the sample gravimetric water content. The Sorta single tangent method trend line has a slope of nearly 1.00 however a high Y-intercept value of 0.18. In this case for the FFT the single tangent method is more accurate and has a better fit of the data as revealed by the much higher R-squared value. However, to draw solid conclusions on this more data would be needed. The calibration equations that were developed for sand do not improve the FFT results. A

custom calibration would be required for FFT. To achieve this a broad range of water content is required.

Pore fluid was collected and analyzed for aqueous chemistry with the results in Table 4.4. Electrical conductivity of the pore fluid was measured and found to be 7.30 dS/m. The dominant ions from Table 4.4 are Sodium and Chloride indicating a high level of Sodium Chloride salt in FFT.

Table 4.4: Collected FFT pore fluid aqueous chemistry.

Ion	Concentration (mg/L)
Na^+	2222.24
K^+	44.79
Ca^+	3.78
Mg^+	24.46
S^+	92.14
Cl^-	1319.39
F^-	10.76
HCO_3^-	1.87
SO_4^-	-
PO_4^-	25.50
NO_3^-	166.49

A chart of volumetric water content and electrical conductivity, similar to Figure 4.4 is presented in Figure 4.10. This chart was created in a similar way to the chart in Figure 4.4 for the sand data. The background contours represented electrical conductivity values from Archie's law, Equation 4-1. Input values that were changed in this were the tortuosity, a is 2 and the porosity ϕ, is 0.75. Pore water electrical conductivity and saturation values increased much the same as the sand data. Pore water electrical conductivity is represented by the X-axis in this case rather than salinity for sand.

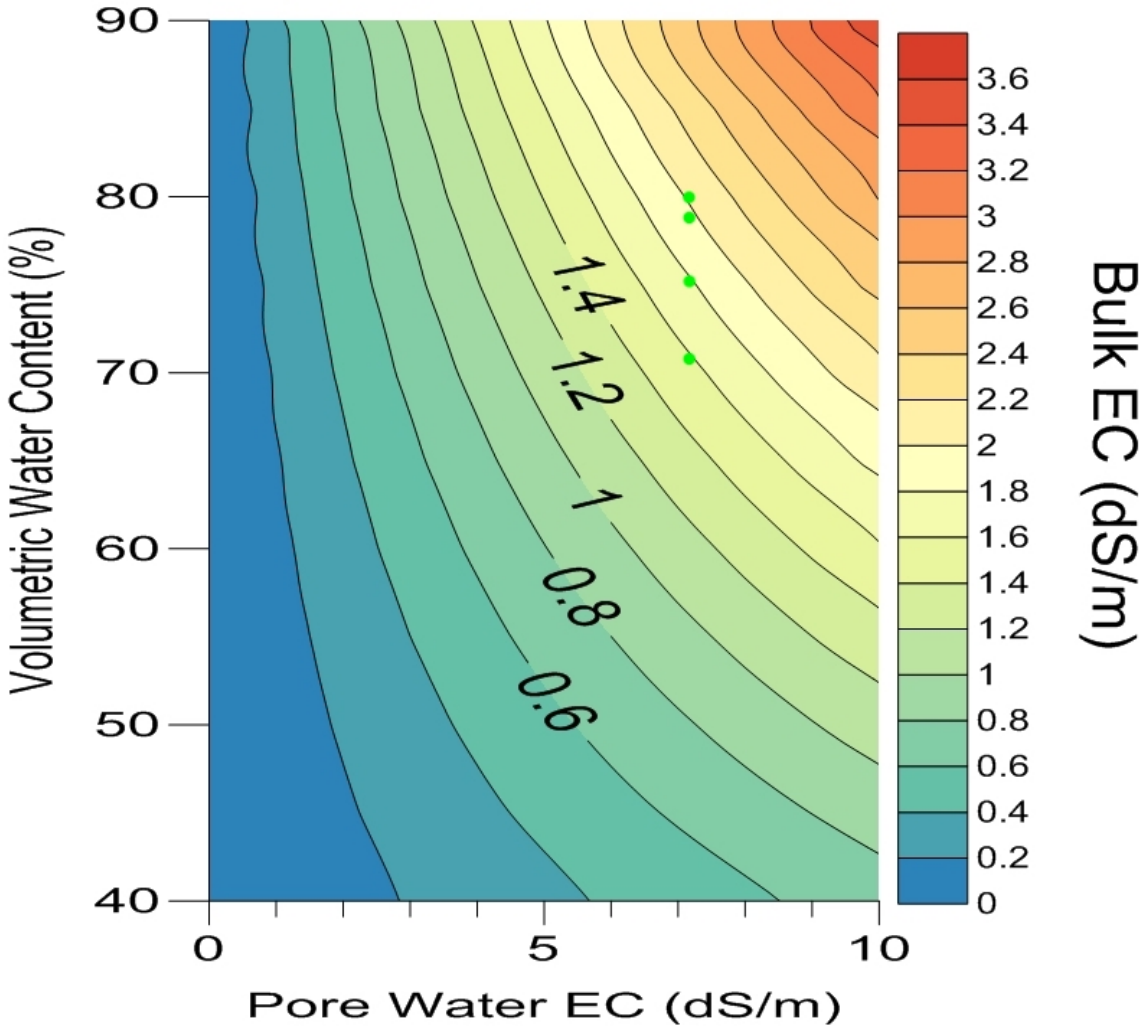

Figure 4.10: Graph defining the operational range of the CPT-TDR over increasing water content and pore water electrical conductivity. Regions of green data points represent where waveforms are well defined.

Bulk electrical conductivity of the FFT was found to be 2.76 dS/m. There is no region of poorly defined waveforms in Figure 4.10 due to limited data. The three data points in Figure 4.10 correspond to specific volumetric water content and pore water electrical conductivity values. These data points plot between bulk electrical conductivity values of 1.5 – 2.0 dS/m. These values are below the measured bulk electrical conductivity of 2.76 dS/m. More data would better define the region of usability for FFT.

4.3 Presentation of Field Data

Field-testing of the CPT-TDR was undertaken during field programs in 2015 and 2016. Both trials follow the methods outlined in sections 3.3 and 3.4. The results and analysis of the field-testing are presented in the following sections.

The tailings dyke where testing took place consisted of tailings sand with less than 30 to 50 cm of fine textured cover soil. This difference in soil texture (within the cover relative to tailings sand) can often result in elevated water contents within this upper layer.

Physical samples of the tailings sand collected close to the water table, or below the water table, are also expected to be subject to errors in measured water content as a result of sample disturbance in loose sand tailings that are close to saturation. It is important to note that the sampling method used in 2015 (piston sampler) is likely less affected by sample disturbance that the drive/sonic sampler used in the 2016 field program. The piston sampler collects clean samples in plastic tubes and although there is potential for densification of the sand as the device is driven into the ground the sample is less subject to vibration. The sonic sampling used in 2016 results in excessive vibration and potential densification of the samples, which when saturated, can result in the accumulation of free water or drainage of the samples as they are removed. Only the gravimetric water contents of the samples were measured in 2016 and consequently the dry density required to calculate volumetric water content had to be estimated for all samples. The dry density value used was the average dry density from the 2015 samples (1750 kg/m^3).

Waveform analysis in 2015 was done using both the single and double tangent methods as the equipment being used had the ability to save waveforms. Due to limitations in 2016 the equipment used did not have the ability to save waveforms and only the single tangent analysis was used. In addition, because the wave form could not be saved digitally, the selection of the X2 point had to be made directly from the oscilloscope in the field.

Both 2015 and 2016 have electrical resistivity included in each depth plot. This provides an indication of the amount of water present however it is also affected by the electrical conductivity of the pore water and the soil minerals. The lowest resistivity values represent the highest electrical conductivity values. By examining the data, the lowest resistivity reading is 4.0 Ohm-m which becomes 2.5 dS/m in electrical conductivity. This value falls into the well-defined region of usability in Figure 4.4. All waveforms from field testing appeared well defined.

4.3.1 2015 Field Testing Results

The 2015 CPT-TDR results from locations, BH-LB07, BH-LB08 and BH-LB09 are plotted with depth in Figures 4.11, 4.13 and 4.15 respectively. Also included in these plots are the volumetric water content calculated for these samples based on the assumed constant dry density value. The plots also present electrical resistivity and the estimated depth of the water table based on pore pressure dissipation tests. Missing CPT-TDR readings over specific intervals are from poorly defined waveforms. This was likely due to damage to the waveguides induced by the extreme forces in the initial field-testing. All CPT-TDR volumetric water content readings have been created using both the single and double tangent methods of analysis and the Topp and Sorta equations. Both methods are shown in all profiles for a total of four CPT-TDR profiles. All data presented is uncalibrated.

For each test location, a plot of the volumetric water content calculated from the samples versus the CPT-TDR volumetric water content is included. These plots are in Figures 4.12, 4.14 and 4.16 respectively. Trend line parameters for each plot are included in Tables 4.5, 4.6 and 4.7 respectively. For these plots only data 0.5 meters above the water table is considered because of potential disturbance of sampling near and below the water table.

Trend line parameters from Figure 4.12 provide a poor fit and poor estimation of volumetric water content no matter which method is used. Visual examination of the plot reveals a high degree of scatter in the data as represented by low R-squared values. Due to damage of the wave guides on the CPT-TDR at the BH-LB07 location, the results are difficult to compare to the physical sample results. However, the overall volumetric water content trend with depth in Figure 4.11 appears to be reasonably consistent for both CPT-TDR and physical samples with the water content increasing from expected ‘field capacity’ values near surface to near saturation values just above the water table. Errors in waveform interpretation due to shaft failure may be the cause for low single tangent volumetric water content readings at depths below 2.00 meters.

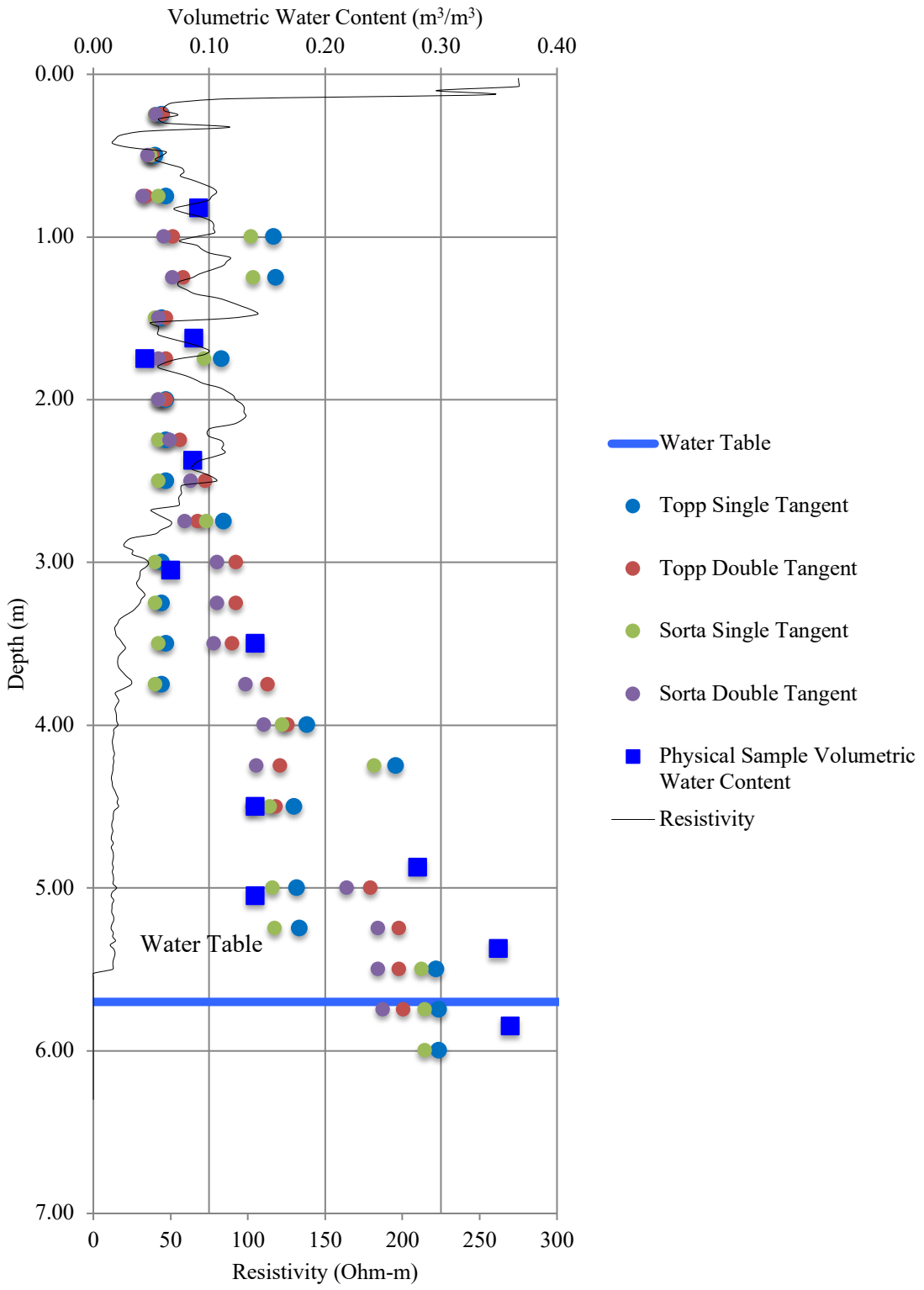

Figure 4.11: Plot of CPT-TDR, physical sample and electrical resistivity results with depth from BH-LB07.

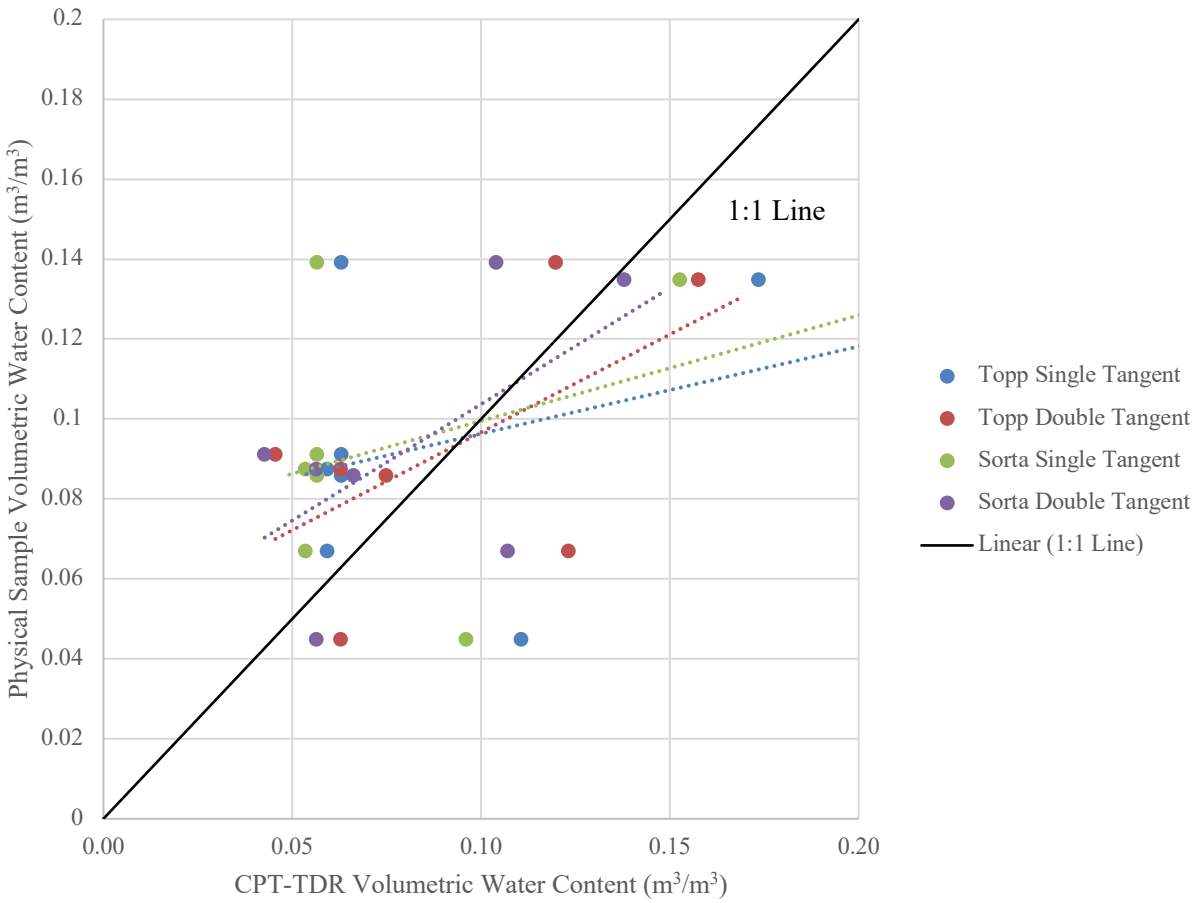

Figure 4.12: Plot of the physical sample volumetric water content versus the CPT-TDR volumetric water content from location BH-LB07.

Table 4.5: Trend line parameters from Figure 4.12.

Trend Line	Slope	Y-Intercept	R^2	RMSE
Topp Single Tangent	0.22	0.08	0.08	0.06
Topp Double Tangent	0.49	0.05	0.35	0.03
Sorta Single Tangent	0.26	0.07	0.08	0.06
Sorta Double Tangent	0.58	0.05	0.36	0.04

Trend line parameters in Table 4.6 from Figure 4.14 provide a poor fit and poor estimation of volumetric water content no matter which method is used. Visual examination of the plot reveals high scatter of the data which is represented with the low R-squared values. It was known that at location BH-LB08 the wave guides had been damaged. The results are difficult to compare due to the damage. Waveform interpretation proved difficult and is revealed in the results with high scatter and no significant increase in volumetric water content reading at and near the water table as seen in Figure 4.13.

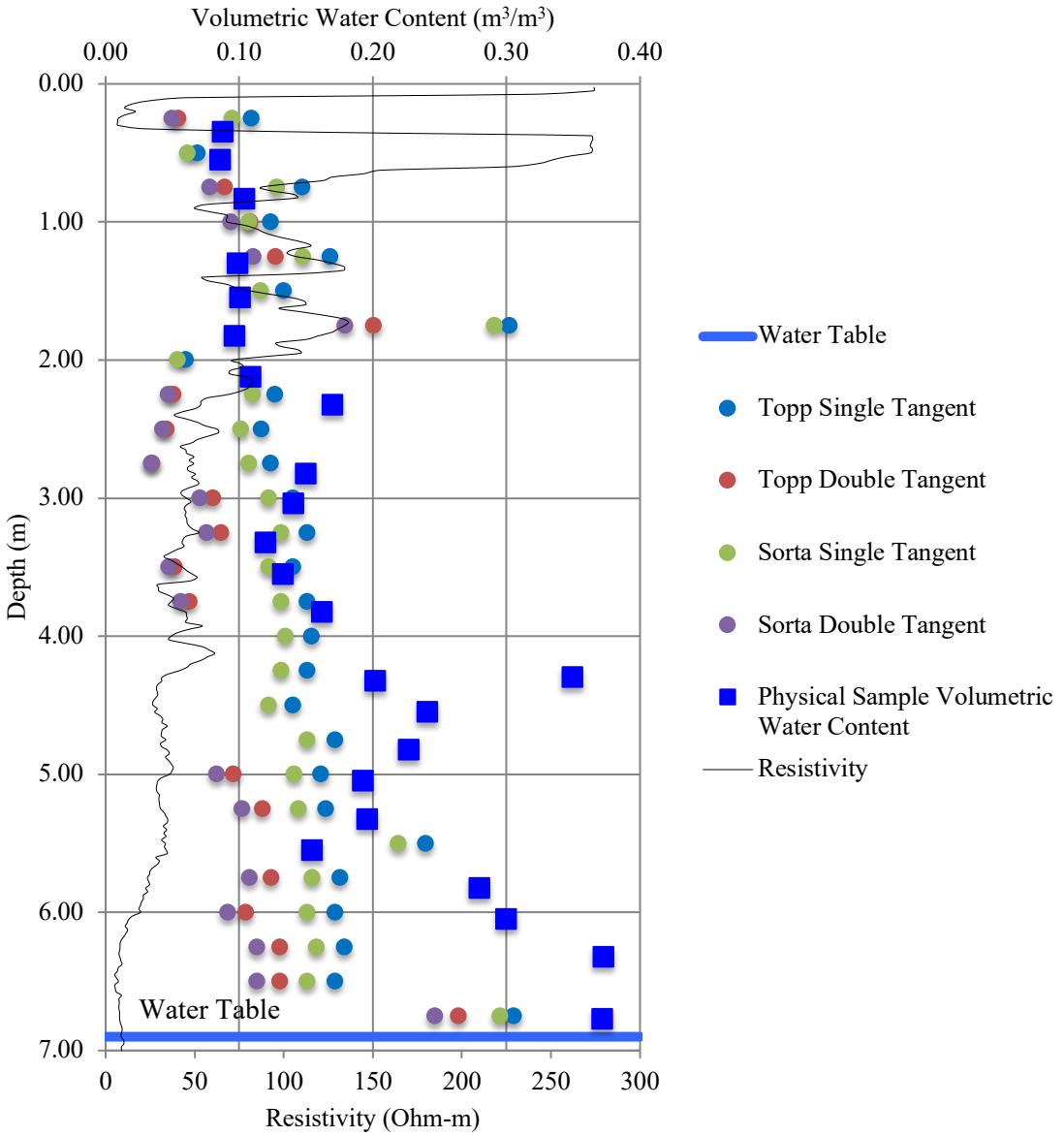

Figure 4.13 - Plot of CPT-TDR, physical sample and electrical resistivity results with depth from BH-LB08.

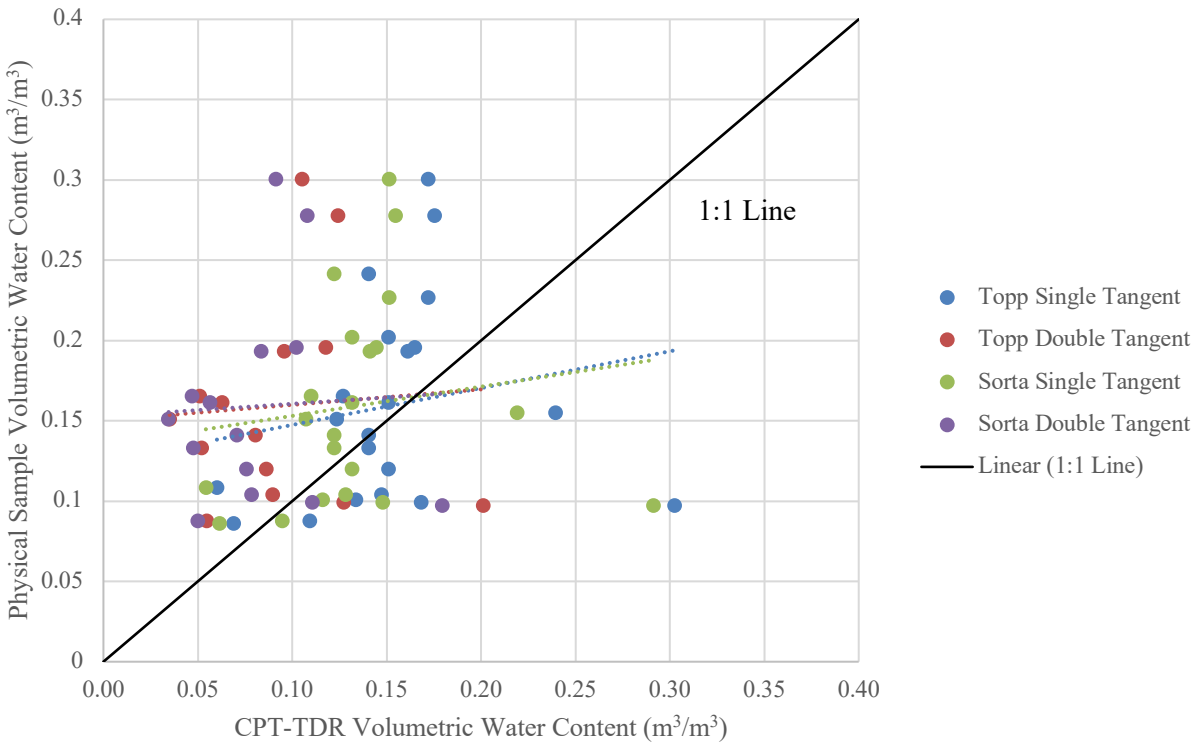

Figure 4.14 - Plot of the physical sample volumetric water content versus the CPT-TDR volumetric water content from location BH-LB08.

Table 4.6: Trend line parameters from Figure 4.14.

Trend Line	Slope	Y-Intercept	R^2	RMSE
Topp Single Tangent	0.23	0.13	0.03	0.07
Topp Double Tangent	0.10	0.15	0.01	0.10
Sorta Single Tangent	0.18	0.13	0.02	0.08
Sorta Double Tangent	0.08	0.15	0.00	0.11

There was no apparent damage to the wave guides during testing at location BH-LB09 and the results at this location appear to be much better than those obtained at other sites. Physical sample and CPT-TDR volumetric water content readings both follow similar trends and approach maximum values at and near the water table as seen in Figure 4.15. At depths below 3.50 m the resistivity values decrease where the volumetric water content values increase. Similar to the

laboratory testing in section 4.3, the single tangent method of analysis values are closer to the physical sample values. The trend line slopes for each method of analysis (Figure 4.16) are closer to the values from laboratory testing described in the earlier section when compared to the results from BH-LB07 and BH-LB08. Trend line parameters from Figure 4.16 resemble an improved fit for both single and double tangent methods. This is represented by the higher R-squared values in Table 4.7. Visual examination also reveals a better fit compared to BH-LB07 and BH-LB08.

This location is most representative of the 2015 portion of field testing since no physical damage occurred to the CPT-TDR device. Assuming that the physical samples are within a reasonable range of error, the results are very similar to the laboratory results. With that the CPT-TDR has performed as expected at this location, using the controlled laboratory results as an indicator of performance.

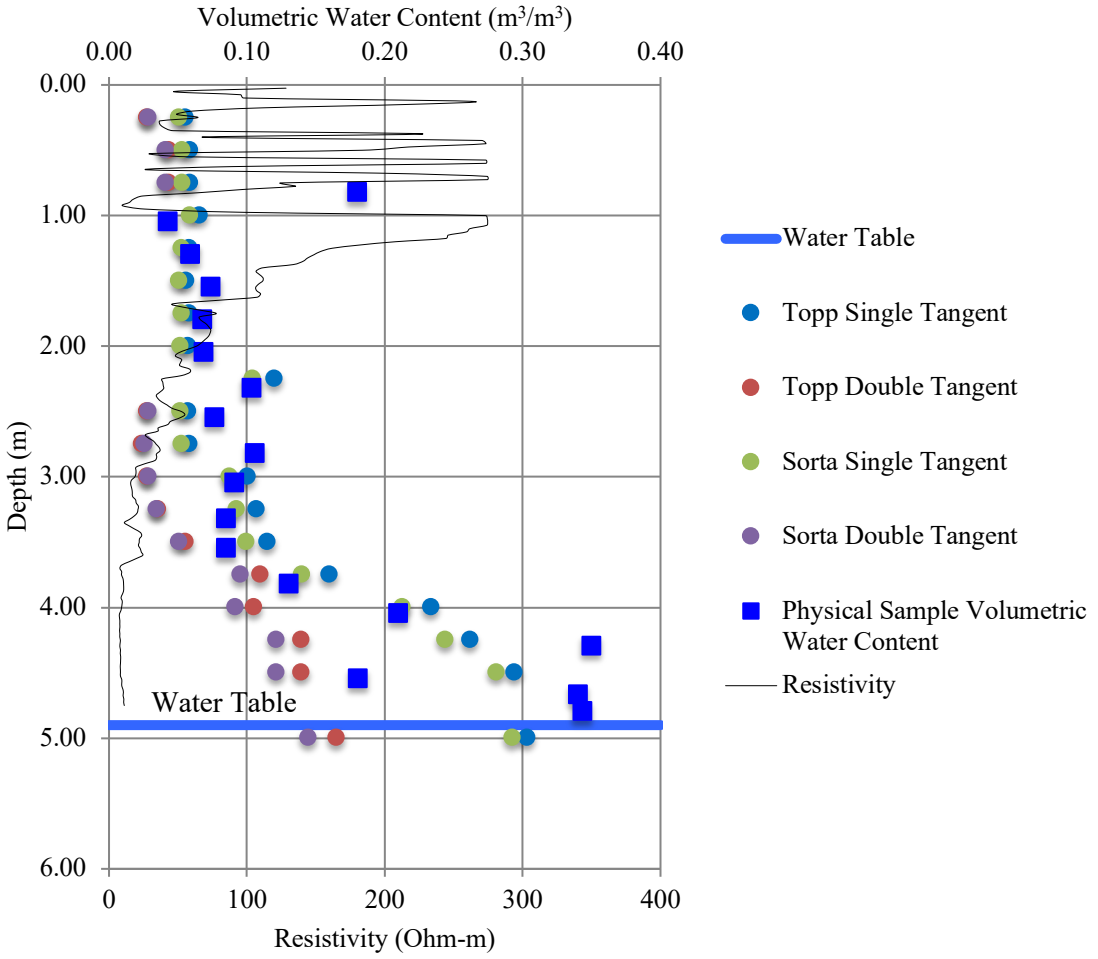

Figure 4.15 - Plot of CPT-TDR, physical sample and electrical resistivity results with depth from BH-LB09.

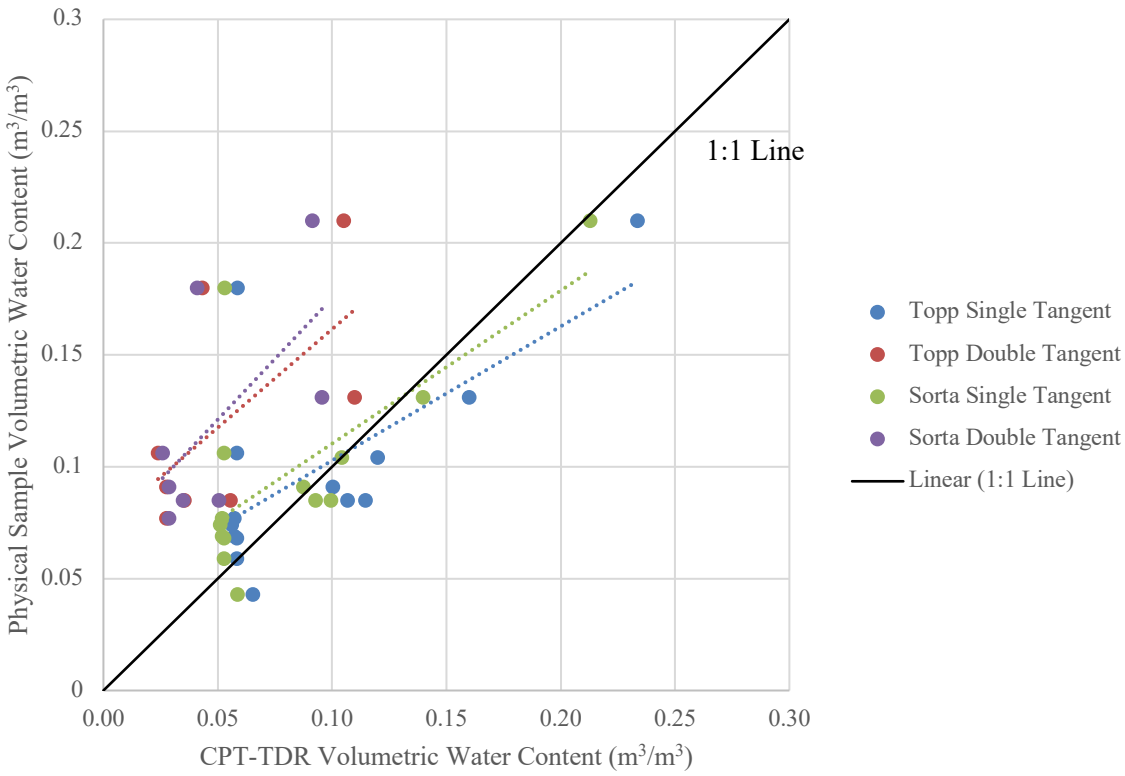

Figure 4.16 - Plot of the physical sample volumetric water content versus the CPT-TDR volumetric water content from location BH-LB09.

Table 4.7: Trend line parameters from Figure 4.16.

Trend Line	Slope	Y-Intercept	R^2	RMSE
Topp Single Tangent	0.60	0.04	0.45	0.04
Topp Double Tangent	0.88	0.07	0.39	0.07
Sorta Single Tangent	0.68	0.04	0.47	0.04
Sorta Double Tangent	1.09	0.07	0.38	0.07

4.3.2 2016 Field Testing Results

The 2016 CPT-TDR results from Locations, 1, 2, 4, 6 and 8 are plotted with depth in Figures 4.17, 4.19, 4.21, 4.23 and 4.25 respectively. Also included in these plots are the volumetric water content results calculated from the gravimetric water content of the soil samples and the assumed dry density of 1750 kg/m^3. The electrical resistivity and the depth of the water table are also shown on these figures. All CPT-TDR volumetric water content readings have been created using only the single tangent methods of analysis due to equipment limitations.

For each test location, a plot of the physical sample measured volumetric water content versus the CPT-TDR volumetric water content is included. The volumetric water content of the physical samples was based on a measured gravimetric water content and an assumed constant value of dry density. These plots are in Figures 4.18, 4.20, 4.22, 4.24 and 4.26 respectively. Similar to the 2015 results, these plots only consider data 0.5 meters above the water table because of potential disturbance of sampling near and below the water table. Trend line parameters for each plot are included in Tables 4.8, 4.9, 4.10, 4.11 and 4.12 respectively.

The test results from Location 1 for both physical samples and the CPT-TDR follow the same depth trend (Fig. 4.17). This is especially true when only results at depths above 6.00 m are considered since disturbance at and near the water table will affect the samples. At depths below 4.50 m the resistivity values drop where the volumetric water content values increase. Trend line slopes from Figure 4.17 are similar to those found during laboratory testing (Section 4.3) but with lower precision. The range of volumetric water content considered for Figure 4.18 is narrow. This is likely the cause for the negative Y-intercept values for each trend line in Table 4.8.

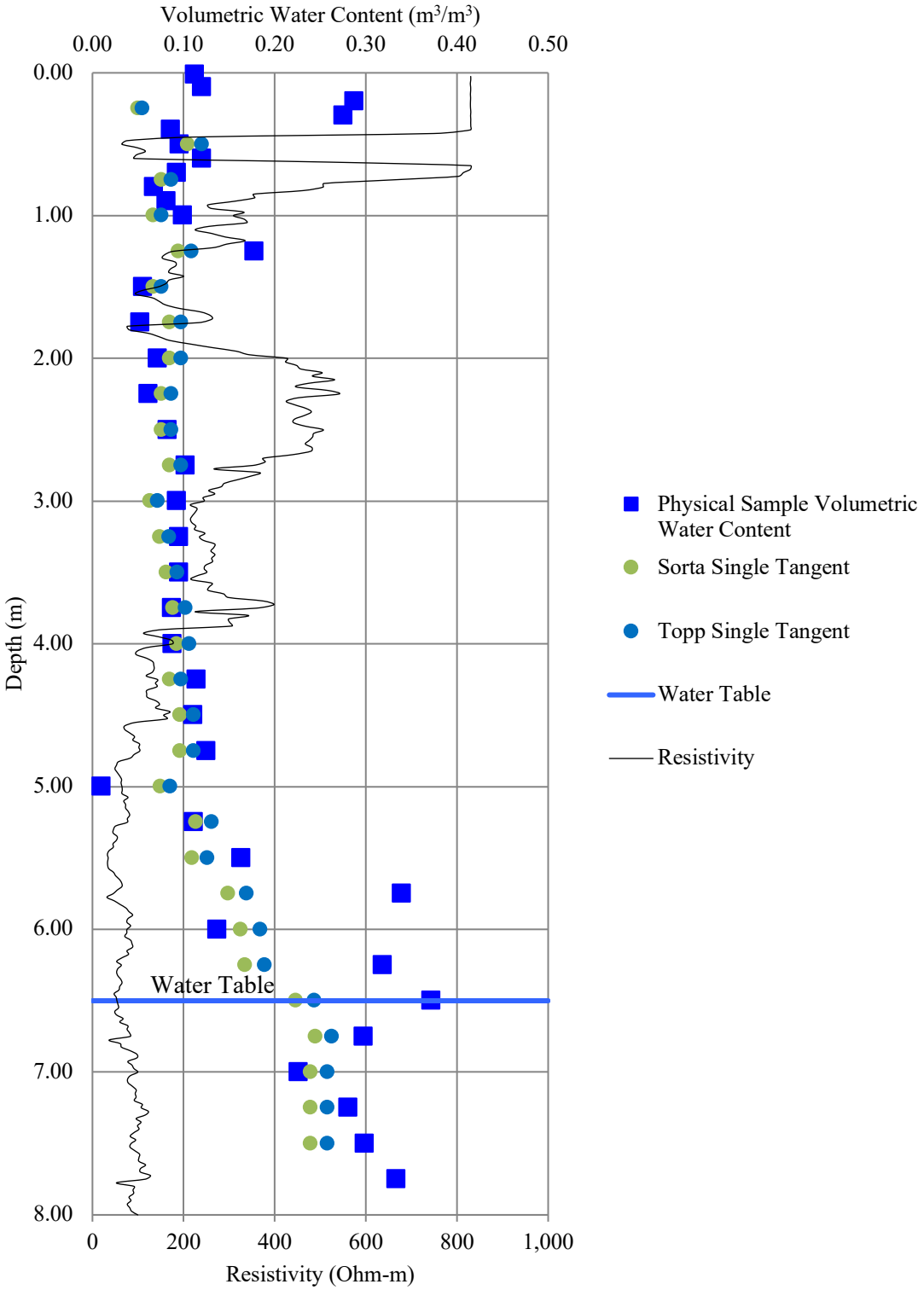

Figure 4.17: Plot of CPT-TDR, physical sample and electrical resistivity results with depth from Location 1.

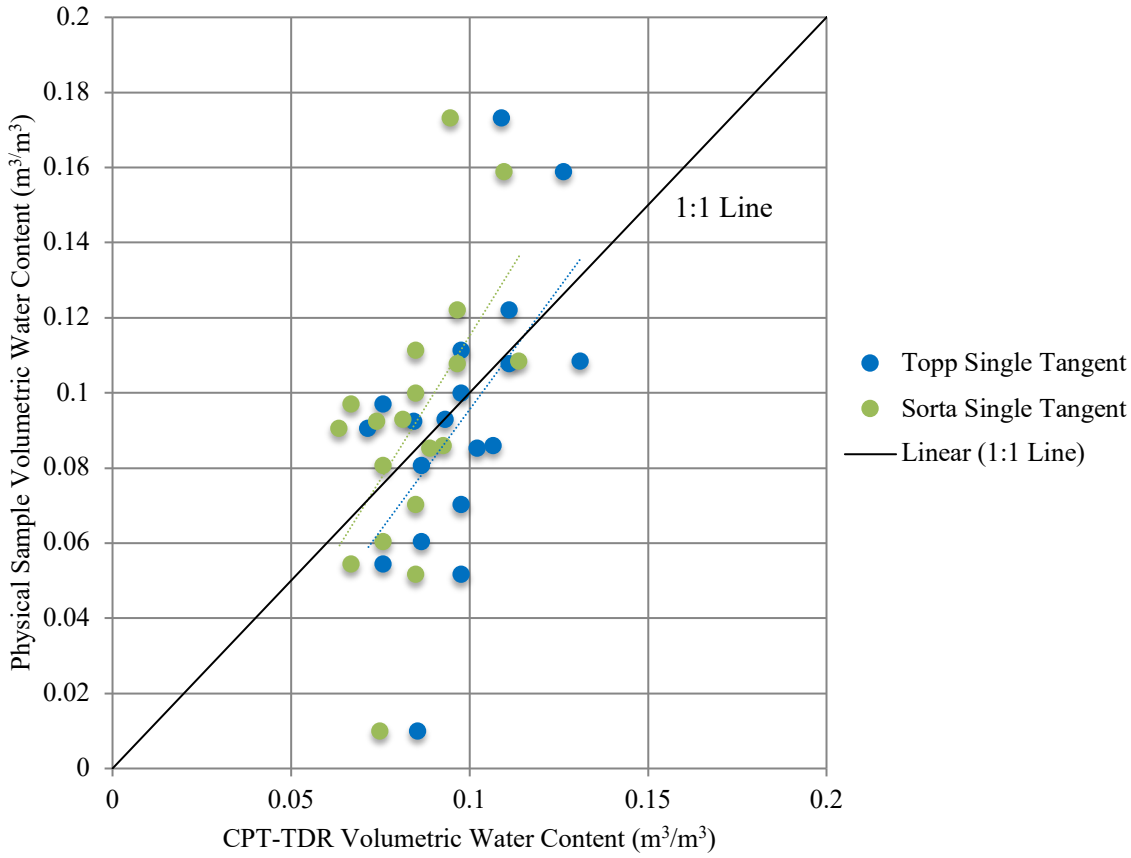

Figure 4.18: Plot of the physical sample volumetric water content versus the CPT-TDR volumetric water content from Location 1.

Table 4.8: Trend line parameters from Figure 4.18.

Trend Line	Slope	Y-Intercept	R^2	RMSE
Topp Single Tangent	1.53	-0.04	0.33	0.03
Sorta Single Tangent	1.29	-0.03	0.33	0.03

Results from both the physical samples and CPT-TDR are fairly consistent for Location 2 in Figure 4.19. However, samples become scattered at depths below 3.00 m. A sharp increase in water content just below 4.50 m is seen from the physical samples and the CPT-TDR. Resistivity also drops at this point. Slopes of the trend lines in Figure 4.20 are relatively high compared to

the results from other single tangent method of analysis. The fit of the data is improved as the R-squared values are higher in Table 4.7. Similar to Location 1, the narrow range of water content is likely the cause of the negative Y-intercept values.

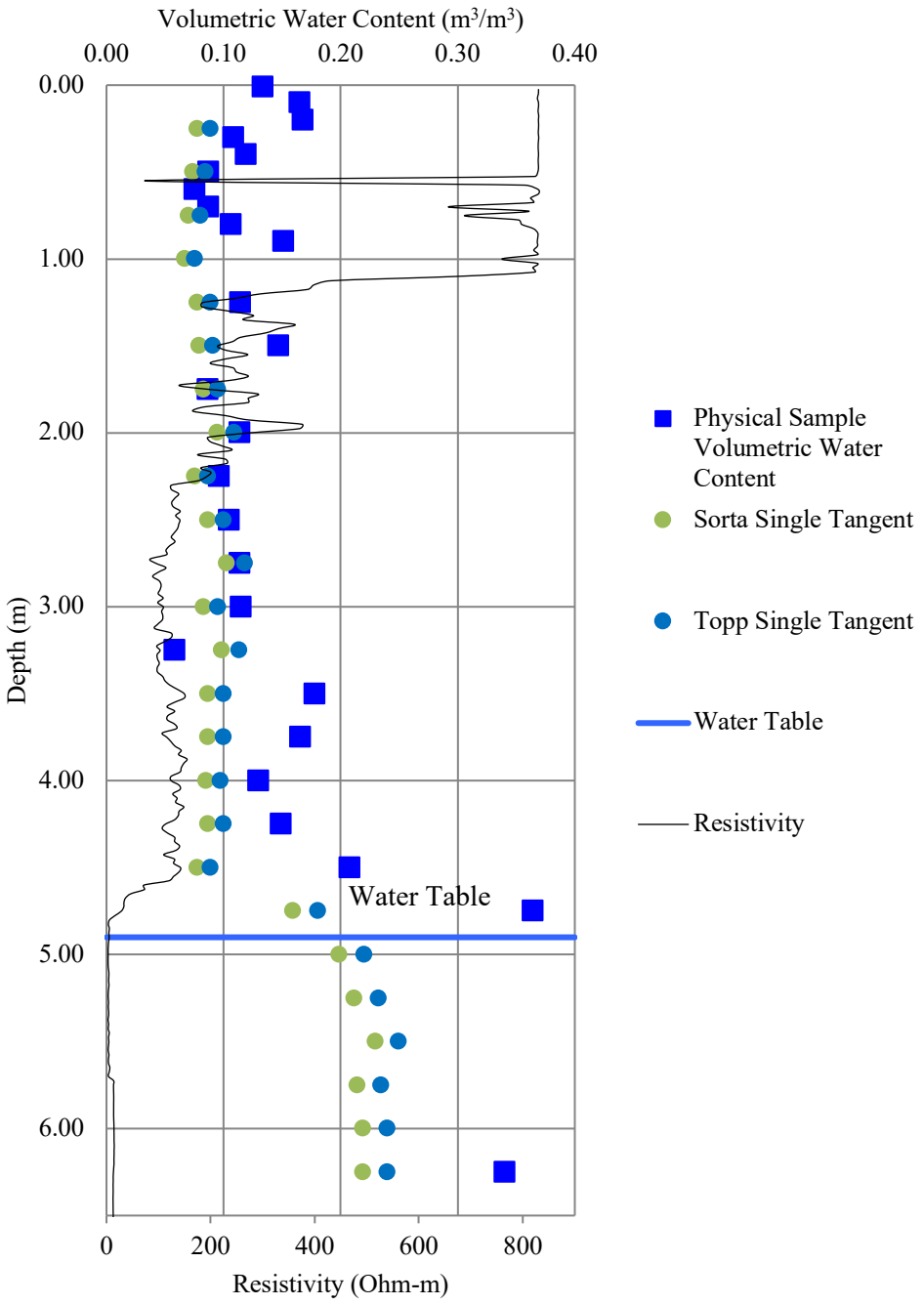

Figure 4.19: Plot of CPT-TDR, physical sample and electrical resistivity results with depth from Location 2.

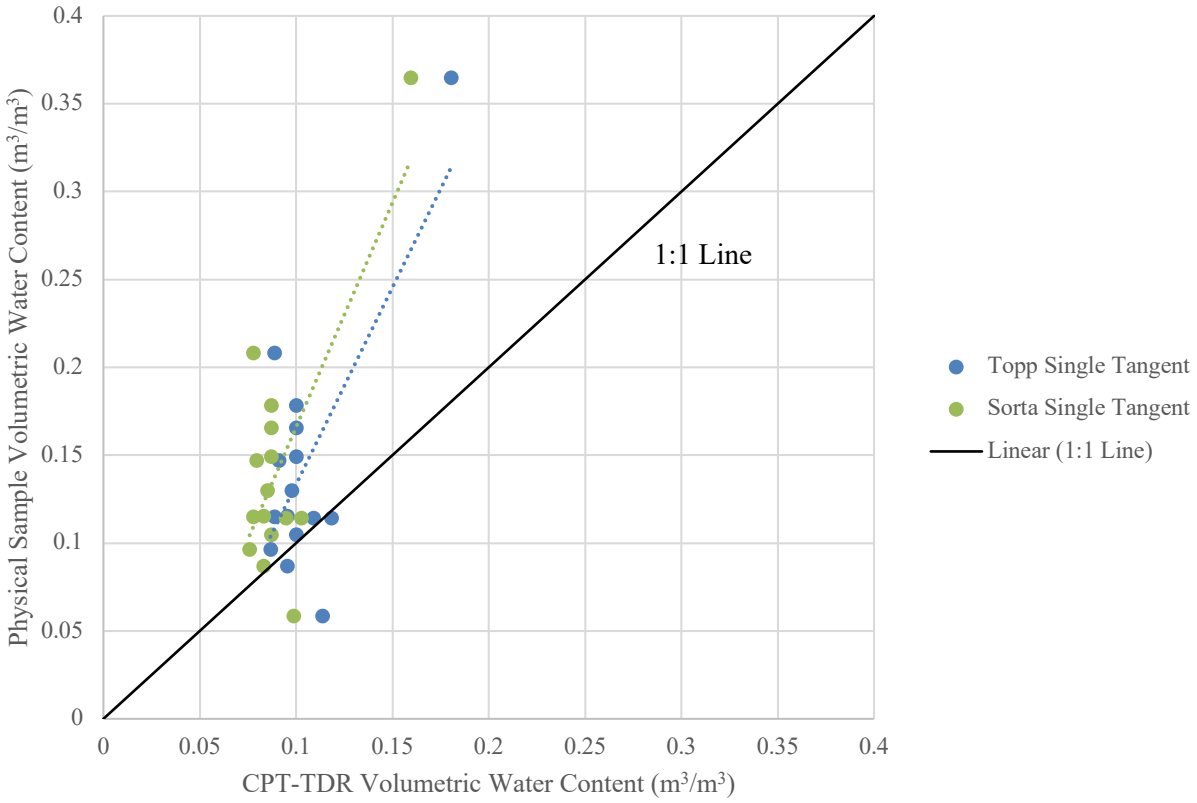

Figure 4.20: Plot of the physical sample volumetric water content versus the CPT-TDR volumetric water content from Location 2.

Table 4.9: Trend line parameters from Figure 4.20.

Trend Line	Slope	Y-Intercept	R^2	RMSE
Topp Single Tangent	2.24	-0.09	0.51	0.07
Sorta Single Tangent	2.55	-0.09	0.52	0.08

The physical sample volumetric water content results at Location 4 (Figure 4.21) are inconsistent throughout the profile. Therefore, the estimated depth of the water table may be used to indicate if the CPT-TDR is providing reasonable results at this location since near the water table is where the CPT-TDR calculated volumetric water content values reach the maximum values. Slopes of the trend lines in Figure 4.22 appear similar to lab results at values just above 1.00. However, the

data is visibly scattered as also indicted by the low R-squared values in Table 4.10. The scatter is caused by the inconsistent volumetric water content results from the physical samples. The plot of data is not only scattered but shifted in way that the CPT-TDR is underestimating the volumetric water content, also shown by the RMSE results. However, this underestimation is typical for this CPT-TDR device.

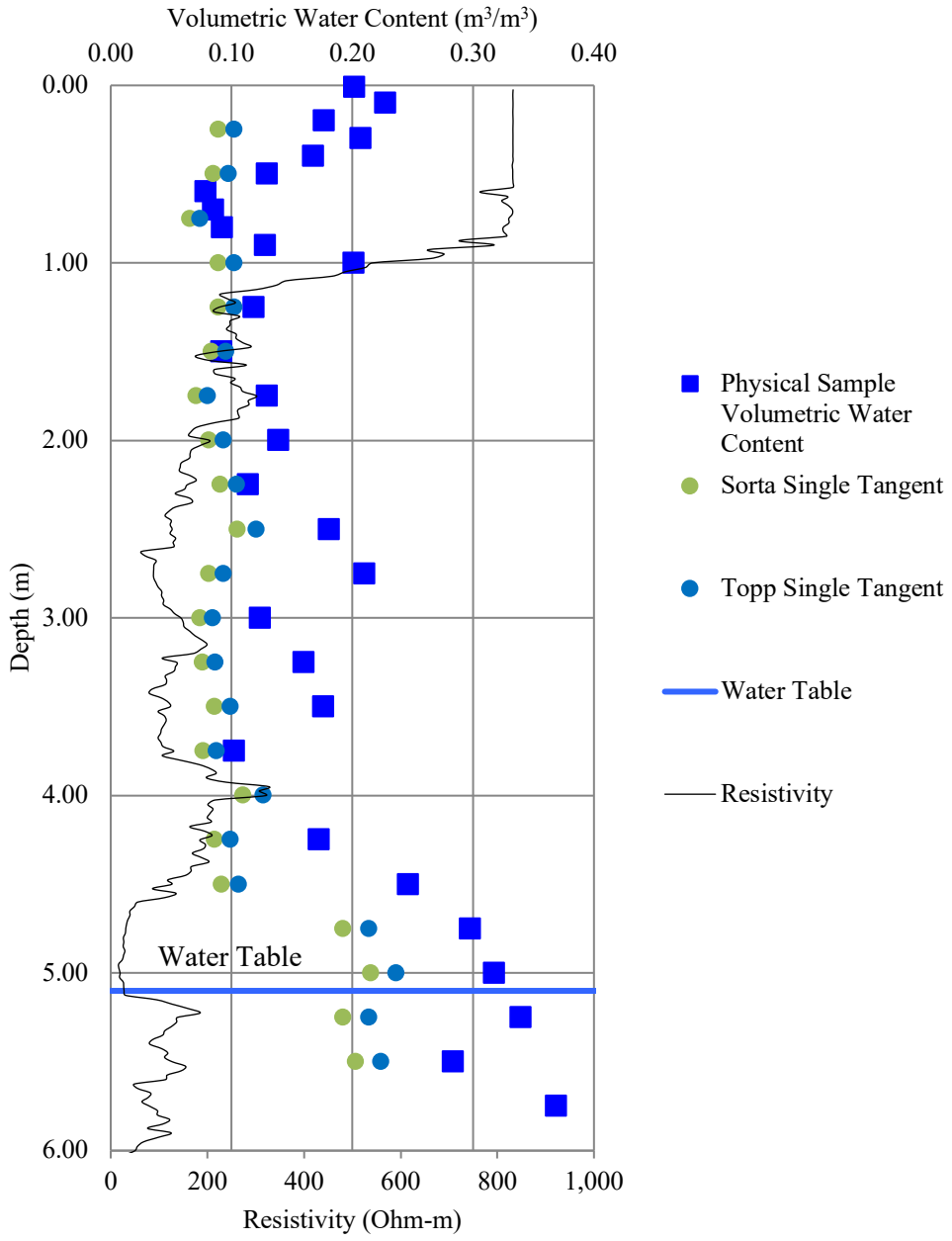

Figure 4.21: Plot of CPT-TDR, physical sample and electrical resistivity results with depth from Location 4.

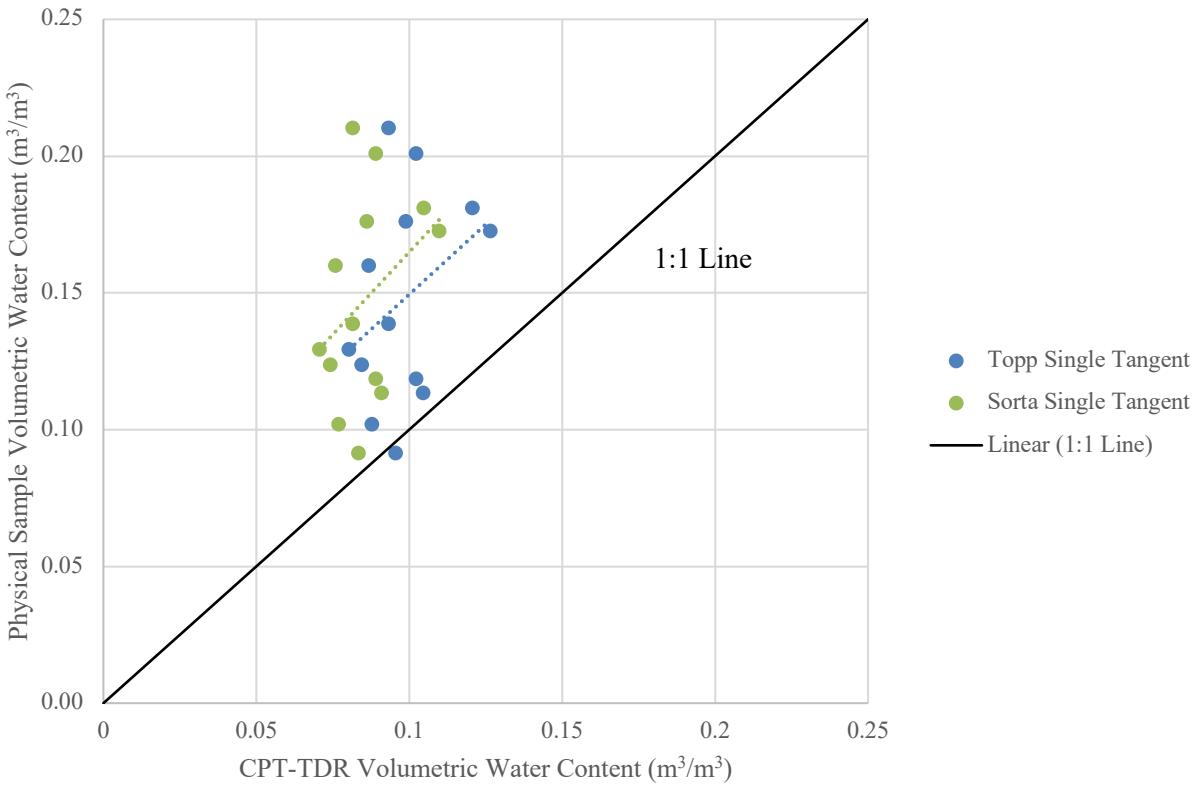

Figure 4.22: Plot of the physical sample volumetric water content versus the CPT-TDR volumetric water content from Location 4.

Table 4.10: Trend line parameters from Figure 4.22.

Trend Line	Slope	Y-Intercept	R^2	RMSE
Topp Single Tangent	1.02	0.05	0.13	0.06
Sorta Single Tangent	1.21	0.04	0.13	0.07

Location 6 physical sample volumetric water content results in Figure 4.23 are inconsistent at depths below 4.00 m. CPT-TDR results are more consistent reaching maximum values below 5.00 m. Slopes of the trend lines in Figure 4.20 are below 1.00 indicating an overestimation of volumetric water content. This is likely due to the inconsistent volumetric water content of the samples. The data points in Figure 4.24 plot above and below the 1:1 line indicating both under and over estimation of volumetric water content by the CPT-TDR. The scatter of the data points is very high, also indicated by the very low R-squared values in Table 4.11.

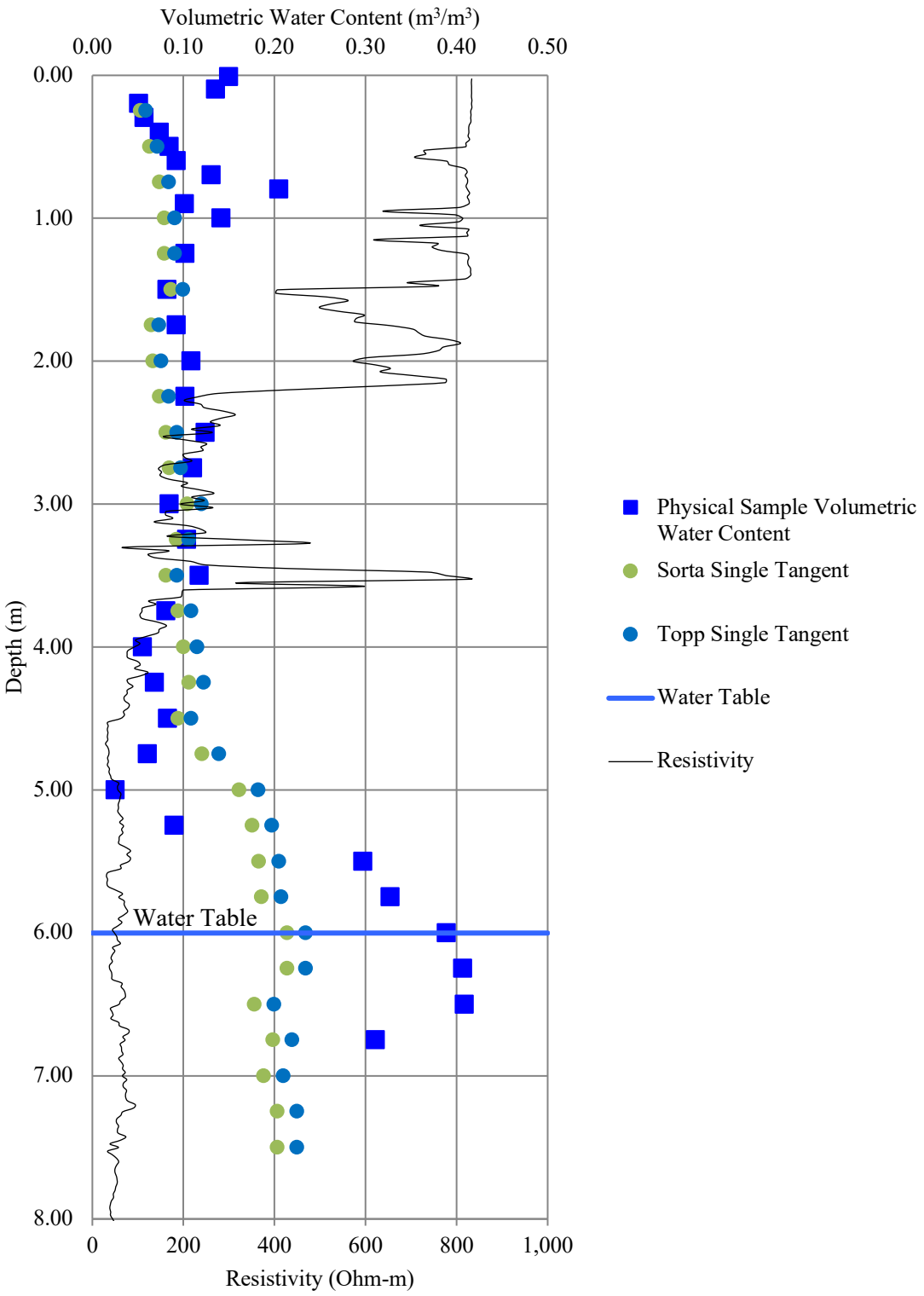

Figure 4.23: Plot of CPT-TDR, physical sample and electrical resistivity results with depth from Location 6.

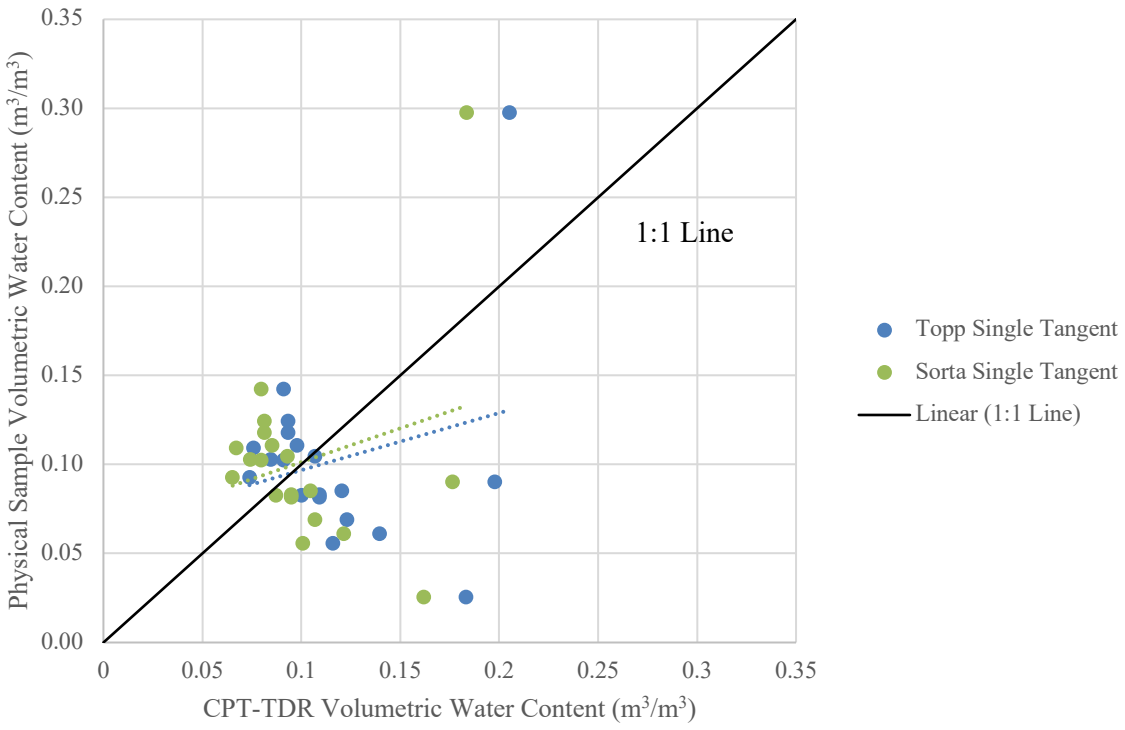

Figure 4.24: Plot of the physical sample volumetric water content versus the CPT-TDR volumetric water content from Location 6.

Table 4.11: Trend line parameters from Figure 4.24.

Trend Line	Slope	Y-Intercept	R^2	RMSE
Topp Single Tangent	0.38	0.06	0.06	0.06
Sorta Single Tangent	0.32	0.07	0.05	0.06

Results from Location 8 are similar to those from Location 6. Physical sample volumetric water content results in Figure 4.25 are inconsistent throughout the profile. CPT-TDR results are more consistent with some scatter. Slopes of the trend lines in Figure 4.26 are below 1.00, normally indicating an overestimation of volumetric water content. However, since the Y-intercept values are high the CPT-TDR still underestimates the volumetric water content as all data points in Figure 4.26 plot above the 1:1 line. The scatter of the data points is very high, indicated by the very low R-squared values in Table 4.112.

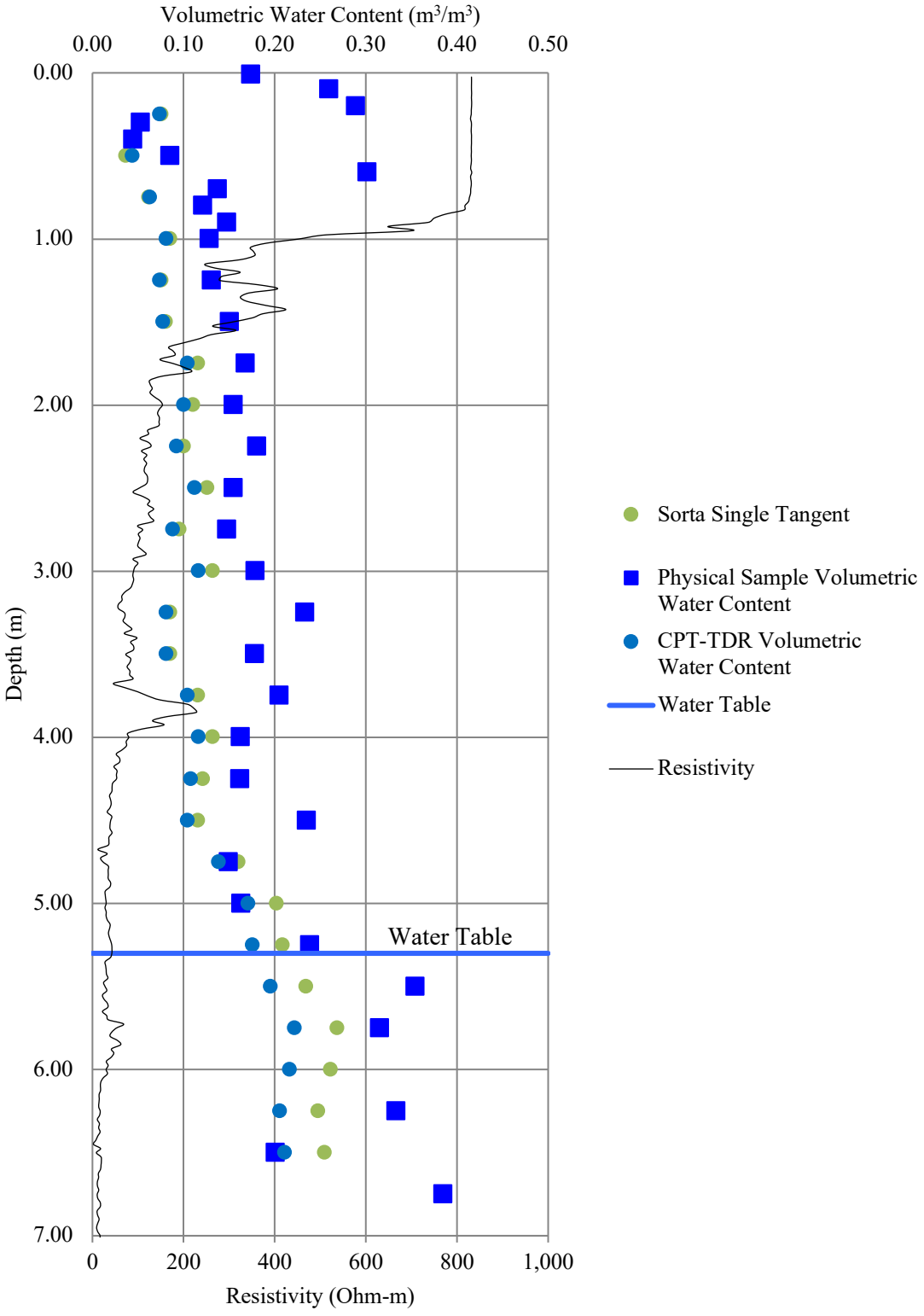

Figure 4.25: Plot of CPT-TDR, physical sample and electrical resistivity results with depth from Location 8.

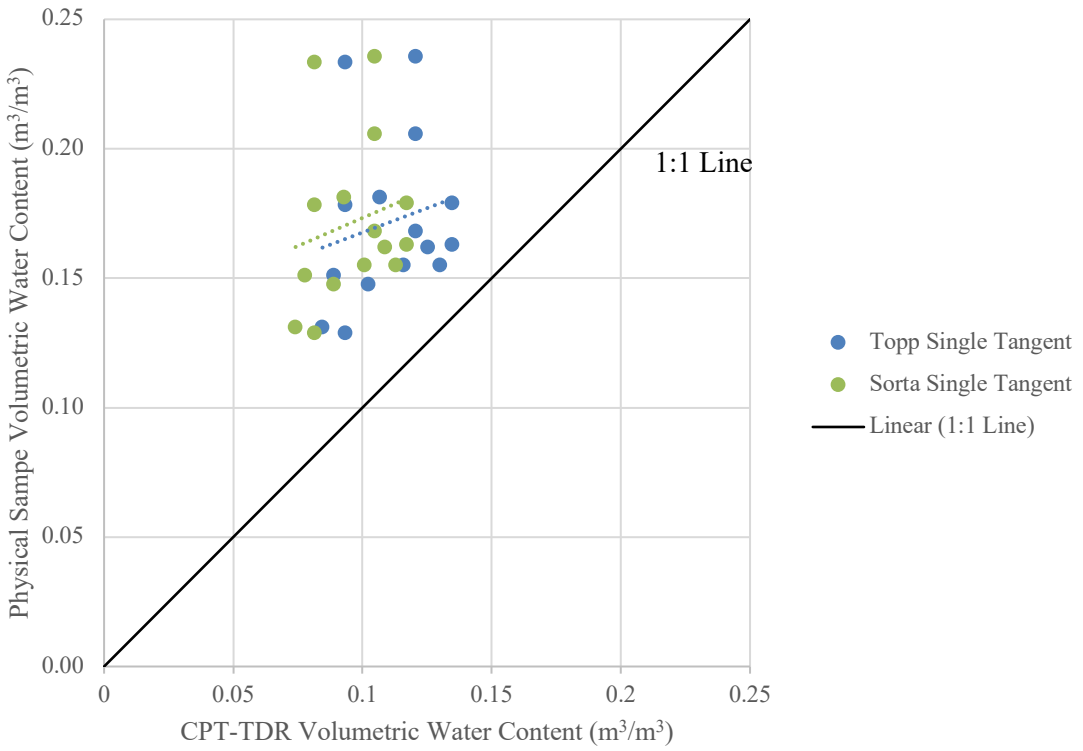

Figure 4.26: Plot of the physical sample volumetric water content versus the CPT-TDR volumetric water content from Location 8.

Table 4.12: Trend line parameters from Figure 4.26.

Trend Line	Slope	Y-Intercept	R^2	RMSE
Topp Single Tangent	0.38	0.13	0.04	0.07
Sorta Single Tangent	0.43	0.13	0.04	0.08

4.3.3 Sensitivity Analysis of Density on Volumetric Water Content

Throughout the 2016 field testing analysis an assumed dry density value of 1750 kg/m^3 was used to calculate the volumetric water content of the physical samples. This density value falls within the range of measured density values from the physical samples of the 2015 field testing. A sensitivity analysis is presented in Figure 4.27 to see how a range of density affects the volumetric water content calculated from the gravimetric water content of the physical samples.

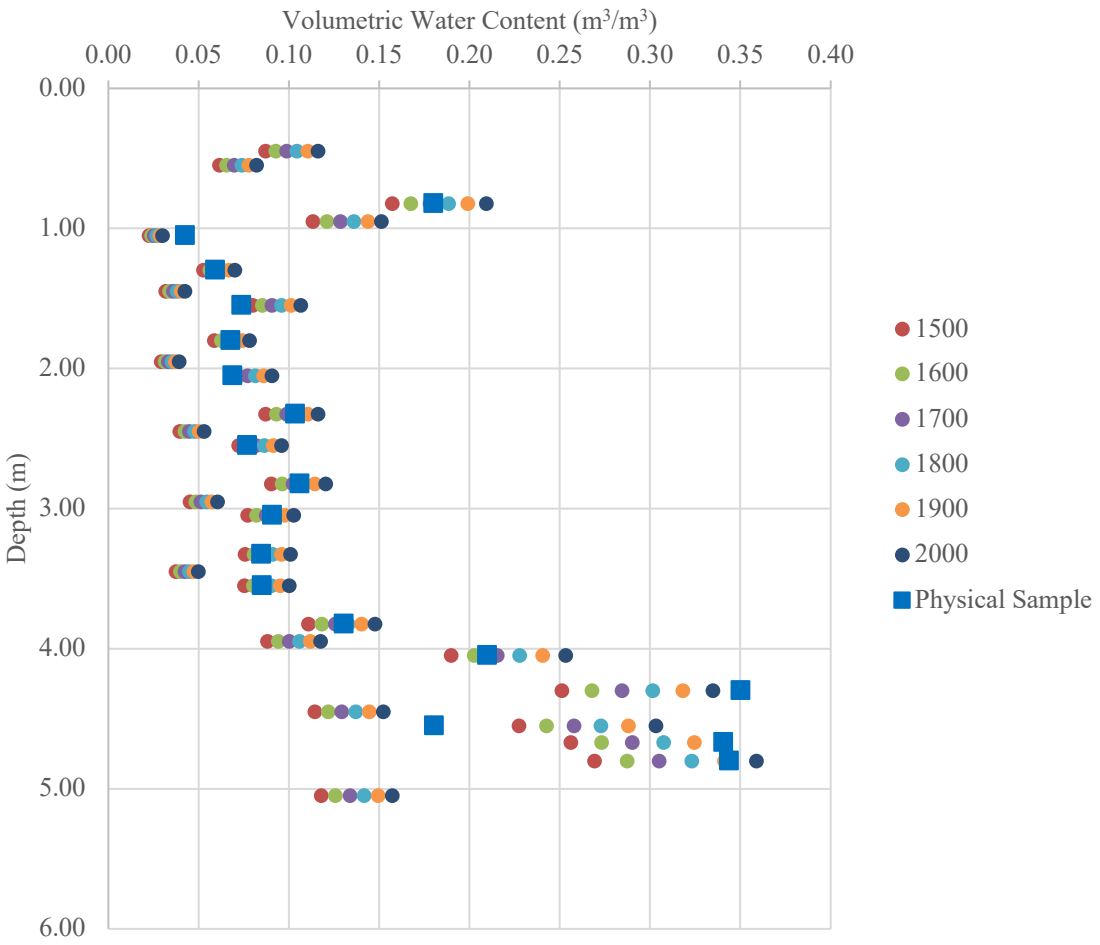

Figure 4.27: Sensitivity analysis of density on the physical sample calculated volumetric water content results. Results are from BH-LB09 from the 2015 field testing. Included in the plot is volumetric water content calculated from an assumed range of densities as well as the measured volumetric water content. The range of assumed density values are from 1500 kg/m^3 to 2000 kg/m^3.

The assumed range of density values increase in separation as the water content increases. The largest difference in calculated volumetric water content from the measured volumetric water content is 0.10 m^3/m^3 a percent difference of 28 %. This is the largest difference with all other comparisons falling below this value. Based upon visual examination most of the physical sample volumetric water contents have results falling within the assumed range of densities volumetric water contents. Each increment in density of 100 kg/m^3 results in an increase of 6.7 % in volumetric water content at the highest water content values.

4.3.4 Discussion of Field Results

The CPT-TDR tip remained intact during testing and although the correlations were poor the field measurements did follow similar trends with the physical samples. The transition of water content from well drained conditions to near saturation at the top of the capillary fringe was captured in most cases. There are a number of possible reasons for the differences in the CPT-TDR measured water contents and those from the physical samples. This includes disturbance of the physical samples causing changes in the gravimetric water content prior to sample collection, errors in the measurement or estimate of the dry density and difficulties in selecting the X_2 values in the field without a digital or hard copy of the wave form. The next section explores whether the application of a calibration method could provide an improvement to the CPT-TDR water contents for the field data.

4.4 Evaluation of Calibration Methods

The hypothesis presented in section 4.2 will be tested as calibration equations are developed and tested for the CPT-TDR using both field and laboratory data. Calibration equations that are developed should correct the CPT-TDR readings closer to the actual volumetric water content.

4.4.1 Development of Calibration Equations

Using the data from laboratory and selected field testing locations, a single calibration equation for each method of analysis is created in Table 4.13. Each equation is created using the average slope and Y-intercept of the trend lines from plots of physical sample versus CPT-TDR volumetric water content. Linear trendline fits are selected due to simplicity and that fact that a polynomial or exponential fit did not have a significant difference on the results. The selection of the values for the equations also considered the precision of each data set, those with very low precision (high scatter) were not considered. The following data sets were used to develop the single tangent method calibrations: laboratory, BH-LB09, Location1, and Location 4. Double tangent method calibrations were developed using data from the laboratory and BH-LB09 since these data sets included the double tangent method of analysis. It should be noted that the calibrations were also tried using just laboratory data, without Amos' data. The results from this trial were poor and therefore not included.

Table 4.13: Calibration equations for the CPT-TDR.

Equation Name	Equation
Topp Single Tangent	$\theta_{actual} = 1.06\theta_{calc} + 0.07$
Topp Double Tangent	$\theta_{actual} = 1.76\theta_{calc} + 0.09$
Sorta Single Tangent	$\theta_{actual} = 1.05\theta_{calc} + 0.09$
Sorta Double Tangent	$\theta_{actual} = 2.16\theta_{calc} + 0.07$

Symbols representing the actual volumetric water content are denoted as θ_{actual}. The symbols denoting the calculated volumetric water content (i.e. from Topp equation) are θ_{calc}. The calibration equations from Table 4.13 have been applied to the laboratory data in Section 4.3 and selected field data in Section 4.4.

4.4.2 Application of Calibration Equations

The data sets from the laboratory results in Figure 4.6 were calibrated and the results shown in Figure 4.28. Trend line parameters for the calibrated results are in Table 4.12.

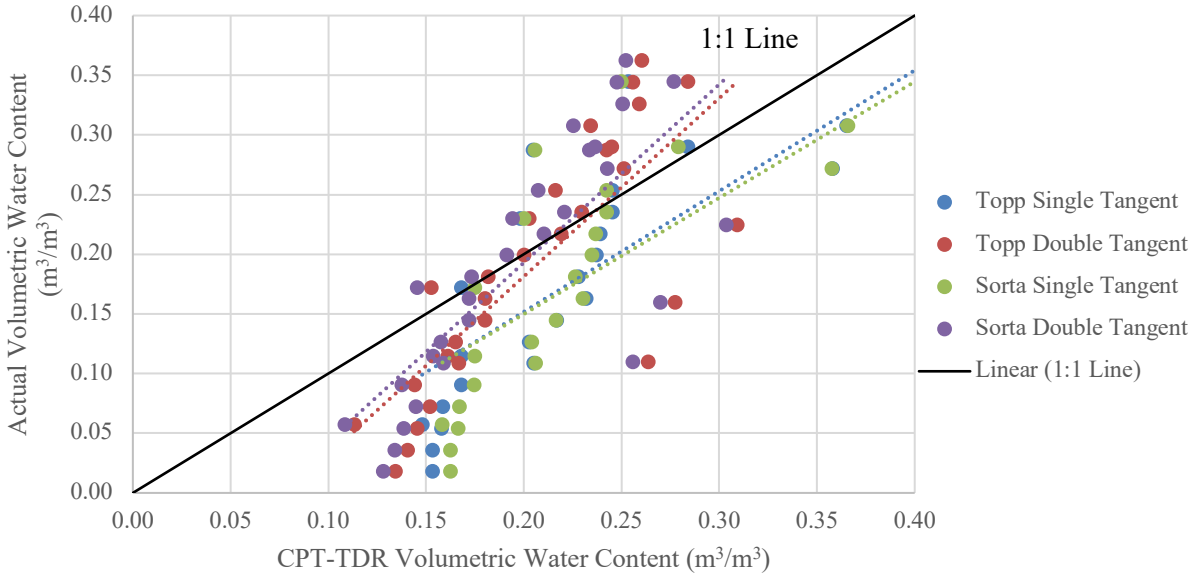

Figure 4.28: Laboratory data calibrated using the equations in Table 4.13 and the data sets in Figure 4.6.

Table 4.14: Trend line parameters from Figure 4.28.

Trend Line	Slope	Y-Intercept	R^2	RMSE
Topp Single Tangent	1.01	-0.05	0.70	0.07
Topp Double Tangent	1.50	-0.12	0.61	0.07
Sorta Single Tangent	0.97	-0.05	0.67	0.08
Sorta Double Tangent	1.50	-0.11	0.60	0.07

The calibration equations do improve the accuracy of the results for the double tangent method as the slopes of the trend lines for the Topp double tangent and Sorta double tangent methods become closer to 1.00. The RMSE for the calibrated results are also improved. Single tangent calibrations show small improvement of the results. The initial uncalibrated single tangent method results have trend line slope values near 1.05 and Y-intercepts near 0.03. The calibration equations for the single tangent methods results in trend line slopes near 1.00 and Y-intercepts of -0.05.

The calibrated results for the 2015 field testing are presented only for BH-LB09. Due to damage of equipment and inconsistent results at the other two locations the calibration equations did not improve the results. Figures 4.29 and 4.30 show the calibrated results for BH-LB09. Trend line parameters from Figure 4.30 are in Table 4.15.

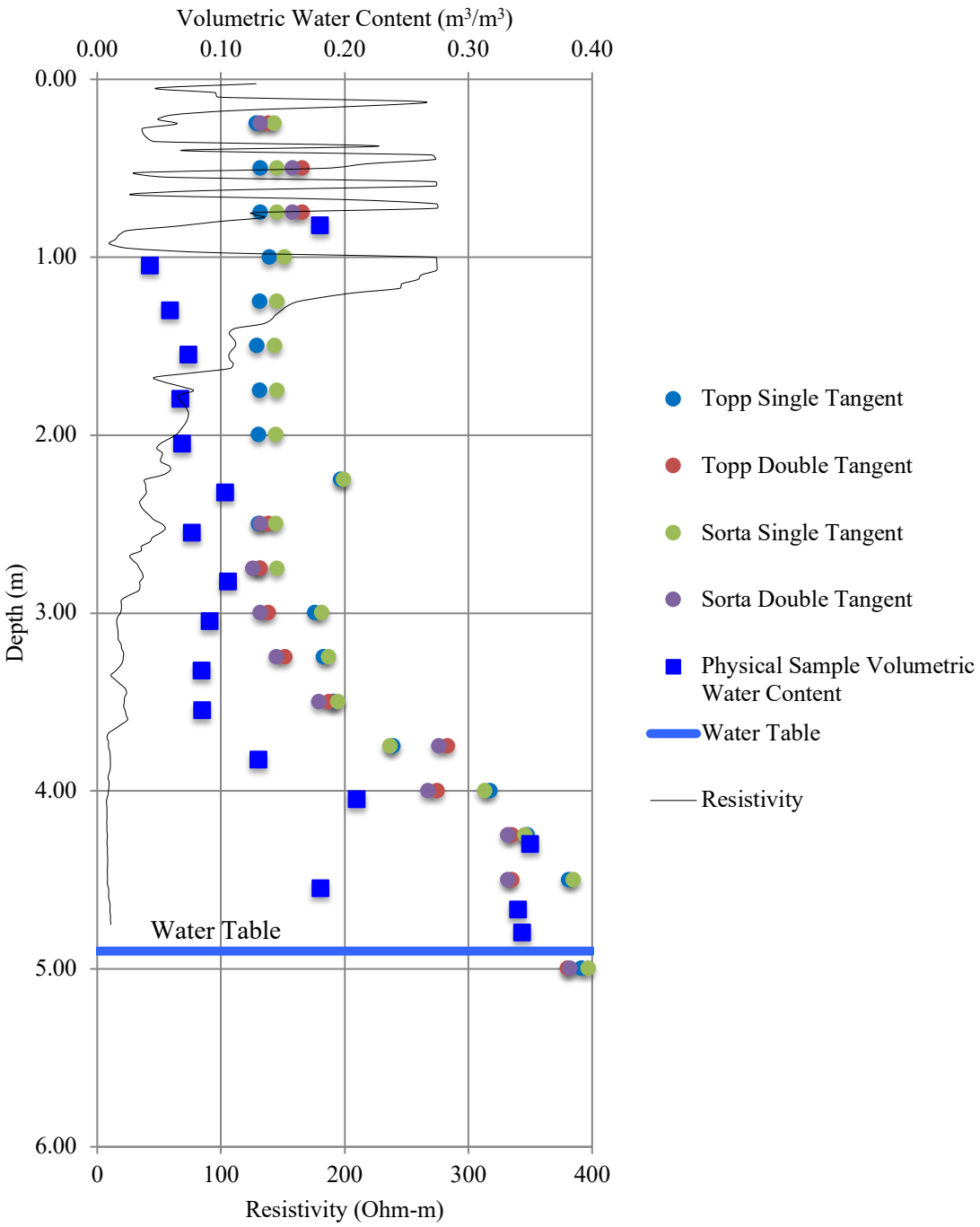

Figure 4.29: Plot of the calibrated CPT-TDR, physical sample and electrical resistivity results with depth from BH-LB09.

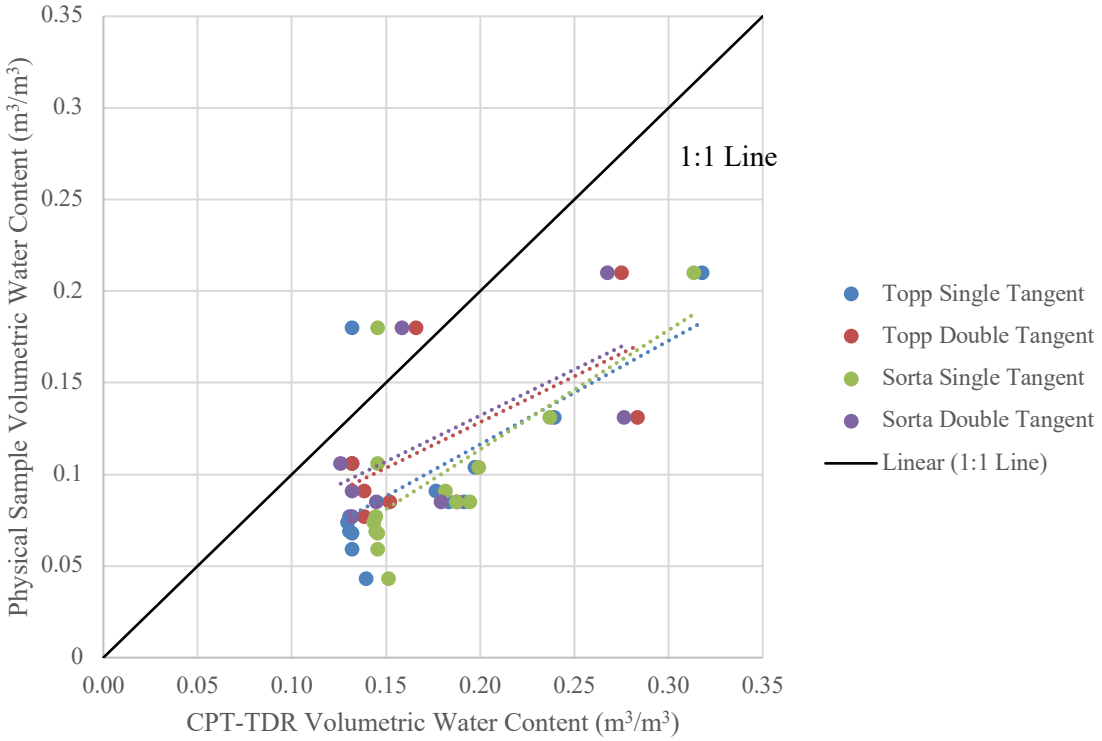

Figure 4.30: Field data from the 2015 testing location BH-LB09, calibrated using the equations in Table 4.13 and the data sets in Figure 4.13.

Table 4.15: Trend line parameters from Figure 4.30.

Trend Line	Slope	Y-Intercept	R^2	RMSE
Topp Single Tangent	0.57	0.00	0.45	0.09
Topp Double Tangent	0.50	0.03	0.39	0.10
Sorta Single Tangent	0.65	-0.02	0.47	0.10
Sorta Double Tangent	0.50	0.03	0.38	0.10

The calibration equations do not improve the accuracy of the results for BH-LB09. The RMSE for all calibrated results are increased thus decreasing the accuracy of the CPT-TDR calculated volumetric water content.

Results for the cumulative stored volume of water plotted with depth are presented in Figure 4.31 for BH-LB09. Both the physical samples and the calibrated CPT-TDR are presented. For the CPT-TDR only the Topp single and double tangent methods are present to avoid clutter. It should be noted for the double tangent method for depths from 1.00m to 2.25m the waveforms were not able to be analyzed using this method. Hence there is no increase in the stored volume of water over that interval.

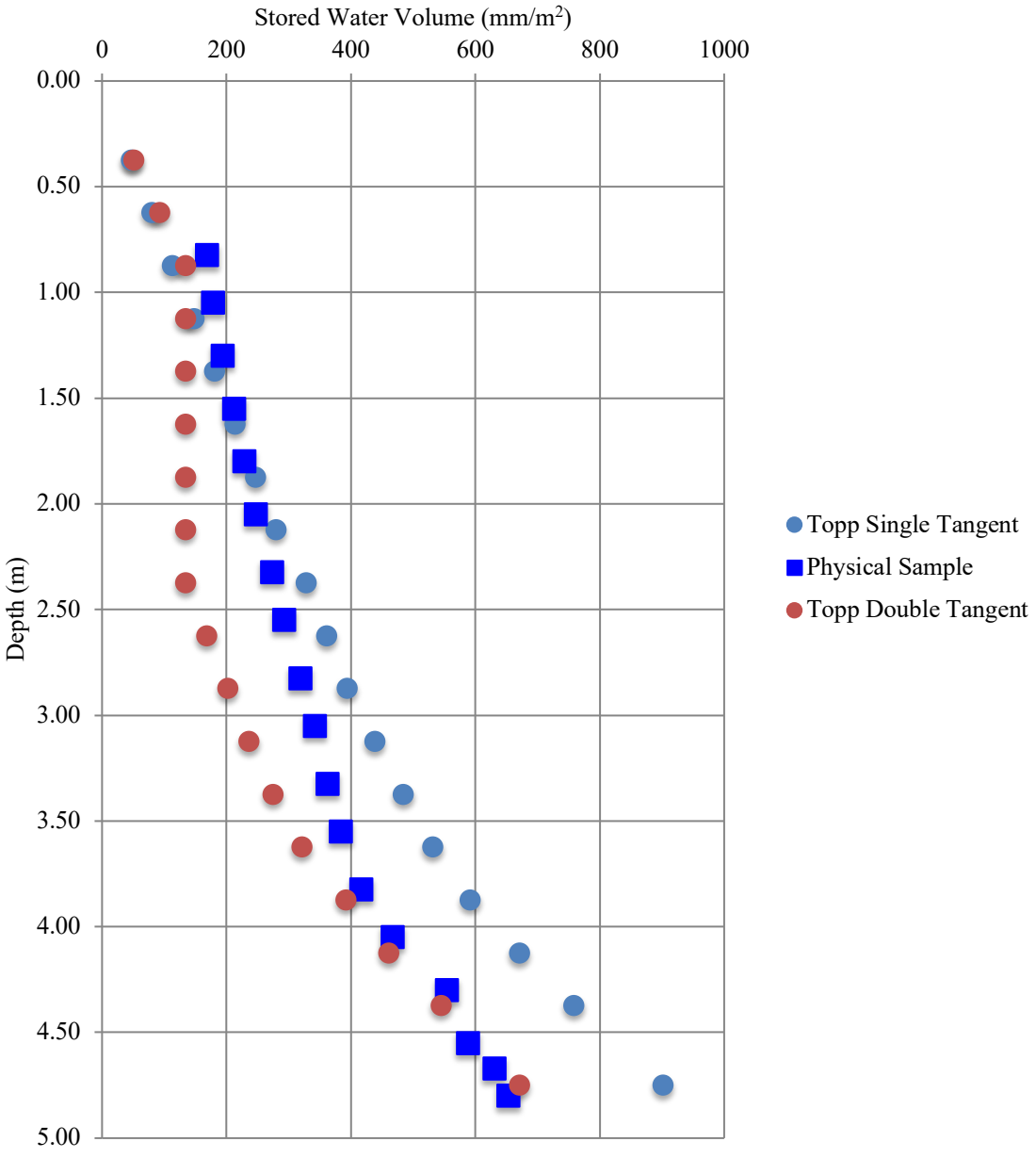

Figure 4.31: Plot of CPT-TDR and physical sample stored water volume with depth.

Figure 4.31 represents the total amount of stored water at each depth interval and is cumulated until the final depth is reached. At the final depth both the Topp double tangent method and physical samples cumulated stored water volumes end near the value of just above 650 mm/m^2. Stored water volume plots are not presented for each location since for the purposes of calibration the linear volumetric water content profiles are most suitable for calibration.

The calibrated results for the 2016 field testing are presented only for Location 4. At the other locations, the calibration results are similar with no improvement and therefore not presented. Figures 4.32 and 4.33 show the calibrated results for Location 4. Trend line parameters for Figure 4.33 are in Table 4.16.

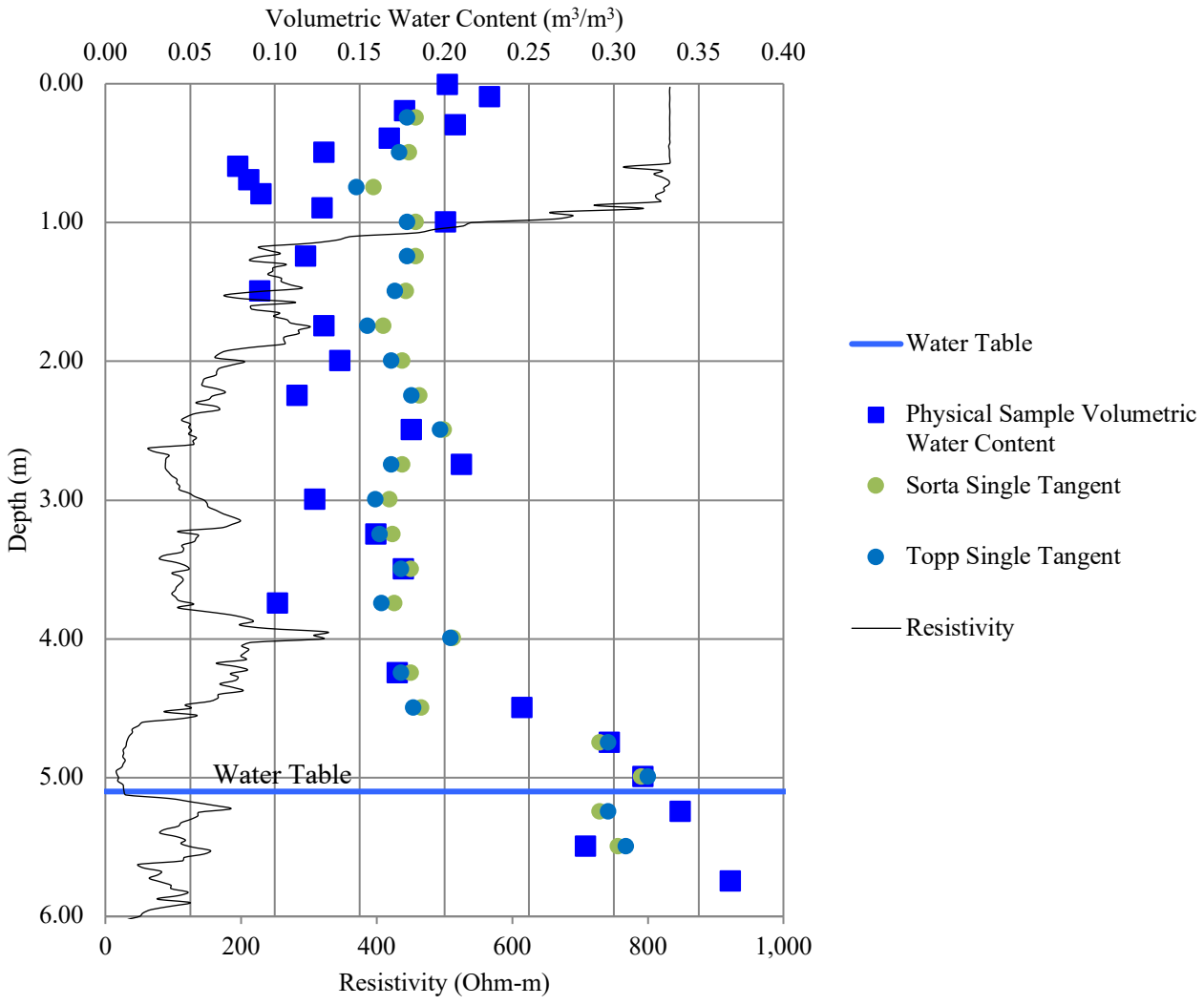

Figure 4.32: Plot of the calibrated CPT-TDR, physical sample and electrical resistivity results with depth from Location 4.

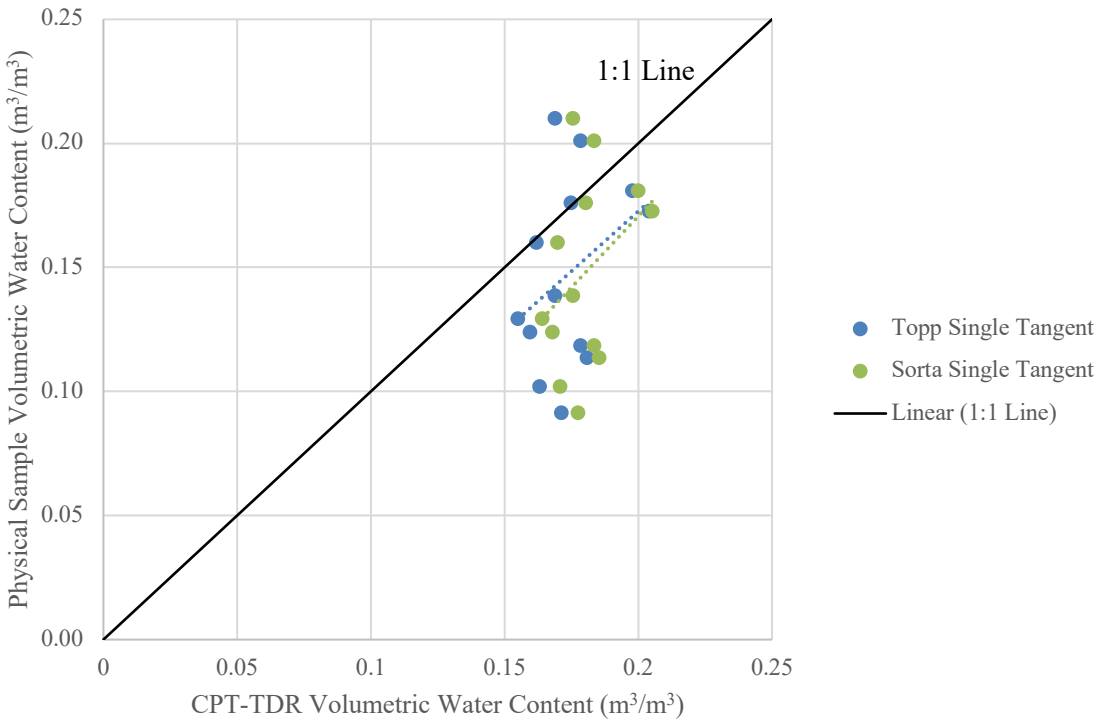

Figure 4.33: Field data from the 2016 testing, Location 4, calibrated using the equations in Table 4.13 and the data sets in Figure 4.21.

Table 4.16: Trend line parameters from Figure 4.33.

Trend Line	Slope	Y-Intercept	R^2	RMSE
Topp Single Tangent	0.97	-0.02	0.13	0.04
Sorta Single Tangent	1.15	-0.06	0.13	0.04

The calibration equations shift the data points with no improvement of the overall trend. The data points remain scattered, plotting both above and below the 1:1 line. Since the scatter of the uncalibrated data is high and due to inconsistencies with the waveform analysis using the single tangent method (similar to Figure 4.7 in section 4.3) the calibration equations do not improve the 2016 results.

4.4.3 Discussion of Calibration Results

Single tangent calibrations did not show improvement in most cases due to high scatter of uncalibrated data. The data scatter makes it difficult to develop a single calibration equation. Scatter of data using the single tangent method is likely caused by uncertainty in waveform interpretation as in Figure 4.7 and error in certain physical samples in the field.

The results were improved with a double tangent calibration where applicable. The laboratory results showed good improvement with the double tangent method. The best indication of performance of the calibration equations is the controlled lab testing results. Error may still be present in actual volumetric water content readings however it is likely small. With that it is apparent that the double tangent calibration method shows improvement of the volumetric water content readings under a controlled laboratory setting.

4.5 Summary

The laboratory testing illustrates the expected trends in the response of the CPT-TDR to changing water content using the two methods of interpretation. Double tangent methods underestimate the actual volumetric water content more when compared to the single tangent methods. However, the single tangent methods are more scattered where the double tangent methods have a linear response. Testing in FFT proved to work to some degree. Waveforms from the CPT-TDR were obtained and readable. However, a calibration is required, much the same as the calibration using sand. For this a large amount of FFT would be required covering broad range of water content.

Field testing proved the structural integrity of the CPT-TDR. Results from the laboratory and field were combined to create four calibration equations depending on the method being used. Laboratory testing was most controlled with respect to water content and the linear response of the double tangent methods proved to have the best calibration results. The field testing, although valuable, had more sources of error in the results from the equipment to the sampling.

5 CONCLUSIONS AND RECOMMENDATIONS

Performance of soil covers over mine waste is evaluated by measuring the stored volume of water within the soil. This is just one method of performance monitoring in addition to other measures. However, measuring the stored volume of water in soil is critical in tracking the overall movement of water throughout the site. Tracking the movement of water is achieved by using the measured stored volume of water as well as other measures of performance. This study investigated a tool to measure volumetric water content in soils with real time results. This tool was developed by adding a shaft section with TDR rods onto CPT equipment. The hypothesis of this study is that the CPT equipment would affect the volumetric water content readings from the TDR probes as the CPT shaft takes the place of soil when compared to traditional TDR.

The objectives of this study were to:

1. Design a shaft that integrates TDR equipment with CPT equipment. Compatibility and strength are critical to the design.
2. Define the accuracy and range of operation in different soil types.

The initial design for the CPT-TDR proved to work in terms of producing volumetric water content readings. However, upon field testing it was discovered that this design was weak structurally as physical failure occurred. A second design was created that modified the initial design addressing the points of weakness. This design proved to work in the field, producing volumetric water content readings and withstanding the extreme forces of CPT.

Overall the CPT-TDR volumetric water content readings are lower than the actual volumetric water content. This is found from both the laboratory and the field results. Two methods of analysis were used the single tangent method and the double tangent method. The single tangent method produced results that were closer to actual volumetric water content values. However, the results using this method of analysis are non-linear and highly scattered in some cases. Double tangent method results underestimate the volumetric water more than the single tangent method. However, this method produces linear results allowing ease in calibrating the CPT-TDR.

Calibration equations were developed using only high-quality results from the field and laboratory results. A total of four equations were developed and applied to the laboratory and field results. The single tangent method calibration equations do not improve the results. Double tangent method calibration equations do not show improvement on the results for the field measurements in sand tailings. However the field data was somewhat limited and prone to error. When the calibration equations were applied to the FFT results there was no improvement on the readings.

Further work on FFT is recommended using the current CPT-TDR design. A custom calibration would be required for the higher water content FFT.

The CPT-TDR was tested in sand with elevated EC. The operational range and limits are outlined in Figure 4.4. This chart may be used to help determine whether or not the CPT-TDR would produce quality waveforms in elevated EC soils. The electrically conductive operational range of the CPT-TDR is up to 1.5 dS/m.

Moving forward it is recommended that the double tangent method of waveform analysis be used to calculate the apparent length and the dielectric constant. Either the Topp or Sorta equation may be used to calculate the volumetric water content. The results may then be calibrated using the Topp Double Tangent or Sorta Double Tangent equation in Table 4.10.

Further work to improve the CPT-TDR includes the creation of a waveform analysis computer program and an integrated processor within the CPT-TDR. Programs and processors exist commercially, however these would need to be customized for this specific application. Benefits of this include the elimination of the fragile coaxial cable, and the removal of user error in waveform analysis.

REFERENCES

Amos, Michael. 2014. *Development of a Time Domain Reflectometry Sensor for Cone Penetration Testing.* Saskatoon, Saskatchewan: University of Saskatchewan.

Amos, Michael J. 2014. *Development of a Time Domain Reflectometry Sensor for Cone Penetration Testing.* MSc Thesis, College of Civil and Geological Engineering, University of Saskatchewan, Saskatoon: Michael Jason Amos.

Anderson, M, and William Woessner. 1992. *Applied groundwater modeling: Simulation of flow and advective transport.* San Diego: Academic Press.

ASTM International D4643-17. 2017. *Standard Test Method for Determination of Water (Moisture) Content of Soil by Microwave Oven Heating.* Standards, West Conshohocken, PA: ASTM International.

ASTM International D6519-15. 2015. *Standard Practice for Sampling of Soil Using the Hydraulically Operated Stationary Piston Sampler.* Standards, West Conshohocken PA: ASTM International.

Atekwana, Eliot A, Estella A Atekwana, Rebecca S Rowe, Dale D Werkema Jr., and Franklyn D Legall. 2004. "The relationship of total dissolved solids measurements to bulk electrical conductivity in an aquifer contaminated with hydrocarbon." *Journal of Applied Geophysics* (Elsevier B.V.) 56: 281-294.

Aubertin, Michel, S Lee Barbour, G Ward Wilson, and Ernest Yanful. 2004. *Design, Construction and Performance Monitoring of Cover Systems for Waste Rock and Tailings.* Edited by O'Kane Consultants Inc. Vol. 2.21.4a. MEND.

Cardoso, Rafaela. 2016. "Porosity and tortuosity influence on geophysical properties of an artificially cemented sand." *Engineering Geology* (Elsevier B.V.) 211: 198-207.

Cereti, Annamaria, Elena Pettinelli, Alessandro Galli, and Francesco Bella. 2003. "Shorted-end probes for accurate permittivity measurements with time-domain reflectometry." *Applied Physics Letters* (American Institute of Physics) 83 (5): 1050-1052.

Dalton, F N, and M Th Van Genuchten. 1986. "The Time-Domain Reflectometry Method for Measuring Soil Water Content and Salinity." *Geoderma* (Elsevier Science Publoshers) 38: 237-250.

Davis, J L, and W J Chudobiak. 1975. "In Situ Meter for Measuring Relative Permittivity of Soils." Paper.

Dompierre, Kathryn A, and S. Lee Barbour. 2016. "Thermal properties of oil sands fluid fine tailings: laboratory and in situ testing methods." *Canadian Geotechnical Journal* (NRC Research Press) 54: 428-440.

DuPont Engineering Polymers. n.d. *Delrin Acetyl Resin Design Guide - Module III.* USA: Dupont Engineering Polymers.

Evett, Steven R. 2003. "Soil Water Measurement by Neutron Thermalization." In *Encyclopedia of Water Science*, 889-893. Bushland, TX: Marcel Dekker, Inc.

Fellner-Feldegg, Hugo. 1969. "The Measurement of Dielectrics in the Time Domain." *The Journal of Physical Chemistry* 73 (3): 616-622.

Ferre, P A, and G C Topp. 2002. "Time domain reflectometry." *Soil Science Society of America Book Series* (Soil Science Society of America, Inc.) 5: 434-436.

Ferre, P. A., J. H. Knight, D. L. Rudolph, and R. G. Kachanoski. 1998. "The sample areas of conventional and altrenative time domain reflectometry probes." *Water Resources Research* 34 (11): 2971-2979.

Fujiyasu, Y, C E Pierce, L Fan, and C P Wong. 2004. "High dielectric coating for time domain reflectometry soil moisture sensor." *Water Resoruces Research* (American Geophysical Union) 40.

Greco, Robert, and Andrea Guida. 2007. "Field measurements of topsoil moisture profiles by vertical TDR probes." *Journal of Hydrology* (Elsevier B.V.) 348: 442-451.

Heimovaara, T. J. 1993. "Design of Triple-Wire Time Domain Reflectometry Probes in Practice and Theory." *Soil Science Society of America Journal* 57 (6): 1410-1417.

Jones, Scott, Jon Wraith, and Dani Or. 2002. *Time domain reflectometry measurement principles and applications.* Logan, Utah: Jon Wiley & Sons, Ltd.

Kahimba, F C, R Sri Ranjan, and M Krishnapillai. 2007. "Impact of cable lengths on the accuracy of dielctric constant measurements by time domain reflectometry." *Candian Biosystems Engineering* 49: 11-18.

Kelly, Shaun F, John S Selker, and James L Green. 1995. "Using Short Soil Moisture Porbes With High-Bandwidth Time Domain Reflectometry Instruments." *Soil Science Society America Journal* 59 (1): 97-102.

Klein, Lawrence A, and Calvin T Swift. 1977. "An Improved Model for the Dielectric Constant of Sea Water at Microwave Frequencies." *IEEE Transcactions on Antennas and Propagation* 25 (1): 104-111.

Knappett, J A, and R F Craig. 2012. *Craig's Soil Mechanics.* New York, New York: Spon Press.

Knight, J H. 1992. "Sensitivity of Time Domain Reflectometry Measurements to Lateral Variations in SOil Water Content." *Water Resources Reasearch* 28 (9): 2345-2352.

Knight, J H, P A Ferre, D L Rudolph, and R G Kachanoski. 1997. "A numerical analysis of the effects of coatings and gaps upon relative dielectric permitivitty measurement with time domain reflectometry." *Water Resources Research* 33 (6): 1455-1460.

Kosugi, Ken'ichirou, Yosuke Yamakawa, Naoya Masaoka, and Takahisa Mizuyama. 2009. "A Combined Penetrometer-Moisture Probe for Surveying Soil Properties of Natural Hillslopes." *Vadose Zone Journal* (Soil Science Society of America) 8 (1): 52-63.

Lapen, D R, G C Topp, M E Edwards, E G Gregorich, and W E Curnoe. 2004. "Combined cone penetration resistance/water content instrumentation to evaluate cone penetration-water content relationships in tillage research." *Soil and Tillage Research* (Elsevier B.V.) 79: 51-62.

Ledieu, J, P De Ridder, P De Clerck, and S Dautrebande. 1986. "A Method of Measuring Soil Moisture by Time-Domain Reflectometry." *Journal of Hydrology* (Elsevier B.V.) 88: 319-328.

Lefebvre, Michel Elzear. 1997. *The Feasability of Coaxial Time Domain Reflectometry as an Insitu Site Characterization Tool for Determining the Moisture Content of Mine Tailings.* MSc Thesis, Department of Civil and Environmental Engineering, University of Alberta, Ottawa: National Library of Canada.

Levesque, Celeste Marie. 2014. "Oil Sands Process Water and Tailings Pond Contaminant Transport and Fate: Physical, Chemical and Biological Processes." MSc Thesis, Vancouver.

Lin, Chih-Ping, Chih-Chung Chung, and Shr-Hong Tang. 2006. *Geoelctric Measurements by TDR Penetrometer.* Purdue University, West Lafayette: Purdue University.

Mann, Prem S. 2010. *Introductory Statistics.* Hoboken, NJ: John Wiley & Sons, Inc.

Miyamoto, H, and J Chikushi. 2006. *Calibration of Column-Attaching TDR Probe Based on Dielectric Mixing Model.* Proceedings, Purdue University, West Lafayette: Purdue University.

MOHR Test and Measurement LLC. 2017. *MOHR CT100 TDR Cable User Guide.* Accessed April 23, 2018. http://www.mohr-engineering.com/documents/CT100_OPMAN/CT100_TDR_Cable_Tester_Guide.php.

Mojid, M A, Guido C.L. Wyseure, and Derek A Rose. 1998. "The use of insulated time-domain reflectometry sensors tom measure water content in highly saline soils." *Irrigation Science* (Springer Verlag) 18: 55-61.

Naderi-Boldaji, Mojtaba, M Younesi, A Sharifi, B Jamshidi, F Abbasi, and S Minaee. 2010. "A combined sensor for on-the-go measurement of soil moisture content and mechanical

resistance: Moisture sensor design and calibration." Department of Mechanical Engineering, University of Tehran.

Nichol, Craig, Roger Beckie, and Leslie Smith. 2002. "Evaluation of Uncoated and Coated Time Domain Reflectometry Probes for High Electrical Conductivity Systems." *Soil Science Society of America* 66: 1454-1456.

Nissen, H H, P Moldrup, and K Henriksen. 1998. "High-Resolution Time Domain Reflectometry Coil Probe for Measuring Soil Water Content." *Soil Science Soiciety of America Journal* (Soil Science Society of America) 62: 1203-1211.

Noborio, K. 2001. "Measurement of soil water content and electrical conductivity by time domain reflectometry: a review." *Computers and electronics in agriculture* (Elsevier B.V.) 31: 213-237.

Pettinelli, Elena, Annamaria Cereti, Alessandro Galli, and Francesco Bella. 2002. "Time domain relfectometry: Calibration techniques for accurate measurement of the dielectric properties of various materials." *Review of Scientific Instruments* (American Institute of Physics) 73 (10): 3552-3562.

Ransom, Robert C. 2017. *A Clarifying Concept of Archie's Resistivity Relationships and Parameters. A Model and Discussion.* 08 01. Accessed 12 15, 2017. www.archieparameters.com.

Reynolds, John M. 2011. *An Introduction to Applied and Environmental Gephysics.* Oxford: John Wiley & Sons, Ltd.

Robertson, P K, and K L Cabal. 2012. *Guide to Cone Penetration Testing for Geotechnical Engineering.* Signal Hill, California: Gregg Drilling & Testing, Inc.

Science Learning Hub. 2010. *Ocean Salinity.* June 22. Accessed December 20, 2017. https://www.sciencelearn.org.nz/resources/686-ocean-salinity.

Shin II, James D, David A Timian, Rexford M Morey, Gayle Mitchell, Chad Antle, and Rocky Hull. 1998. "Development of a CPT Deployed Probe for In Situ Measurement of Volumetric Soil Moisture Content and Electrical Resistivity." *Field Analytical Chemistry and Technology* (John Wiley & Sons, Inc.) 2 (2): 103-109.

Teixeira, W, G Schroth, J Marques, and B Huwe. 2003. "Sampling and TDR probe insertion in the determination of the volumetric soil water content." *SciELO.* 07. Accessed 12 1, 2015. www.scielo.br/scielo.php?script=sci_arttext&pid=S0100-06832003000400001.

The Engineering Toolbox. n.d. *Density of some Common Materials.* Accessed 12 1, 2015. www.engineeringtoolbox.com/density-materials-d_1652.html.

Topp, G C. 1980. *Electromagnetic Determination of Soil Water Content: Measurements in Coaxial Transmission Lines.* Ottawa, Ontario: Water Resources Research.

Vaz, Carlos Manoel Pedro, and W Jan Hopmans. 2001. "Simultaneous Measurement of Soil Penetration Resistance and Water Content with a Combined Penetrometer-TDR Probe." *Soil Science Society of America* 65: 4-12.

Whalley, W R. 1993. "Considerations on the use of time-domain reflectometry (TDR) for measuring soil water content." *Journal of Soil Science* 44: 1-9.

Wyseure, G C.L., M A Mojid, and M A Malik. 1997. "Measurement of volumetric water content by TDR in saline soils." *European Journal of Soil Science* (Blackwell Science Ltd.) 48: 347-354.

Zegelin, S J, and I White. 1989. "Improved Field Probes for Soil Water Content and Electrical Conductivity Measurement Using Time Domain Reflectometry." *Water Resources Research* 25 (11): 2367-2376.

APPENDIX A: RAW LABORATORY DATA

Table A.1: Sand mixture data and CPT-TDR testing results from comparison of CPT-TDR to conventional TDR.

Mixture Identification	Mass Sand (kg)	Mass Water (kg)	Dry Density (kg/m^3)	Volumetric Water Content (m^3/m^3)	X_1 (m)	X_2 (m)	Dielectric Constant
5	19.829	0.55	1500.00	0.04	18.3394	18.5171	3.1577
10	19.829	1.10	1500.00	0.08	18.3394	18.5391	3.9880
15	19.829	1.65	1500.00	0.12	18.3394	18.5410	4.0643
20	19.829	2.20	1500.00	0.17	18.3394	18.5550	4.6483
25	19.829	2.75	1500.00	0.21	18.3394	18.5830	5.9341

Table A.2: Sand mixture data and conventional TDR testing results from comparison of CPT-TDR to conventional TDR.

Mixture Identification	Mass Sand (kg)	Mass Water (kg)	Dry Density (kg/m^3)	Volumetric Water Content (m^3/m^3)	X_1 (m)	X_2 (m)	Dielectric Constant
5	19.829	0.55	1500.00	0.04	14.6686	14.8044	1.8442
10	19.829	1.10	1500.00	0.08	14.6686	14.8702	4.0643
15	19.829	1.65	1500.00	0.12	14.6686	14.8782	4.3932
20	19.829	2.20	1500.00	0.17	14.6686	14.9681	8.9700
25	19.829	2.75	1500.00	0.21	14.6686	15.0878	17.5729

Table A.3: Sand mixture data from sand testing part one.

Mixture Identification	Dry Mass Sand & Pail (kg)	Mass of Water Added (g)	Volume of Sand (L)	Approximate Dry Density (kg/m^3)	Approximate Volumetric Water Content (m^3/m^3)
0 g/L	28.837	4100.8	14.6	1973.0	0.28
5 g/L	25.223	1918.6	14.0	1796.9	0.14
10 g/L	25.820	1921.4	14.5	1783.4	0.13
15 g/L	25.865	1928.0	14.1	1831.9	0.14
20 g/L	25.076	1959.1	14.0	1786.4	0.14
25 g/L	25.617	1962.0	14.2	1800.2	0.14
30 g/L	23.987	1939.6	13.1	1831.2	0.15

Table A.4: CPT-TDR results from sand testing part one.

Mixture Identification	Waveform X_1 (m)	Waveform X_2 Single Tangent (m)	Waveform X_2 Double Tangent	Dielectric Constant Single Tangent	Dielectric Constant Double Tangent
0 g/L	18.3024	18.6473	18.5915	11.8956	8.3579
5 g/L	18.3003	18.5231	18.5041	4.9639	4.1534
10 g/L	18.3043	18.5913	18.5915	8.2369	8.2484
15 g/L	18.3023	18.6063	18.5694	9.2416	7.1342
20 g/L	18.2993	18.5736	18.5252	7.5240	5.1031
25 g/L	18.3143	18.5410	18.5252	5.1392	4.4479
30 g/L	18.3133	18.6252	-	9.7281	-

Table A.5: Sand mixture data from sand testing part two.

Mixture #	Dry Mass Sand (kg)	Mass of Water Added (g)	Volume of Sand (L)	Approximate Dry Density (kg/m^3)	Approximate Volumetric Water Content (m^3/m^3)
1	25.293	250.0	13.8	1834.2	0.02
2	25.293	500.0	13.8	1834.2	0.04
3	25.293	750.0	13.8	1834.2	0.05
4	25.293	1000.0	13.8	1834.2	0.07
5	25.293	1250.0	13.8	1834.2	0.09
6	25.293	1500.0	13.8	1834.2	0.11
7	25.293	1750.0	13.8	1834.2	0.13
8	25.293	2000.0	13.8	1834.2	0.15
9	25.293	2250.0	13.8	1834.2	0.16
10	25.293	2500.0	13.8	1834.2	0.18
11	25.293	2750.0	13.8	1834.2	0.20
12	25.293	3000.0	13.8	1834.2	0.22

13	25.293	3250.0	13.8	1834.2	0.24
14	25.293	3500.0	13.8	1834.2	0.25
15	25.293	3750.0	13.8	1834.2	0.27
16	25.293	4000.0	13.8	1834.2	0.29
17	25.293	4250.0	13.8	1834.2	0.31
18	25.293	4500.0	13.8	1834.2	0.33
19	25.293	4750.0	13.8	1834.2	0.34
20	25.293	5000.0	13.8	1834.2	0.36

Table A.6: CPT-TDR results from sand testing part two.

Mixture #	Waveform X_1 (m)	Waveform X_2 Single Tangent (m)	Waveform X_2 Double Tangent (m)	Dielectric Constant Single Tangent	Dielectric Constant Double Tangent
1	18.3370	18.5594	18.5050	4.9462	2.8224
2	18.3370	18.5594	18.5090	4.9462	2.9584
3	18.3370	18.5634	18.5122	5.1257	3.0695
4	18.3370	18.5642	18.5162	5.1620	3.2113
5	18.3370	18.5722	18.5114	5.5319	3.0415
6	18.3370	18.6028	18.5250	7.0650	3.5344
7	18.3370	18.6010	18.5242	6.9696	3.5044
8	18.3370	18.6122	18.5330	7.5735	3.8416
9	18.3370	18.6242	18.5330	8.2484	3.8416
10	18.3370	18.6210	18.5338	8.0656	3.8730
11	18.3370	18.6282	18.5442	8.4797	4.2932
12	18.3370	18.6298	18.5546	8.5732	4.7350

13	18.3370	18.6345	18.5602	8.8506	4.9818
14	18.3370	18.6346	18.5530	8.8566	4.6656
15	18.3370	18.7210	18.5714	14.7456	5.4943
16	18.3370	18.6642	18.5682	10.7060	5.3453
17	18.3370	18.7266	18.5626	15.1788	5.0895
18	18.3370	18.7618	18.5754	18.0455	5.6835
19	18.3370	18.7770	18.5738	19.3600	5.6074
20	18.3370	18.7786	18.5762	19.5011	5.7217

Table A.7: FFT mixture data from FFT testing.

Reading Date	Sample Wet Mass (g)	Sample Dry Mass (g)	Sample Gravimetric Water Content (%)	Volumetric Water Content (m^3/m^3)
Jan. 15	71.10	26.40	1.69	0.80
Jan. 19	89.80	35.00	1.57	0.79
Feb. 16	24.50	10.50	1.33	0.76
Feb. 21	60.10	29.50	1.04	0.71

Table A.8: CPT-TDR results from FFT testing.

Reading Date	Waveform X_1 (m)	Waveform X_2 Tangent (m)	Waveform X_2 Double Tangent (m)	Dielectric Constant Tangent	Dielectric Constant Double Tangent
Jan. 15	18.2873	18.9013	18.8229	37.6996	28.6867
Jan. 19	18.2960	18.8822	18.7868	34.3630	24.0885
Feb. 16	18.2822	18.8632	18.8186	33.7561	28.7725
Feb. 21	18.2978	18.8632	18.8017	31.9677	25.3915

APPENDIX B: 2015 RAW FIELD DATA

Table B.1: Sample data from BH-LB07.

Average Depth (m)	Dry Density (kg/m3)	Volumetric Water Content (m^3/m^3)
0.83	1614.45	0.09
1.63	1685.42	0.09
1.75	1660.64	0.05
2.38	1683.17	0.09
3.05	1647.53	0.07
3.50	1771.81	0.14
4.50	1553.85	0.14
4.88	1744.30	0.28
5.05	1989.39	0.14
5.38	1731.45	0.35
5.85	1926.73	0.36

Table B.2: CPT-TDR results from BH-LB07.

Depth (m)	X_1 (m)	X_2 Single Tangent (m)	X_2 Double Tangent (m)	Dielectric Constant Single Tangent	Dielectric Constant Double Tangent
0.25	15.4979	15.7018	15.7024	4.1575	4.1820
0.50	15.4979	15.6964	15.6938	3.9402	3.8377
0.75	15.4979	15.7055	15.688	4.3098	3.6138
1.00	15.4979	15.7874	15.7111	8.3810	4.5454
1.25	15.4979	15.7892	15.7197	8.4856	4.9195
1.50	15.4979	15.7018	15.7053	4.1575	4.3015
1.75	15.4979	15.7492	15.7053	6.3152	4.3015
2.00	15.4979	15.7055	15.7053	4.3098	4.3015
2.25	15.4979	15.7055	15.7169	4.3098	4.7961
2.50	15.4979	15.7055	15.7371	4.3098	5.7217
2.75	15.4979	15.751	15.7313	6.4060	5.4476
3.00	15.4979	15.7018	15.7601	4.1575	6.8749
3.25	15.4979	15.7018	15.7601	4.1575	6.8749
3.50	15.4979	15.7055	15.7572	4.3098	6.7236
3.75	15.4979	15.7018	15.7832	4.1575	8.1396
4.00	15.4979	15.8111	15.7976	9.8094	8.9820
4.25	15.4979	15.873	15.7919	14.0700	8.6436
4.50	15.4979	15.802	15.789	9.2477	8.4739
5.00	15.4979	15.8038	15.8553	9.3575	12.7735

5.25	15.4979	15.8056	15.8755	9.4679	14.2582
5.50	15.4979	15.9021	15.8755	16.3378	14.2582
5.75	15.4979	15.904	15.8784	16.4917	14.4780
6.00	15.4979	15.904		16.4917	

Table B.3: Sample data from BH-LB08.

Average Depth (m)	Dry Density (kg/m^3)	Volumetric Water Content (m^3/m^3)
0.35	1717.3	0.09
0.55	1545.7	0.09
0.84	1594.1	0.10
1.30	1780.0	0.10
1.55	1762.4	0.10
1.83	1790.9	0.10
2.13	1791.6	0.11
2.33	1740.1	0.17
2.83	1711.3	0.15
3.04	1703.6	0.14
3.33	1812.1	0.12
3.55	1592.8	0.13
3.83	1844.2	0.16

4.33	1844.3	0.20
4.30	2092.8	0.35
4.55	1905.7	0.24
4.83	1861.2	0.23
5.05	1948.8	0.19
5.33	1643.0	0.20
5.55	1688.7	0.16
5.83	1782.1	0.28
6.05	2007.2	0.30
6.33	1819.1	0.37
6.78	1962.7	0.37

Table B.4: CPT-TDR results from BH-LB08.

CPT-TDR Depth (m)	X_1 (m)	X_2 Single Tangent (m)	X_2 Double Tangent (m)	Dielectric Constant Single Tangent	Dielectric Constant Double Tangent
0.25	15.4310	15.6811	15.6304	6.2550	3.9760
0.50	15.4310	15.6444		4.5540	
0.75	15.4310	15.7136	15.6636	7.9863	5.4103
1.00	15.4310	15.6935	15.6802	6.8906	6.2101
1.25	15.4310	15.7310	15.6967	9.0000	7.0596
1.50	15.4310	15.7021		7.3495	
1.75	15.4310	15.8406	15.7575	16.7772	10.6602
2.00	16.1520	16.3568		4.1943	
2.25	16.1809	16.4462	16.3765	7.0384	3.8259
2.50	16.1809	16.4376	16.3710	6.5895	3.6138
2.75	16.1809	16.4434	16.3599	6.8906	3.2041
3.00	16.1578	16.4347	16.3820	7.6674	5.0266
3.25	16.1578	16.4434	16.3875	8.1567	5.2762
3.50	16.1578	16.4347	16.3544	7.6674	3.8652
3.75	16.1578	16.4434	16.3654	8.1567	4.3098
4.00	16.1578	16.4462		8.3175	
4.25	16.1549	16.4405		8.1567	
4.50	16.1549	16.4318		7.6674	
4.75	16.1549	16.4578		9.1748	

5.00	16.1549	16.4491	16.3931	8.6554	5.6739
5.25	16.1520	16.4491	16.4096	8.8268	6.6358
5.50	16.1520	16.5097		12.7949	
5.75	16.1520	16.4578	16.4152	9.3514	6.9274
6.00	16.1520	16.4549	16.3986	9.1748	6.0812
6.25	16.1520	16.4607	16.4207	9.5296	7.2200
6.50	16.1520	16.4549	16.4207	9.1748	7.2200
6.75	16.0482	16.4607	16.4262	17.0156	14.2884

Table B.5: Sample data from BH-LB-09.

Average Depth (m)	Dry Density (kg/m^3)	Volumetric Water Content (m^3/m^3)
0.83	1722.3	0.18
1.05	2861.1	0.04
1.30	1689.7	0.06
1.55	1389.9	0.07
1.80	1737.4	0.07
2.05	1524.4	0.07
2.33	1783.7	0.10
2.55	1602.7	0.08
2.83	1761.3	0.11

3.05	1773.9	0.09
3.33	1685.1	0.09
3.55	1700.7	0.09
3.83	1770.4	0.13
4.05	1660.5	0.21
4.30	2092.8	0.35
4.55	1191.4	0.18
4.67	1995.0	0.34
4.80	1915.7	0.34

Table B.6: CPT-TDR results from BH-LB09.

Depth (m)	X_1 (m)	X_2 Single Tangent (m)	X_2 Double Tangent (m)	Dielectric Constant Single Tangent	Dielectric Constant Double Tangent
0.25	15.5011	15.7015	15.6719	4.0160	2.9173
0.50	15.5011	15.7044	15.6888	4.1331	3.5231
0.75	15.5011	15.7044	15.6888	4.1331	3.5231
1.00	15.5011	15.7111		4.4100	
1.25	15.5011	15.7042		4.1250	
1.50	15.5011	15.7019		4.0321	
1.75	15.5011	15.7042		4.1250	
2.00	15.5011	15.7030		4.0764	
2.25	15.5011	15.7606		6.7340	
2.50	15.5011	15.7030	15.6719	4.0764	2.9173
2.75	15.5011	15.7042	15.6677	4.1250	2.7756
3.00	15.5011	15.7434	15.6719	5.8709	2.9173
3.25	15.5011	15.7491	15.6804	6.1504	3.2148
3.50	15.5011	15.7560	15.7014	6.4974	4.0120
3.75	15.5011	15.7941	15.7519	8.5849	6.2901
4.00	15.5011	15.8540	15.7477	12.4538	6.0812
4.25	15.5011	15.8771	15.7772	14.1376	7.6231
4.50	15.5011	15.9036	15.7772	16.2006	7.6231
5.00	15.5011	15.9117	15.7983	16.8592	8.8328

APPENDIX C: 2016 RAW FIELD DATA

Table C.1: Sample data from Location 1.

Depth (m)	Sample Gravimetric Water Content (%)
0.01	6.4
0.10	6.9
0.20	16.4
0.30	15.7
0.40	4.9
0.50	5.5
0.60	6.9
0.70	5.3
0.80	3.9
0.90	4.7
1.00	5.7
1.25	10.2
1.50	3.2
1.75	3.0
2.00	4.1
2.25	3.5
2.50	4.7
2.75	5.9
3.00	5.3

3.25	5.4
3.50	5.5
3.75	5.0
4.00	5.1
4.25	6.5
4.50	6.3
4.75	7.2
5.00	0.6
5.25	6.4
5.50	9.3
5.75	19.4
6.00	7.9
6.25	18.2
6.50	21.3
6.75	17.0
7.00	12.9
7.25	16.1
7.50	17.1
7.75	19.1

Table C.2: CPT-TDR results from Location 1.

Depth (m)	X_1 (m)	X_2 Single Tangent (m)	Dielectric Constant Single Tangent
0.250	17.588	17.788	4.000
0.500	17.588	17.848	6.760
0.750	17.588	17.818	5.290
1.000	17.588	17.808	4.840
1.250	17.588	17.838	6.250
1.500	17.588	17.808	4.840
1.750	17.588	17.828	5.760
2.000	17.588	17.828	5.760
2.250	17.588	17.818	5.290
2.500	17.588	17.818	5.290
2.750	17.588	17.828	5.760
3.000	17.582	17.798	4.666
3.250	17.582	17.810	5.198
3.500	17.582	17.818	5.570
3.750	17.582	17.826	5.954
4.000	17.582	17.830	6.150
4.250	17.582	17.822	5.760
4.500	17.582	17.834	6.350
4.750	28.650	28.902	6.350

5.000	28.650	28.879	5.244
5.250	28.650	28.919	7.236
5.500	28.650	28.915	7.023
5.750	28.650	28.951	9.060
6.000	28.650	28.963	9.797
6.250	28.650	28.967	10.049
6.500	28.650	29.011	13.032
6.750	28.650	29.027	14.213
7.000	28.650	29.023	13.913
7.250	28.650	29.023	13.913
7.500	28.650	29.023	13.913

Table C.3: Sample data from Location 2.

Depth (m)	Gravimetric Water Content (%)
0.01	7.7
0.10	9.4
0.20	9.6
0.30	6.2
0.40	6.8

0.50	5.0
0.60	4.3
0.70	5.0
0.80	6.1
0.90	8.7
1.25	6.6
1.50	8.4
1.75	5.0
2.00	6.5
2.25	5.5
2.50	6.0
2.75	6.5
3.00	6.6
3.25	3.3
3.50	10.2
3.75	9.5
4.00	7.4
4.25	8.5
4.50	11.9
4.75	20.8
6.25	19.5
6.50	25.3
6.75	20.3

Table C.4: CPT-TDR results from Location 2.

Depth (m)	X_1 (m)	X_2 Single Tangent (m)	Dielectric Constant Single Tangent
0.250	17.582	17.814	5.382
0.500	17.582	17.810	5.198
0.750	17.582	17.806	5.018
1.000	17.582	17.802	4.840
1.250	17.582	17.814	5.382
1.500	17.582	17.816	5.476
1.750	17.582	17.820	5.664
2.000	17.582	17.832	6.250
2.250	17.582	17.812	5.290
2.500	17.582	17.824	5.856
2.750	17.582	17.840	6.656
3.000	17.582	17.820	5.664
3.250	17.582	17.836	6.452
3.500	17.582	17.824	5.856
3.750	17.582	17.824	5.856
4.000	17.582	17.822	5.760
4.250	17.582	17.824	5.856
4.500	17.582	17.814	5.382
4.750	17.582	17.892	9.610

5.000	17.582	17.924	11.696
5.250	17.582	17.934	12.390
5.500	17.582	17.948	13.396
5.750	17.582	17.936	12.532
6.000	17.582	17.940	12.816
6.250	17.582	17.940	12.816

Table C.5: Sample data from Location 4.

Depth (m)	Gravimetric Water Content (%)
0.01	11.5
0.10	13.0
0.20	10.1
0.30	11.8
0.40	9.6
0.50	7.4
0.60	4.5
0.70	4.8
0.80	5.3
0.90	7.3

1.00	11.5
1.25	6.8
1.50	5.2
1.75	7.4
2.00	7.9
2.25	6.5
2.50	10.3
2.75	12.0
3.00	7.1
3.25	9.1
3.50	10.1
3.75	5.8
4.25	9.9
4.50	14.1
4.75	17.0
5.00	18.1
5.25	19.4
5.50	16.2
5.75	21.1

Table C.6: CPT-TDR results from Location 4.

Depth (m)	X_1 (m)	X_2 Single Tangent (m)	Dielectric Constant Single Tangent
0.250	17.588	17.832	5.954
0.500	17.588	17.828	5.760
0.750	17.588	17.806	4.752
1.000	17.588	17.832	5.954
1.250	17.588	17.832	5.954
1.500	17.588	17.826	5.664
1.750	17.588	17.812	5.018
2.000	17.588	17.824	5.570
2.250	17.588	17.834	6.052
2.500	17.588	17.848	6.760
2.750	17.588	17.824	5.570
3.000	17.588	17.816	5.198
3.250	17.588	17.818	5.290
3.500	17.588	17.829	5.808
3.750	17.588	17.819	5.336
4.000	17.588	17.853	7.023
4.250	17.588	17.829	5.808
4.500	17.588	17.835	6.101
4.750	17.588	17.925	11.357

5.000	17.588	17.943	12.603
5.250	17.588	17.925	11.357
5.500	17.588	17.933	11.902

Table C.7: Sample data from Location 6.

Depth (m)	Gravimetric Water Content (%)
0.01	8.6
0.10	7.8
0.20	2.9
0.30	3.3
0.40	4.3
0.50	4.9
0.60	5.3
0.70	7.5
0.80	11.7
0.90	5.8
1.00	8.1
1.25	5.9
1.50	4.7

1.75	5.3
2.00	6.2
2.25	5.9
2.50	7.1
2.75	6.3
3.00	4.9
3.25	6.0
3.50	6.7
3.75	4.7
4.00	3.2
4.25	4.0
4.50	4.7
4.75	3.5
5.00	1.5
5.25	5.2
5.50	17.0
5.75	18.7
6.00	22.2
6.25	23.3
6.50	23.4
6.75	17.8

Table C.8: CPT-TDR results from Location 6.

Depth (m)	X_1 (m)	X_2 Single Tangent (m)	Dielectric Constant Single Tangent
0.250	17.600	17.804	4.162
0.500	17.600	17.816	4.666
0.750	17.600	17.828	5.198
1.000	17.600	17.834	5.476
1.250	17.600	17.834	5.476
1.500	17.600	17.842	5.856
1.750	17.600	17.818	4.752
2.000	17.600	17.820	4.840
2.250	17.600	17.828	5.198
2.500	17.600	17.836	5.570
2.750	17.600	17.840	5.760
3.000	17.600	17.860	6.760
3.250	17.600	17.848	6.150
3.500	17.600	17.836	5.570
3.750	17.600	17.850	6.250
4.000	17.600	17.856	6.554
4.250	17.600	17.862	6.864
4.500	17.600	17.850	6.250
4.750	17.600	17.876	7.618

5.000	17.600	17.912	9.734
5.250	17.600	17.924	10.498
5.500	17.600	17.930	10.890
5.750	17.600	17.932	11.022
6.000	17.600	17.954	12.532
6.250	17.600	17.954	12.532
6.500	17.600	17.926	10.628
6.750	17.600	17.942	11.696
7.000	17.600	17.934	11.156
7.250	17.600	17.946	11.972
7.500	17.600	17.946	11.972

Table C.9: Sample data from Location 8.

Depth (m)	Gravimetric Water Content (%)
0.01	10.0
0.10	14.9
0.20	16.5
0.30	3.0
0.40	2.6
0.50	4.9

0.60	17.3
0.70	7.9
0.80	7.0
0.90	8.5
1.00	7.4
1.25	7.5
1.50	8.6
1.75	9.6
2.00	8.9
2.25	10.4
2.50	8.9
2.75	8.4
3.00	10.2
3.25	13.3
3.50	10.2
3.75	11.8
4.00	9.3
4.25	9.3
4.50	13.5
4.75	8.6
5.00	9.4
5.25	13.7
5.50	20.3
5.75	18.0

6.00	29.0
6.25	19.1
6.50	11.5
6.75	22.0

Table C.10: CPT-TDR results from Location 8.

Depth (m)	X_1 (m)	X_2 Single Tangent (m)	Dielectric Constant Single Tangent
0.250	17.588	17.816	5.198
0.500	17.588	17.780	3.686
0.750	17.588	17.804	4.666
1.000	17.588	17.824	5.570
1.250	17.588	17.816	5.198
1.500	17.588	17.820	5.382
1.750	17.588	17.848	6.760
2.000	17.588	17.844	6.554
2.250	17.588	17.836	6.150
2.500	17.588	17.856	7.182
2.750	17.588	17.832	5.954
3.000	17.588	17.860	7.398
3.250	17.588	17.824	5.570

3.500	17.588	17.824	5.570
3.750	17.588	17.848	6.760
4.000	17.588	17.860	7.398
4.250	17.588	17.852	6.970
4.500	17.588	17.848	6.760
4.750	17.588	17.880	8.526
5.000	17.588	17.908	10.240
5.250	17.588	17.912	10.498
5.500	17.588	17.928	11.560
5.750	17.588	17.948	12.960
6.000	17.588	17.944	12.674
6.250	17.588	17.936	12.110
6.500	17.588	17.940	12.390